Seismic Behavior and Evaluation of Concrete Members Made of A Large Quantity of Fly Ash

Wang, Junhua

(Degree)
博士（学術）

(Date of Degree)
2016-09-25

(Date of Publication)
2017-09-01

(Resource Type)
doctoral thesis

(Report Number)
甲第6734号

(URL)
https://hdl.handle.net/20.500.14094/D1006734

博士論文

Seismic Behavior and Evaluation of Concrete Members Made of A Large Quantity of Fly Ash

フライアッシュを大量配合した **RC** 部材の耐震性能と評価方法

平成 28 年 7 月

神戸大学大学院工学研究科

汪　俊華

Seismic Behavior and Evaluation of Concrete Members Made of A Large Quantity of Fly Ash

Kobe University
Graduate School of Engineering

A Dissertation
Submitted to the Kobe University
for the Degree of Doctor of Philosophy

By

Junhua Wang
Kobe, Hyogo, Japan

May, 2016

Acknowledgements

I am very grateful to my supervisor Prof. Yuping Sun for providing the opportunity for me to study in his laboratory and for his technical guidance throughout the period of my research work in Kobe University and for keeping patience to teach me in my research and life during the three and half years, letting me become real researcher from a young man only having a naïve dream to research, this thesis would not be possible without his hard guidance and dedication. Moreover, the rigorous attitude to research and profound knowledge embodied by Prof. Sun will be direction I should hardly study in the future research work and life.

The thesis could not have been completed without the professional guidance, scrupulous examinations and precious advices from Profs. Akinori Tani and Hidenori Morikawa, from Departments of Architecture and Civil Engineering at Kobe University, respectively, whom I wish to sincerely thank.

I would also like to thank Assistant Prof. Takashi, Takeuchi largely for his help and suggestions in my research. And meanwhile thank Associated Prof. Koyama Tomoyuki of Kyushu University for his guidance on production of fly ash concrete and Associate Prof. Takashi, Fujinaga of Kobe University for his technical advice.

I am really grateful to my master supervisor Prof. Qing Wu in Jiangsu University of Science and Technology of China for his financial support and inspiration in particular, and Prof. Xingzhu Pei for all his kind help to me. And I am also grateful to my friends, Miss. Lili Bao, Miss. Fangqian He, Mr. Sheng Gu, Mr. Xiaoen Zhang, Mr. Dingfa Du, Miss. Ping Wang for their financial support and encourage.

I would like to express my gratitude to the Ministry of Education, Culture, Sports, Science and Technology of Japan for providing the financial support for my life.

I am particularly thankful to Doctor Huajia Zhu and Doctor Gaochuang Cai for their help and teaching in my study and life. I am thankful to my colleagues in the Sun Laboratory of the Kobe University Engineering Department for their cooperation in the test work in the laboratory, Doctor Grigor Sargsyan, Doctor Hua Zhao, Ms. Aono Youka, Ms. Shibada Kazuyuki, Ms. Ohada Yusyunn, Ms. Higasiyama Ryofutoshi, Ms. Fuji Syunnsukei, Ms. Kume Kidai, and Ms. Hu Hongyu in special. Thank Mr. Kaneou for his help in setting up the experiment and my friend Grigor for his talks and patient listening.

I also want to thank my parents, my sister, and my brother for their inspiration, in spite of being far away from me. Specially, I want to say thanks to my girlfriend, Yun Wang, for her company and encourage during the last hard period. I also thank my grandfather and grandmother, uncles, aunt, and all other family members.

I want say that there are a large number of people who I owe thanks to. At the confused and wander moments, they gave me courage, power and confidence to keep going for my dream during the past years.

Junhua Wang
2016. 07. 04

Contents

List of Figures

List of Tables

Chapter 1

Introduction

It is true that the grasping of truth is not possible without empirical basis. However, the deeper we penetrate and the more extensive and embracing our theories become, the less empirical knowledge is needed to determine those theories.

Albert Einstein, December 1952.

1.1 RESEARCH IMPETUS AND BACKGROUND

Modern industry development has brought massive wealth, meanwhile it has also caused serious environment problems such as greenhouse effect and air pollution, and more serious industry resource shortage. It was reported that the amount of CO_2 has reached 30.3 billion tons as of 2011. Therefore, building sustainable society which can save energy, make less carbon and protect environment has gradually become the consensus in the world in the 21st century. Based on the above social background, particular emphasis has been placed on new technology development and improvement to enhance utilization efficiency of resource for reducing the usage amount of resource and energy. As the field consuming lots of resource and energy, researchers and designer in civil engineering are also devoting to make some contributions to the sustainable society development.

As we know, the thermal power generation produces huge amount of dust, more than 90 percent of which is fly ash, causing a series of environment problems. For example, the serious air pollution by PM2.5 will be caused if directly discharging the fly ash dust into air, as shown Fig1.1, and the river will be jammed if delivering the fly ash dust into river. Therefore, there will be significant social meaning for the sustainable development in the use the fly ash in the civil engineering construction as the substitute of other resources such as cement and sand, since this utilization of fly ash can reduce the environmental problems stated in the above and save the resources and energy.

(a) Thermal power generation industry [1.1] (b) Shanghai in the polluted air[1.2]

Fig.1 - 1 Environmental problem caused by thermal power generation

In the last several decades extensive researches on fly ash concrete as a kind of energy saving material have been comprehensively conducted in the world. Since 1950s, fly ash has found its wide applications in cement and concrete industries. In North America, fly ash has been used mainly as a supplementary cementitious material in the production of Portland cement concrete at replacement levels ranging from 15% to 30% by mass of the total cementitious material [1.3]. Since 2000, high volume fly ash concrete with fly ash replacement level larger than 30% has gained increasing attention from the standpoint of reducing environmental burden caused by the production of cement [1.4-1.6]. In Japan, the last two decades has seen the recycling ratio of fly ash increase from 67% to about 97% with about 65% of fly ash being used as raw material for Portland cement [1.7]. On the other hand, while the annual domestic consumption of Portland cement declined from its peak of 86.5 million tons in 1990 to 43.7 million tons as of 2013.

However, the thermal power generation is boosted due to the security consideration after The 2011 Great East Japan Earthquake , and the amount of fly ash produced by thermal power generation is gradually increasing, while the cement production, the main filed to consume fly ash now, is decreasing because of the depressed construction market. This fact implies that further use of fly ash as raw material for cement can no longer be expected in Japan. A new application of fly ash is desirable.

From the viewpoint of maximizing environmental and economic benefits simultaneously, Matsufuji et al. [1.8] have proposed to utilize fly ash to partially replace fine aggregate and make high-performance structural concrete. Through extensive experimental works, Matsufuji et al. demonstrated that compressive strength of the concrete with fly ash partially replacing not Portland cement but sand kept increasing along with the fly ash content till the replacement level reached 640 kg/m^3 if the concrete mixture met the minimum requirements prescribed in JASS5 [1.9] for structural concrete. Matsufuji et al. have also developed an empirical formula to predict compressive strength of the concrete with fly ash partially replacing fine aggregate, and verified that the optimum upper replacement level of fly ash would be about 455 kg/m^3 without compromising workability and casting of the produced concrete [1.8]. The advantage of the method proposed by Matsufuji et al. to largely use fine fly ash lies in that it could provide high concrete strength and sounder durability simultaneously, and reduce the amount of sand from river, mountain and sea, which significantly contribute to mitigate environmental burden by concrete industry.

As compared with steel structures and wooden structures, concrete structures are still most widely used in the world due to good structural performances, excellent durability, fire resistance efficiency, and high cost performance. However, concrete structures have inherent shortage such as brittle characteristics. The method increasing the amount of stirrups in the concrete structure has been proposed in current concrete structural design codes in many countries to improve the ductility of concrete, and the largest spacing of stirrup for the concrete columns in buildings has been limited to 100mm in Japan.

Fig.1 - 2 Damaged concrete buildings in earthquake[1.14-1.17]

It has been found that the performances of many buildings designed according to current design codes can attain the goal of life safety, but some buildings can't reach that goal although they were designed by ductility design method as summarized in the survey reports of observed damage of buildings in recent mega earthquakes such as the 2008 Sichuan Earthquake and The 2011 Great East Japan Earthquake [1.10-1.13]. In addition, as shown in Fig. 1-2, several buildings which didn't collapsed during the earthquakes had to be demolished because the residual deformation of them was so large that they couldn't been used anymore or the repair costs would be very expensive [1.14-1.17]. These phenomenon indicates that ductile concrete structures could no longer be regarded as the only solution for the buildings constructed in earthquake-prone regions. From the lessons from the 1995 Kobe earthquake, Ohtani and Kawasima pointed out the importance of limiting the residual deformation in 1997, respectively [1.18, 1.19].

Based on the backgrounds described above, a new type of building structure needs to be developed to mitigate the environmental burden and enhance the robustness and reparability of buildings structures. In other words, sustainability and resilience shall be two key words for the next generation of building structures located in seismic regions.

1.2 STUDY ON PERFORMANCES OF FLY ASH CONCRETE STRUCTURE

1.2.1 Study on material properties of fly ash concrete

As described previously, fly ash had been mainly used to replace cement in concrete. Such kind of fly ash concrete exhibits lower early stage strength than the concrete without fly ash, but may have equivalent or higher strength at later ages due to the continued pozzolanic activity of fly ash [1.20]. Siddique studied basic mechanical properties, including compressive, splitting tensile and flexural strengths, modulus of elasticity and abrasion resistance of concrete with fly ash up, and experimentally demonstrated that the use of high volumes of fly ash as a partial replacement of cement in concrete would decreased mechanical properties of conventional fly ash concrete [1.21].

Matsufuji et al. have pointed out that while conventional fly ash concrete has several advantages such as reduction of the cement content, enhancement of fluidity and reduction of the hydration heat in concrete, the compressive strength and durability of produced concrete, in particular at early age, tended to be less than concrete without fly ash [1.22]. Furthermore, the replacement level of fly ash should be kept less than 30 %, which obviously hinders effective application of fly ash to make structural concrete.

As a new and effective application of fly ash in concrete, Matsufuji et al. have proposed to use fine fly ash rather as partial replacement of fine aggregate than as replacement of cement. Through extensive and comprehensive experiments on mechanical properties of the concrete with fly ash replacing sand, they have revealed that the early-age compressive strength including 28 days strength could be higher than the concrete without fly ash, that the optimum upper replacement level of fly ash would be about 455 kg/m^3 without compromising workability and casting of the produced concrete [1.22], and that the initial stiffness of the produced concrete didn't declined [1.23]. The same experimental results could be found even concrete was cured in 40℃ air environment [1.24-1.25]. The difference between the mechanical properties of conventional fly ash concrete and the new type of fly ash concrete can be attributed to that the amount of micro pores larger than 50μm are reduced because the micro pores were filled by fly ash with the largest grain size of 10μm, leading to denser internal structures than the concrete without fly ash [1.26].

1.2.2 Study on mechanical properties of fly ash concrete structures

In order to make the best use of high-strength and sound durability of fly ash, Sun and his research team have conducted a series of studies on mechanical properties of concrete members containing a large quantity of fly ash. Koyama et al. have demonstrated that LQFA concrete exhibited the same compressive stress-strain behavior as general concrete with identical compressive strength, and the stress-strain response of LQFA concrete can be accurately evaluated by the equation for general concrete [1.23]. Sun et al. have demonstrated that shear strength and deformability of the fly ash concrete (FAC) beams increased along with the mixed quantity of fly ash, that the failure mode of concrete short beams could be improved from brittle shear failure to relatively ductile flexural-shear mode due to the increased compressive strength, and that shear strength could be reasonably calculated by the formulas in current design codes [1.27]. Through experimental works on mechanical behavior of square FAC columns, Sun et al. have also verified that combination of FAC and ultra-high strength rebars could ensure square concrete columns to behave in a ductile manner up to large drift of 3.0 % and that flexural and shear strength of square FAC columns could be reasonably predicted by the AIJ-prescribed equations [1.28-1.31].

However, for concrete members made of large quantity of fly ash, due to greatly increased concrete strength, the specimens did not fail in shear till large deformation, and information on shear behavior and ultimate shear capacities of these FAC members is scarce.

1.3 STUDY ON PERFORMANCE OF TUBED CONCRETE COLUMN

Tubed concrete column, tube of which is used to confine concrete in lateral direction and don't carry the vertical stress by bending or axial load, was proposed by Tomii et al. to avoid the shear failure and increase the ductility of the short concrete columns in frame structure and the boundary columns of shear wall structure[1.32,1.33]. Advantages of tubed concrete column are, 1) large amount of shear reinforcement can be easily provided; 2) tube confinement contains whole column section and avoids degradation in lateral resistance of columns at large deformation due to the spalling off of the cover concrete; 3) the buckling of longitudinal rebar can be effectively prevented; and 4) the tube can be used as a form for columns [1.34].

Xiao and Sun have studied the stress-strain relationship of concrete confined by circular tube and square tube [1.35, 1.36], and proposed stress-strain relationships for circularly and squarely tubed concrete, respectively. Sun has also proposed the equation to calculate the flexural strength of tubed concrete column [1.37]. Sakino et al. have studied seismic behavior of square tubed concrete column under high axial compression [1.38], and experimentally verified that square tubed concrete columns could exhibit high deformability and seismic performances even under high axial load with the axial load ratio of 0.99. Matsuo et al. have investigated the performances of tubed high strength concrete columns reinforced by high strength rebars, and verified their high deformability and low residual deformation [1.39].

The first application of the tubed concrete column in bridge structures was the design of a bridge by Transportation Department of Las Vegas in USA. Silva et al. bent three full scale tubed concrete columns, and verified that tube confinement was effective in enhancing both the flexural strength and ductility of the columns [1.40]. Priestley et al. [1.41] systematically studied the mechanical properties of concrete members confined by steel jacket and proposed a series of seismic evaluation method and strengthening design method which are now used in the strengthening engineering for bridge in California.

The tube used in the aforementioned tubed concrete columns were made by welding two pieces of L-shape or channel-shape steel plates. Since there are potential defects in the welding all of which couldn’t be completely detected, these hideous defects may seriously affect the performances of tubed concrete columns. To mitigate negative effect of potential defect in the welding portion of tube, Fukuhara et al. have proposed to connect two pieces of L-shape plates by bolts and nuts and demonstrated that this connection method could provide the same confinement effect to concrete columns as the welded tube [1.42]. However, effect of this confinement method on circular concrete columns, in particular those made of high-strength concrete, has not yet been verified and evaluated.

1.4 STUDY ON PERFORMANCES OF RESILIENT CONCRETE STRUCTURES

Importance of the residual deformation of concrete structures hit by an earthquake has been widely recognized in structural engineering community. So far, two methods have been proposed to design and construct the resilient concrete structure. One is using post-tensioned pre-stressed (PTPS) bar to reinforce the section of concrete components, and the other is using ultra-high strength (UHS) rebar having low bond strength or un-bond rebar as longitudinal rebars in concrete components.

Watanabe et al. [1.43] focused on using PTPS high strength (HS) rebar into conventional concrete columns to take advantages of the high resistance of conventional concrete columns and the long elastic region of pre-stressed HS bar and to construct the resilient concrete columns. Their experimental results showed that residual deformation of concrete columns could largely be decreased due to the resilience of PTPS HS bar. Priestley et al. [1.44] have applied this method to concrete bridges to reduce residual deformation. Panian et al. [1.45] have actually applied the PTPS bar into the construction of David Brown Center to resist the potential earthquake.

He and Xin et al. [1.46-1.48] studied the seismic behavior of a self-centering bridge pier system connected by un-bond post-tensioned (PT) tendon locating at the center of cross section of bridge pier with mild steel distributed around the perimeter of the pier section. The PT tendon was intended to dissipate seismic energy and to minimize the residual deformation of bridge pier. Hu et al. [1.49] also utilized PT tendon into concrete walls.

The above-mentioned studies have demonstrated effectiveness of the PTPS bar on reduction of the residual deformation of concrete structures. However, there are several problems for using the PTPS bar remain to be solved. These problem include the evaluation of the loss in the stress of the PTPS bar at large lateral deformation and the appropriate level of the pre-stress that should be applied to the PTPS bar.

Pandey et al. [1.50] have studied the influence of the bond strength of longitudinal rebars on the shear resistance and ductility of concrete columns and demonstrated that the damage of column was greatly reduced and the failure mode was changed from brittle shear to ductile flexure by reducing the bond stress of longitudinal rebar. According to their study, the less the bond stress, the larger the improved ductility, and increasing the length of un-bond region of longitudinal rebar could also greatly improve the ductility. Tanaka et al. [1.51] studied seismic behavior of concrete columns with their longitudinal rebars being completely un-bonded by surrounding them with a pre-installed steel pipe into concrete and revealed that these columns could exhibited self-centering hysteresis response performance.

On the other hand, the use of un-bond rebars leads to lower lateral resistance and is hard to enable concrete columns to develop the calculated capacity by the current design codes.

To overcome the problems in the method of using PTPS bar or un-bond rebars, Sun et al. have recently proposed using special ultra-high strength rebar (SBPDN 1275/1420 rebar) with low bond strength as longitudinal rebar in concrete members. The SBPDN rebar has spiral groove on its surface and has low bond strength of about 1/5 of deformed rebar [1.52]. They demonstrated that square concrete columns using SBPDN rebar exhibited stable cyclic behavior up to large deformation and reduced residual deformation as compared with the columns using conventional HS rebar (USD685) [1.53-1.56]. Meanwhile, Sun et al. also revealed that the square concrete columns using SBPDN rebar under double curvature deformation need careful detailing to fix the rebar at the middle of column in order for the columns to exhibit identical resilience as the cantilever columns [1.57].

Sun and Cai et al. have researched the resilience and seismic performances of circular concrete columns reinforced by SBPDN in detail, and verified that circular concrete columns exhibited more stable performance and smaller residual deformation because circular hoops or spirals can provide more effective confinement to core concrete[1.58-1.60].

1.5 STUDY ON MODEL FOR SHEAR STRENGTH DEGRADATION

The nominal shear capacity of concrete columns is generally evaluated as the sum of three contributions, namely; concrete V_c, axial load V_n and transverse steel V_s. Most of the current design codes assume that shear capacity of concrete columns is a constant, independent of the deformation level of the column, as shown in Fig.1-3. Priestley et al [1.61], however, illustrated that the shear capacity of a concrete column tends to degrade along with deformation level because the shear contribution by concrete and axial load decrease at large deformation.

As one can see from Fig. 1-3, a reliable and sound model of shear strength, which can account for effect of deformation on the shear strength, is of great importance in design. According to the relative value of shear strength model and the actual response envelop curve, one can predict the failure mode of a concrete component at the stage of design.

So far, only New Zealand design code recommends a complete shear strength model for circular concrete columns account for effect of deformation. However, the model needs transformation of circular section into an equivalent square or rectangular section or adoption of the concept of effective shear strength area. Apparently, the transformation of column section causes evitable error in the calculated shear strength.

In order to overcome the disadvantage induced by the deformation of column section, since 1980s several complete shear strength models have been proposed by Ang and Wong et al.[1.62,1.63], Aschheim and Meohle [1.64], Priestley et al.[1.65], California Department of Transportation [1.66], Applied Technology Council [1.67] and Kowalsky et al.[1.68]. There is, however, a crucial problem in these models. All models define the relationship between the shear strength and displacement ductility, but the definition of yield displacement is rather arbitrary and varies among researches, which may result in unreliable prediction.

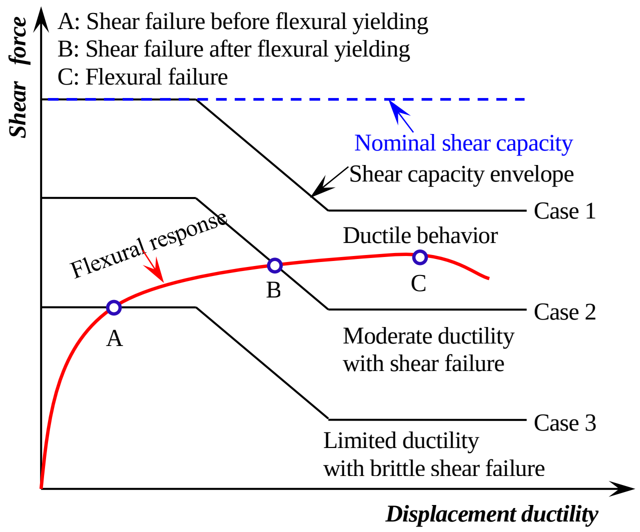

Fig.1 - 3 Representative lateral resistance of concrete columns

Another problem needs to be solved in the current shear strength models is the upper limitation on the lateral stress of hoop or spiral used in the calculation of shear strength because the high strength spirals or hoops may not yield at the peak resistance[1.69]. While Architecture Institute of Japan (AIJ) has recommended an upper limit of 700MPa on the lateral stress of rectilinear hoop in calculating the so-called confinement effect [1.70, 1.71], however, AIJ design guideline doesn’t specify upper yield stress to circular hoop, in particular to the circular hoop as shear reinforcement. The upper limitation of transverse reinforcement is proposed to be 550MPa in ACI Committee for circular spirals used to confine concrete and based on the tests by Richart el al [1.72]. In other design codes [1.73-1.75], the upper yield strength for transverse steels has been assumed to be 500MPa. Scattering among the upper lateral stresses of shear steel can be observed. .

While Cai et al. have developed a complete seismic shear strength model for circular concrete columns [1.76]. The model can only be applied to circular concrete columns with compressive strength less than 50 MPa. Since the use of LQFA may increase concrete strength over 70 MPa, a new model which can cover high-strength concrete columns, both circular and square, needs to be developed.

1.6 OBJECTIVES AND SCOPE

On the basis of the above-mentioned backgrounds and reviews of previous studies, it is reasonable to presume that the utilization of LQFA in concrete and the use of ultra-high strength SBPDN rebar as longitudinal steel in concrete columns are a feasible way to the development of sustainable and resilient concrete components.

Objectives of this doctor dissertation are to develop a new type of sustainable and resilient concrete columns and experimentally investigate their seismic performance, to propose design equations for predicting ultimate shear strength and deformation of concrete components made of LQFA, to develop a skeleton model for the proposed concrete columns, and finally to propose a cyclic loop model of the proposed columns.

The concrete contents of this doctor desertion are summarized as follows:

1) Experimental investigation of seismic behavior of circular concrete cantilever columns made of LQFA and reinforced with SBPDN rebars to clarify if the LQFA concrete beams can exhibit the same resilience as the conventional circular concrete columns and if the resilience may change due to the increased compressive strength of LQFA concrete. These columns simulates the columns at the lower stories of high-rise frame structures, which are expected to exhibit a strong column-weak beam lateral resistance mechanism.

2) Experimental investigation of seismic behavior of circular concrete columns made of LQFA and reinforced with SBPDN rebars under double-curvature deformation. These columns simulate the columns in a frame expected to exhibit the weak column-strong beam failure mechanism, which was well observed in low- and middle-rise building structures damaged during recent strong earthquakes.

3) Proposal of design equations to calculate the ultimate shear strength and corresponding drift or chord rotation of LQFA concrete beams. These proposed equations are intended not only for LQFA concrete beams but also for LQFA concrete columns. With the proposed equations, one can conduct reasonable and reliable design of the developed sustainable and resilient concrete columns.

4) Modeling of skeleton curve of lateral force versus drift ratio relationship for circular

LQFA concrete columns. In this paper, the model will be referred to as capacity curve, which is indispensable in performance-based design of the proposed sustainable and resilient concrete columns as shown in Fig. 1-4.

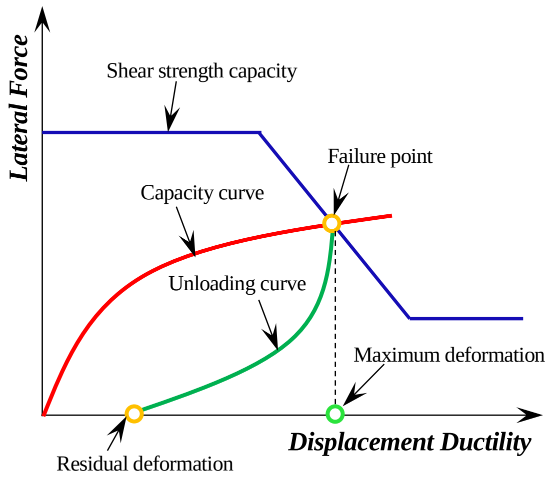

Fig.1 - 4 Characteristics of the next generation structure

1.7 FORMAT OF THE DOCTOR DISSERTATION

This doctor dissertation comprises six chapters. Each chapter deals with one of the above-mentioned issues except chapter one and chapter six. Core points of each chapter are written below:

Chapter one introduces backgrounds of this doctor dissertation, reviews previous study in the literature, and presents research objectives and research issues.

Chapter two is devoted to the investigation of seismic behavior of circular concrete cantilever columns. Four specimens were fabricated and tested under combined reversed cyclic loading and constant axial compression. Experimental variables were the type of longitudinal rebar and the confinement method. All specimens were 250mm in diameter and had shear span ratio of 2.0. Two specimens were reinforced by eight SBPDN (12.6mm in nominal diameter) rebars, and two specimens by eight high-strength deformed USD685 rebars. Longitudinal rebars were uniformly distributed along the perimeter of column section with concrete shell of 30mm and gave steel ratios of 2.05% and 2.07%, respectively. Objectives of this experimental work are to investigate effect of the high compressive strength of LQFA concrete on the resilience of columns, and to verify effectiveness of partial confinement of columns by steel plates on seismic capacity of high-strength concrete columns.

Chapter three presents experimental study on seismic performance of circular LQFA concrete columns under double curvature deformation. Four circular columns with diameter of 250mm were made and tested under reversed cyclic loading while the axial load was kept constant. All specimens were made of concrete with fly ash replacement of 455 kg/m3 of sand and partially confined by circular steel plates within end region of 375mm from the column base. Experimental variables were the connecting method of steel plates for confinement, the type of longitudinal rebars (USD685 and SBPDN) and the anchorage length of SBPDN rebars within the loading stubs. The shear span ratio and axial load level expressed in terms of axial load ratio were kept constant for all specimens and had values of 2.0 and 0.33, respectively.

Chapter four describes an experimental program to investigate shear behavior of LQFA concrete beams. Emphasis of the program was placed on the assessment of ultimate shear strength and deformability of LQFA concrete members, whose shear capacities have been little known because the use of fly ash in large quantities leads to high strength concrete that tends to fail after the yielding of longitudinal rebars. To obtain experimental information on the ultimate shear capacities of LQFA concrete members, the SBPDN rebars were used as tensile steels for all twenty specimens, all of which were prismatic beams with rectangular section of 250 x 150 mm. Experimental variables among specimens were the shear span ratio of beams (1.0 – 4.0) and the steel ratio of tensile rebar (0.76%, 1.14%). Based on the test results, the equilibrium of forces acting on the diagonal shear plane and Mohr-Coulomb failure criterion for LQFA concrete, a complete shear strength model is developed and its validity and accuracy is verified by comparing the experimental results with the calculated results.

A skeleton envelop curve is developed in Chapter five for circular LQFA concrete columns. The capacity curve model is developed on the basis of the test results described in Chapters two and three of this dissertation. The proposed model takes effect of slippage of SBPDN rebars on capacity curve into consideration. Test results described in this study are used to verify validity and accuracy of the developed model.

Chapter six summarizes all findings and observations obtained through Chapters two and five, and presents several future issues concerning with the proposed sustainable and resilient concrete components.

REFERENCES

[1.1] http://image.so.com/i?src=rel&q=%E7%81%AB%E5%8A%9B%E5%8F%91%E7%94%B5%E5%8E%82%E6%B1%A1%E6%9F%93%E5%9B%BE%E7%89%87. July, 10, 2016.

[1.2] https://www.google.co.jp/search?q=%E9%9B%BE%E9%9C%BE+%E5%8C%97%E4%BA%AC&biw=1422&bih=1032&tbm=isch&tbo=u&source=univ&sa=X&ved=0ahUKEwiNkqK16KjMAhVm26YKHQ5IDicQsAQIGg&dpr=0.9#tbm=isch&q=%E9%9B%BE%E9%9C%BE+%E4%B8%8A%E6%B5%B. July, 10, 2016.

[1.3] Thomas, M.D.A., "Optimizing the use of fly ash in concrete," PCA report IS548, Portland Cement Association, Stokie, Illinois, 2007.

[1.4] Bilodeau, A., Malhotra, V.M., "High-volume fly ash system: concrete solution for sustainable development," ACI Materials Journal, V.97, No.1, 2000, pp. 41-50.

[1.5] Mehta, P., Manhoman, D., "Sustainable high-performance concrete structures," Concrete International, V. 28, No.7, 2006, pp. 37-42.

[1.6] Myadarabonia, H., Solikin, M., Patnaikuni, I., Setunge, S., "Development of high volume fly ash concrete using ultra-fine fly ash," Proceedings of 23rd Australasian Conference on the Mechanics of Structures and Materials, Byron Bay, Italy, 2014, pp.65-70.

[1.7] Japan Coal Energy Center, "Fly ash application survey from 1995 to 2013," JCOAL 2013, www.jcoal.or.jp. [in Japanese]

[1.8] Matsufuji, Y., Koyama, T., Funamoto, K., Ito, K., "Mix proportion principle of concrete containing large quantity of coal ash with constant cement content," Concrete Research and Technology, Japan Concrete institute 2001, V.12, No.2, 2001, pp. 51-60.

[1.9] Architectural Institute of Japan, "Japanese Architectural Standard Specification 5 – Construction of Reinforced Concrete Structures," AIJ 2005, Maruzen, Tokyo. [in Japanese]

[1.10] Wang, D.S., Guo, X., Sun, Z.G., "Damage to Highway during Wenchuan Earthquake," Journal of Earthquake Engineering and Engineering Vibration, V.29, 2009, No. 3, pp. 84-94.

[1.11] Sun, Z.G., Wang, D.S., Li, H.G., et al., "Damage Investigation of RC frames in Wenchuan Earthquake and Suggestion for Post-earthquake Rehabilitation," Journal of Natural Disasters, V.19, No.4, 2010, pp. 114 – 123.

[1.12] Wen, Z.P., Xu, C., Lu, M., et al., "Damage Features of R. C Frame Structures in Wenchuan Earthquake," Journal of Beijing University of Technology, V.35, No.6, 2009, pp. 753 – 760.

[1.13] Zhuang, W.L., Liu, Z.Y., Jiang, J.S., "Earthquake-induced Damage Analysis of Highway Bridges in Wenchuan Earthquake and Counter Measures," Chinese Journal of Rock Mechanics and Engineering, V.28, No.7, 2009, pp.1377 – 1387.

[1.14] https://zh.wikipedia.org/wiki/%E6%B1%B6%E5%B7%9D%E5%A4%A7%E5%9C%B0%E9%9C%87#/media/File:ADBC_Branch_in_BeiChuan_after_earthquake.jpg. July, 10, 2016.

[1.15] https://zh.wikipedia.org/wiki/%E6%B1%B6%E5%B7%9D%E5%A4%A7%E5%9C%B0%E9%9C%87#/media/File:Sichuan_earthquake_building_collasped..JPG. July, 10, 2016.

[1.16] http://natural-hazard.blogspot.jp/. July, 10, 2016.

[1.17] http://encoresources.com/index.html. July, 10, 2016.

[1.18] Ohtani, S., "Development of Performance-Based Design Methodology in Japan," Proceedings of International Conference at Bled, Slovenia, 1997, pp.59-68.

[1.19] Kawashima, K., "The 1996 Japanese Seismic Design Specifications of Highway Bridges and the Performance-Based Design," Proceedings of International Conference at Bled, Slovenia, 1997, pp.229-240.

[1.20] Orville, R., Werner, I., Edward, A., Abdum, N., Pierre-Claude, A., Leonard W. Bell, Floyd, J. B., et al, "Use of Fly Ash in Concrete, " ACI Materials Journal-Committee Report 226, No.84-M39, 1988, pp.381-409.

[1.21] Rafat, S., "Performance Characteristics of High-Volumes Class F Fly Ash Concrete," Cement and Concrete Research, No.34, 2004, pp.487-493.

[1.22] Yasunori, M.F., Tomoyiki, K. Y., Korekiyo, I.T., "Mix Proportion Theory of Strength Controlling Concrete Containing Large Quantity of Coal Ash, " The Society of Materials Science, Vol.51, No.10, pp.1111-1116, 2002

[1.23] Koyama, T., Sun, Y.P., Koyamada, H., Fujinaga, T., "Behavior and modelling of compressive stress-strain relationship of concrete with a large quantity of fly ash in partial place of sand," Proceedings of the Japan Concrete Institute, V.30, No.3, 2008, pp. 85-90. [in Japanese]

[1.24] Takasu, K., and Matsufuji Y., "Strength properties of concrete using recycled aggregates and fly ash," Proceedings of the Japan Concrete Institute, Vol. 29, No.2, 2007, pp. 379-384. [in Japanese]

[1.25] Takasu, K., and Matsufuji Y., "Strength properties of concrete made of recycled aggregates and fly ash under hot environment with 40℃," Proceedings of the Japan Concrete Institute, Vol. 30, No.1, 2008, pp. 201-206. [in Japanese]

[1.26] Suyama H., Koyama T., Ito K. and Matsufuji Y., "Strength development of concrete using by-product system inorganic powder," Proceedings of the Japan Concrete Institute, Vol. 28, No.1, 2006, pp. 269-274. [in Japanese]

[1.27] Koyama, T., Sun, Y.P., Fujinaga, T., et al.. , "Mechanical Properties of Beam Made of a Large Amount of Fine Fly Ash," The 14th World Conference on Earthquake Engineering, Beijing, 2008.

[1.28] Tani, M., Sun, Y.P., Koyama, T. and Koyamada H., "Mechanical properties of concrete members made of a large quantity of fly ash," Proceedings of the Japan Concrete Institute, Vol. 32, No.2, 2010, pp. 73-78. [in Japanese]

[1.29] Yoshino, K., Tani, M., Koyama T. and Sun Y.P., "Shear behavior of concrete columns made of a large quantity of fly ash," Proceedings of the Japan Concrete Institute, Vol. 33, No.2, 2011, pp. 181-186. [in Japanese]

[1.30] Takeuchi T., Koyama, T., Fujinaga, T. and Sun Y.P., "Effect of yield strength of longitudinal rebar on seismic properties of high volume fly ash concrete columns," Proceedings of the Japan Concrete Institute, Vol. 34, No.2, 2012, pp. 145-150. [in Japanese]

[1.31] Takeuchi T., Koyama, T., Yoshino K. and Sun, Y. P., "Experimental study of seismic performance of high volume fly ash concrete columns confined by steel plates," Proceedings of the Japan Concrete Institute, Vol. 35, No.2, 2013, pp. 151-156. [in Japanese]

[1.32] Tomii, M., Sakino, K., Xiao, Y., Watanabe, K., "Earthquake Resisting Hysteretic Behavior of Reinforced Concrete Short Columns Confined by Steel Tube," Proceedings of the International Conference on Concrete Filled Steel Tubular Structures, 1985, pp.119-125, China.

[1.33] Xiao, Y., Tomii, M., Sakino, K., "Experimental Study on Design Method to Prevent Shear Failure of Reinforced Concrete Short Circular Columns by Confining in Steel Tube," Transactions of Japan Concrete Institute,V.8, 1986, pp.119-125.

[1.34] Xiao, Y., "Development and Prospects of Tubed Reinforced Concrete Column Structures," China Civil Engineering Journal, V.37, No.4, 2004, pp. 8-12.

[1.35] Xiao Y., "Constitutive law for confined concrete," Dissertation paper submitted to Kyushu University for doctor in engineering, January 1989. [in Japanese]

[1.36] Sakino, K. and Sun, Y. P., "Stress-Strain Curve of Concrete Confined by Rectilinear Hoop," J. of Struct. Constr. Eng., AIJ, No. 461, 1994, pp. 95 – 104. (in Japanese)

[1.37] Sun, Y. P., Sakino, K. and Aklan, A., "Flexural Behaviour of High Strength RC Columns Confined by Rectilinear Reinforcement," Proceedings of the Japan Concrete Institute, V.18, No.2, 1996, pp.131-136.

[1.38] Sakino, K. and Sun, Y. P., "Seismic behavior of RC columns confined by square steel tube under high axial compression," Transaction of JCI, Vol. 14, 1992, pp. 483-490.

[1.39] Matsuo, H., Sun, Y. P., Fukuhara, T., and Sakino K., "Cyclic behavior of confined high strength concrete columns," Proceedings of the Japan Concrete Institute, Vol. 26, No.2, 2004, pp. 775-780. [in Japanese]

[1.40] Silva, P., Sritharan, S., Seible, F., Priestley, M.J.N., "Full Scale Test of the Alaska Cast in Place Steel Shell Three Column Bridge Bent," Research Report of Charles Lee Powell Structural Research Laboratories, No. SSRP 98/13, pp.157.

[1.41] Priestley, M.J.N., Seible, F., Calvi, M., "Seismic Design and Retrofit of Bridge," John Wiley & Sons, pp.686.

[1.42] Fukuhara, T., Nakahara, Y., Matsuo, H., and Sun, Y. P., "Proposal of an analytical method to predict seismic behavior of PCa columns made of high strength concrete,"

Proceedings of the Japan Concrete Institute, Vol. 29, No.3, 2007, pp. 559-564. [in Japanese]
[1.43] Watanabe, F., Miyazaki, S., Tani, M., Kono, S., "Seismic Strengthening Using Precast Prestressed Concrete Braces," 3th World Conference on Earthquake Engineering, Vancouver, August.2004, pp.3406.
[1.44] Priestley, M.J.N., Macrae, G., "Seismic tests of Precast beam-to-column joint subassemblies with unbonded tendons," PCI Journal, V.1, No.41, 1996, pp.64-81.
[1.45] Panian, L., et al, "Post-tensioned Concrete Walls for Seismic Resistance," PTI Journal, V.10, No.29, 2007, pp. 39-45.
[1.46] Guo, J., Xin, K.G., He, M.H., Hu, L., "Experimental Study and Analysis on the Seismic Performance of a Self-Centering Bridge Pire," Engineering Mechanics, V.29, Suppl I, 2012, pp.29-34.
[1.47] He, M.H., Xin, K.G., Guo, J., Guo, Y.M., "Research on the Intrinsic Lateral Stiffness and Hysteretic Mechanics of Self-Centering Pire," China Railway Science, V.33, No.5, 2012, pp.22-28.
[1.48] He, M.H., Xin, K.G., Guo, J., "Local Stability Study of New Bridge Pire with Self-Centering Joints," Engineering Mechanics, V.29, No.4, 2012, pp.122-127.
[1.49] Hu, X.B., He, H.G., Peng, Z., Cao, W.Q., "Study on Hysteretic Performance of Self-Centering Wall Subjected to Cyclic Loading," Journal of Building Structures, V.34, No.11, 2013, pp.18-23.
[1.50] Pandey, R.A.J., Hiroshi, Mutsuyoshi, H., "Seismic Performance of Reinforced Concrete Piers with Bond-Controlled Reinforcements," ACI Structural Journal, V.102, No.2, 2005, pp. 295-304.
[1.51] Tanaka, M. et al., "Cyclic properties of RC columns with un-bonded high-strength rebars," Proceedings of the Japan Concrete Institute, Vol. 26, No.2, 2004, pp. 181-186. [in Japanese]
[1.52] Funato, Y., Sun, Y. P., Takeuchi, T., and Cai, G., "Modeling and Application of Bond Characteristic of High-strength Reinforcing Bar with Spiral Grooves," Proceedings of the Japan Concrete Institute, V.34, No.2, 2012, pp.157-162.
[1.53] Nakai, S., Kittaka, M., Tani, M., and Sun, Y. P., "Influence of steel ratio and axial load ratio on seismic behavior of concrete columns made of ultra-high strength rebars," Proceedings of the Japan Concrete Institute, V.33, No.2, 2011, pp.157-162. [in Japanese]
[1.54] M., Tani, M., and Sun, Y. P., et al., "Experimental study of concrete columns with high resilience,“ Proceedings of the Japan Concrete Institute, V.31, No.2, 2009, pp.565-570. [in Japanese]
[1.55] Kittaka, M., Tani, M., Fujinaga, T., and Sun, Y. P., "Seismic behavior of concrete columns with ultra-high strength rebars," Proceedings of the Japan Concrete Institute,

Vol. 32, No.2, 2010, pp. 79-84. [in Japanese].
[1.56] Wang, J.H., Takeuchi, T., Koyama, T., "Seismic behavior of circular fly ash concrete columns reinforced by ultra-high strength rebar and steel plates," Proceedings of the Japan Concrete Institute, V.36, No.2, 2014, pp: 115-120.
[1.57] Sun, Y. P., et al., "Fundamental study of earthquake-resilient concrete columns," Proceedings of the Japan Concrete Institute, Vol. 35, No. 2, 2013, pp. 1501-1506. [in Japanese]
[1.58] Cai, G., and Sun, Y. P., et al., "Experimental study of seismic performance of circular concrete columns with high yield strength and low bond strength rebars," Proceedings of the Japan Concrete Institute, Vol. 35, No.2, 2013, pp.145-150. [in Japanese]
[1.59] Sun, Y.P., Cai, G.C., Takeuchi, T., "Seismic Behavior and Performance-Based Design of Resilient Concrete Columns," International Journal of Applied Mechanics and Materials, Vols. 438-439, 2013, pp. 1453-1460.
[1.60] Cai, G.C., "Seismic Performance and Evaluation of Resilient Circular Concrete Columns," Doctoral dissertation, Kobe University, 2014.
[1.61] Priestley, M.J.N., Verma, R., and Xiao, Y., "Seismic Shear Strength of Reinforced Concrete Columns," Journal of Structural Engineering, ASCE, V.120, No.8, 1994, pp.2310-2329.
[1.62] Ang, B.G., Priestley, M.J.N., Paulay, T., "Seismic Shear Strength of Circular Reinforced Concrete Columns," ACI Struct J, 1989; V.86, No.1, 1989, pp.45-59.
[1.63] Wong, Y.L., Paulay, T., Priestley, M.J.N., "Response of circular reinforced concrete beams to multi-directional seismic attack". ACI Struct J, V.90, No.2, 1993, pp.180–91.
[1.64] Aschheim, M., Moehle, J.P., "Shear Strength and Deformability of RC Bridge Columns Subjected to Inelastic Cyclic Displacements," Rep. No. UCB/EERC -92/04, Earthquake Engineering Research Center, University of California at Berkeley, Berkeley, CA, 1992.
[1.65] Priestley, M.J.N., Verma. R., Xiao, Y., "Seismic Shear Strength of Reinforced Concrete Columns," Journal of Structural Engineering ASCE, V.20, No.8, 1994, pp.2310-2329.
[1.66] Caltrans, "Memo to Designers Change Letter 02," Sacramento, Calif. California Department of Transportation, 1995.
[1.67] Applied Technology Council, "Seismic Evaluation and Retrofit of Concrete Buildings Volume 1," Calif. (Redwood City), Report No. SSC 96-01, 1996.
[1.68] Kowalsky, M.J., Priestley. M.J.N., "Improved Analytical Model for Shear Strength of Circular Reinforced Concrete Columns in Seismic Regions," ACI Struct J, V.97, No.3, 2000, pp. 388-396.
[1.69] Sun, Y.P., et al, "Ductility Improvement of Reinforced Concrete Columns with

High-Strength Materials," Transactions of the Japan Concrete Institute, No.15, 1993, pp. 455-462.

[1.70] Architecture Institute of Japan, "Guidelines for Performance Evaluation of Earthquake-Resistant Reinforced Concrete Buildings (Draft)," Maruzen, Tokyo, 2004.

[1.71] Otani, S., Nagai, S., Aoyama, H., "Load-Deformation Relationship of High-Strength Reinforced Concrete Beams. Mete A. Sozen Symposium: a Tribute from his Students, " ACI SP 162, J. K. Wight and M. E. Kreger, eds., American Concrete Institute, Farmington Hills, MI, pp. 35-52.

[1.72] Richart, F.E., Brown, R.L., "An investigation of reinforced concrete columns. Bulletin" No. 267. Urbana (IL): Univ. of Illinois Engineering Experiment Station, 1934.

[1.73] AS3600, Concrete Structures, "New Australian Standard, Standards Association of Australia," Sydney, 2009.

[1.74] CSA A23.3, "Design of Concrete Structures (CSA A23.3-04), Canada standard Association, Mississauga," ON, Canada, 2004, pp.214.

[1.75] NZS 3101, "Concrete Structures Standard, Part 1: The Design of Concrete Structures, Standard Association of New Zealand," New Zealand, 2006, pp.293.

[1.76] Cai, G., Sun, Y.P., Takeuchi, T., Zhang, J., "Proposal of A Complete Seismic Shear Strength Model for Circular Concrete Columns," Engineering Structures, V.100, 2015, pp.309-409.

Chapter 2

Seismic Behavior of Circular LQFA Concrete Cantilever Columns Reinforced by Ultra High Strength Rebar and Steel Plates

2.1 INTRODUCTION

The design philosophy of the strong column – weak beam has been utilized in the structural design of buildings since 1960s. The strong column-weak beam lateral force-resisting mechanism works only if the column bases at the lowest story of a building have been assigned sufficient robustness and ductility. Recent earthquakes have proved that ductile concrete columns at the lowest story could attain the goal of preventing the buildings from total collapse and saving human life during a mega-earthquake. As shown in Fig.1-2, however, ductile columns may be deformed to large drift by a strong earthquake and result in severe damage within the column bases and too large residual deformation for the columns to be repaired after the ground motion.

One of solutions for constructing idealistic strong column-weak beam frames for building is the utilization of LQFA concrete and SBPDN rebars into the columns at the lowest story, because combination of both materials may ensure adequate robustness and resilience to the columns. As the first step to the development of seismic assessment method for the sustainable and resilient concrete members, this chapter focuses on the following items: 1) to experimentally verify effectiveness of combination of LQFA concrete and SBPDN rebars on enhancement of robustness and resilience of circular concrete cantilever columns which simulate the columns at the lowest story; 2) to clarify effect of bond strength of longitudinal rebars on overall seismic performance of LQFA concrete cantilever columns, and 3) to present experimental information on hysteresis feature, residual drift, and variation of steel strains along with deformation, of the columns.

2.2 EXPERIMENTAL PROGRAM

2.2.1 Description of test specimen

To achieve the aforementioned goals, four 1/3-scale circular concrete columns with diameter of 250mm were fabricated and tested under combined constant axial compression and reversed cyclic lateral load. Table 2-1 shows outlines of test specimens. All specimens had a shear span of 500 mm to give a shear span ratio of 2.0. Concrete with fly ash replacement level of 455 kg/m^3 was used to make the specimens and give a targeted compressive strength over 70MPa. The experimental variables were the type of longitudinal rebars and the confinement method of column. The specimens were divided into two groups, SB and US, according to the type of longitudinal rebar. SB series specimens were reinforced by eight SBPDN 1275/1420 rebars, while US series specimens were reinforced by eight deformed USD 685 rebars. Specimens FANSB and FANUS were confined with D6 spirals having spacing of 30mm. For specimens FATSB and FATUS, the end region from the column bottom with a length of 1.4D (D = diameter of column section) were confined by steel plates, and the left portion were confined by circular D6 hoops having spacing of 30mm. Within the tube-confined region of specimens FATSB and FATUS, D6 hoops were also provided with spacing of 90mm just to keep the position of longitudinal rebars as shown in Fig.2-1. To prevent the steel plates to directly sustain the axial stresses induced by axial load and bending, clearance of 6mm was provided between lower end of steel plates and the loading beam.

Table 2 - 1 Outlines of test specimens

Specimen	f'_c (N/mm^2)	a/D	n	Longitudinal Bar		Transverse reinforcement				
				Type	p_g (%)	s (mm)	ρ_h (%)	Steel Plate	t (mm)	ρ_t (%)
FANSB	80	2	0.33	SBPDN rebar	2.05	30	1.98	No	-	-
FATSB						90	0.57	Yes	3.2	2.5
FANUS				USD rebar	2.07	30	1.98	No	-	-
FATUS						90	0.57	Yes	3.2	2.5

Note: f'_c: concrete cylinder strength; *a/D*: shear span ratio; *n*: axial load ratio; p_g: the ratio of rebars; *s*: spacing of spirals; ρ_h: the volumetric ratio of spirals; ρ_t= the volumetric ratio of steel plate.

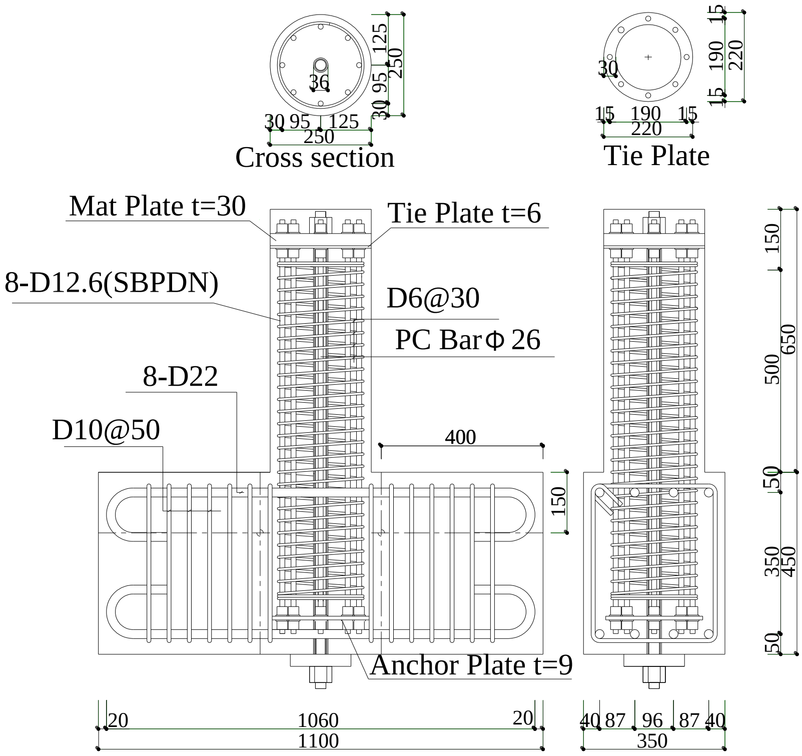

(a) FANSB

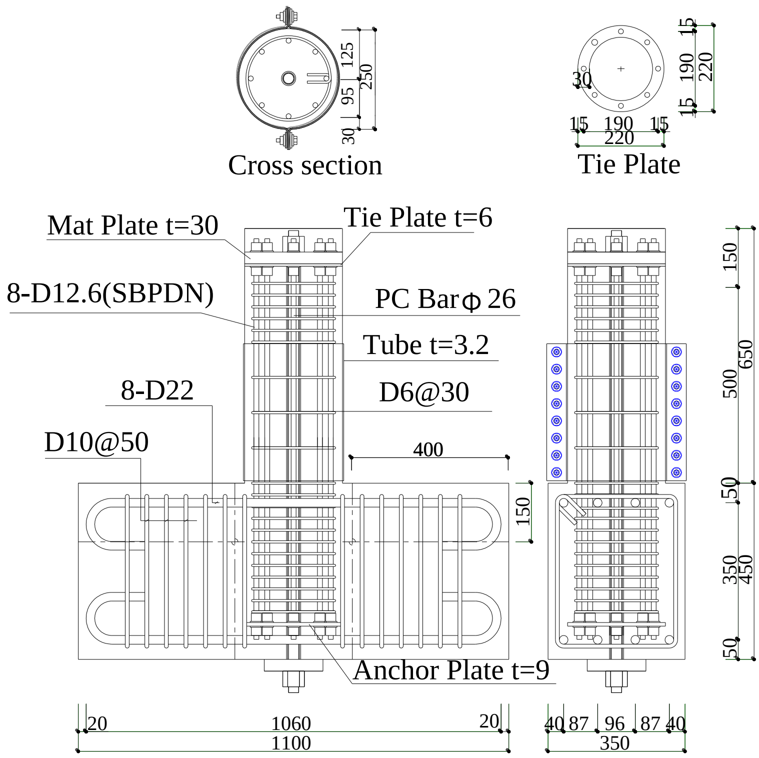

(b) FATSB

Fig. 2-1 Details of test columns (Continued)

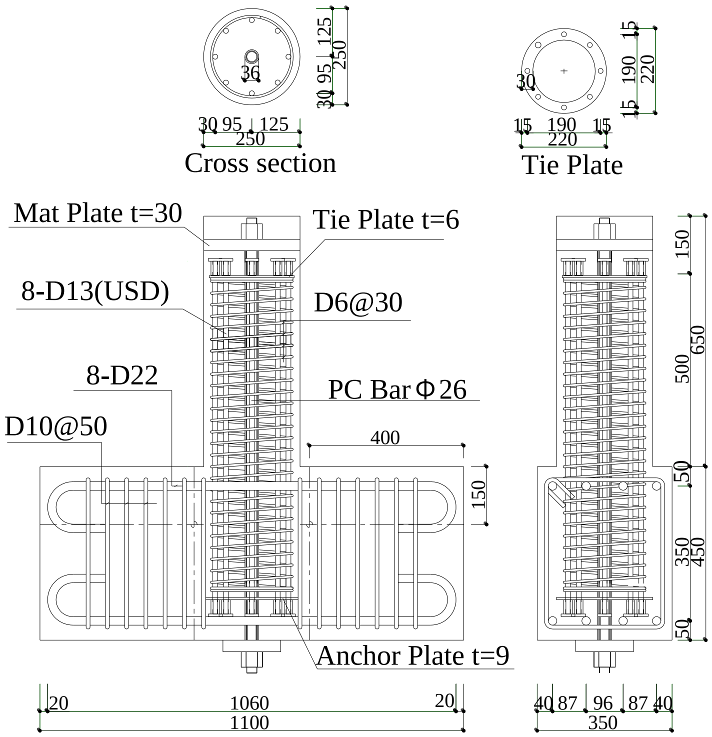

(c) FANUS

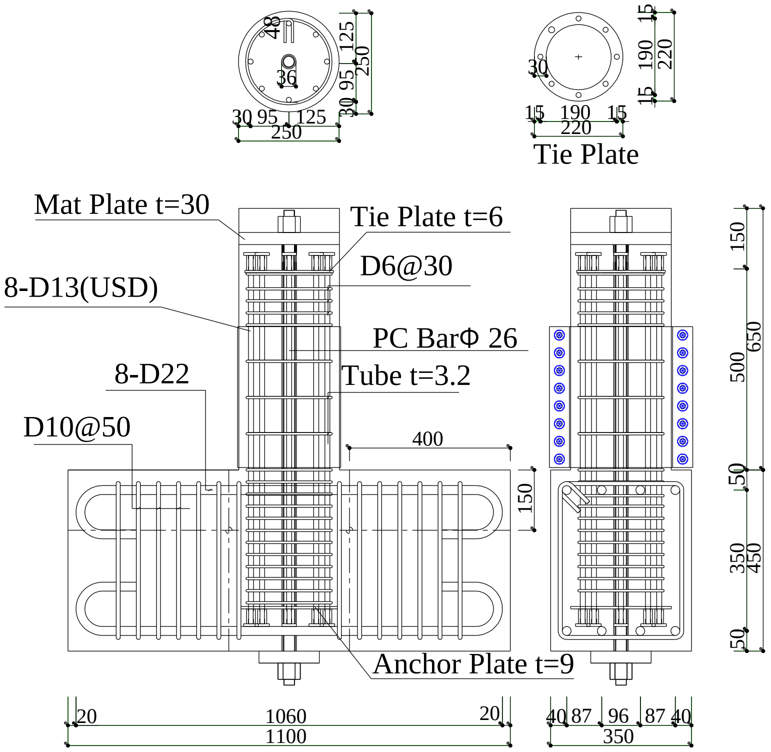

(d) FATUS

Fig. 2- 1 Details of test columns

Each end of SBPDN rebars was anchored to end plate by nuts and bolts as shown in Fig.2-1, while both ends of each USD rebars were anchored by anchor caps. In addition, one piece of mat plate with thickness of 30 mm was embedded in the top of each specimen to disperse the pre-stressed axial compression. Each specimen was under constant axial compression with axial load ratio of 0.33. Due to the limitation of facility capacity, about 30% of the targeted axial compression was provided via a PC bar.

2.2.2 Material properties

Ready-mix concrete was used to fabricate test specimens. Table 2-2 shows details of mix proportion of the concrete. As can be seen from Table 2-2, up to 455kg of fine fly ash was used to replace fine aggregate in per unit volume of concrete. The specimens were cured in the forms with their tops covered by wet burlaps for four weeks after casting and then were air-cured till the time of testing. The actual concrete strength at the testing day was about 78.8MPa.

Table 2 - 2 Mix proportion of concrete

Fly Ash (kg/m^3)	W/C	Water (kg/m^3)	Cement (kg/m^3)	Fine Aggregate		Coarse Aggregate (kg/m^3)	Admixture (kg/m^3)
				Sand (kg/m^3)	Crushed Sand (kg/m^3)		
455	0.65	185	285	334	146	833	5.92

Table 2 - 3 Mechanical properties of the steels

Name	Type	f_y (N/mm^2)	f_u (N/mm^2)	E_s (N/mm^2)	ε (%)	*Elongation* (%)
SBPDN bars	SBPDN 1275/1420	1423**	1499	215000	0.86**	9.7
USD bars	USD 685*	961**	1037	182000	0.72**	25.7
PL3.2	SS400	325**	503	194000	0.37**	
D6	SD295	426	517	190000	0.23	25.9

Note: f_y=yield stress; f_u=ultimate stress; E_s= young modulus; ε= yield strain; USD685* is hardening strength; ε=0.37%**, ε=0.86%** are obtained according to the 0.2% offset method.

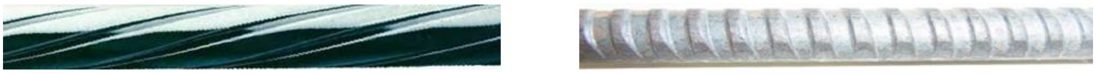

(a) SBPDN 1275/1420 rebar (b) USD 685 rebar

Fig.2- 2 View of the longitudinal rebars used

The ultra-high strength SBPDN 1275/1420 rebar has yield strength of 1423 MPa and 12.6 mm in diameter with spiral grooves on its surface as shown in Fig.2-2 along with conventional high-strength deformed USD 685 rebar whose yield strength was 961 MPa. According to Funato et al. [2-1], the bond strength of SBPDN rebar was about 3.0 MPa and about one-fifth of that of USD rebar. The steel plates used to confine concrete in specimens FATSB and FATUS had a thickness of 3.2mm and yield strength of 325 MPa. Fig.2-3 and Table 2-3 shows the tensile stress-strain curves and mechanical properties of the steels used, respectively.

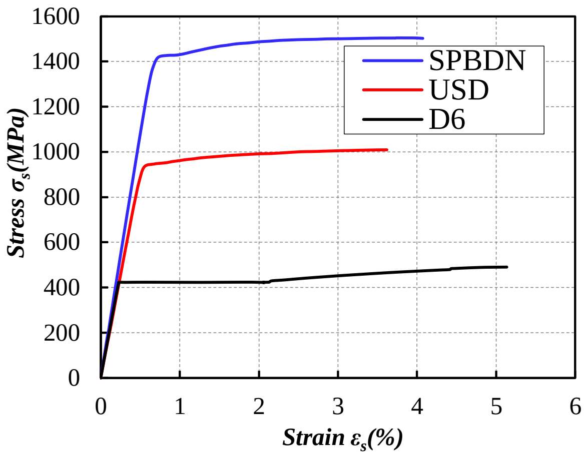

Fig. 2- 3 Stress-strain curves of steels used

2.2.3 Test setup

The test setup is shown in Fig.2-4. The axial compression was applied by a hydraulic jack while the reversed cyclic lateral force was applied by another hydraulic jack. About 250 kN of axial compression was applied to each specimen by post-tensioning a PC bar before the testing. Since the stress of the PC bar would vary along with the drift of column, the axial compression applied through hydraulic jack was adjusted to keep the axial load applied to columns as constant as possible.

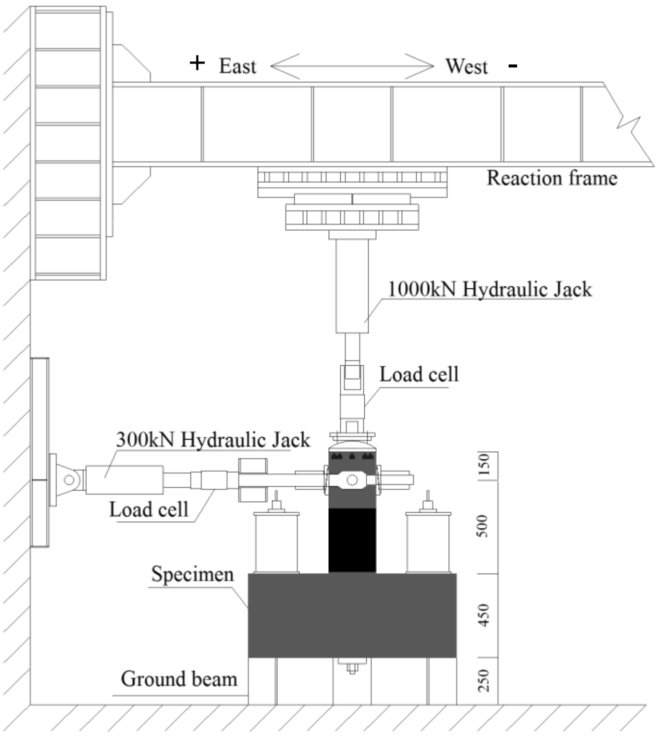

Fig.2- 4 Schematic view of test setup (Unit: mm)

Fig.2-5 shows overall view of actual loading. The horizontal hydraulic jack was attached to a rigid concrete reaction wall, and the reversed cyclic lateral load was basically controlled by drift angle R (=Δ/L, where Δ is the lateral displacement at the rotation center of the column measured by a displacement transducer (DT), and L is the shear span). The planned loading program for the lateral force is shown in Fig.2-6.

Lateral load was initially force-controlled until the first flexural crack was observed, and then controlled by drift angle (R). Two complete cycles were applied at each level of drift level before R reached 0.02rad, from which on only one cycle was applied at each level of drift level. For specimens FATSB and specimen FATUS, however, because the ultimate capacities of them exceeded capacity of the horizontal hydraulic jack in the pull direction, these two specimens were deformed only up to 0.03 rad. and 0.02 rad. in the pull direction.

Fig.2- 5 Overall view of loading

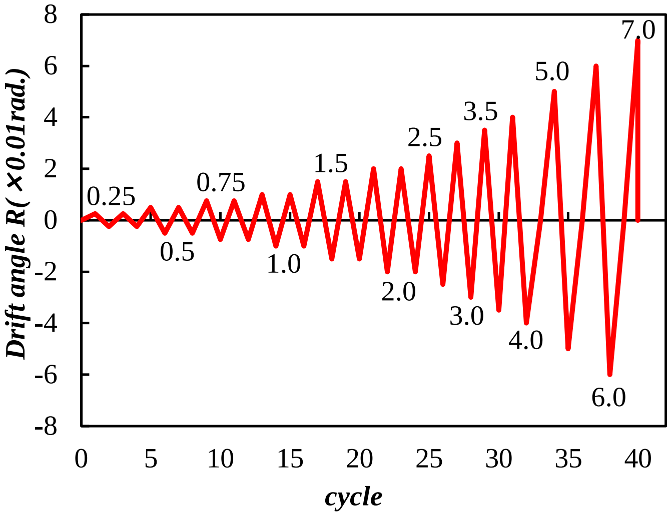

Fig.2- 6 Loading program

2.2.4 Instrumentation and measurement

As shown in Fig.2-7 and Fig.2-8, for each specimen, there were nine DTs and fourteen strain gages used for measuring the displacement and steel strain. The No.1 DT measured the lateral displacement while No. 2 through No.7 DTs measured the axial deformation within different gage lengths. No. 8 and No. 9 DTs were attached to monitor the shift of the loading stub and the base rigid beam.

Locations of strain gages for the longitudinal and transverse reinforcements are shown in Fig.2-8. In addition, two strain gages were attached to the PC bar to monitor variation of the stress, and six bi-axial strain gages were attached on the external surface of the steel plates to measure the surface strains located 16 mm, 181 mm and 346 mm, respectively, away from the column base as shown in Fig.2-8 (e).

2.3 TEST RESULTS AND OBSERVATIONS

2.3.1 Observations of test columns

Crack patterns of specimen FANSB at several representative drift angle are shown in Fig.2-9(a) in the form of extend elevation of the specimen. In Fig.2-9(a), the terms “east” and “west” represent the initial tensile and compressive flanges, respectively. Before the testing, several hairline cracks due to shrinkage of concrete were observed, but they were very subtle. Flexural cracks were firstly observed near the bottom section and the section 100mm away from the column base when R reached 0.0025rad in the push and pull direction, respectively.

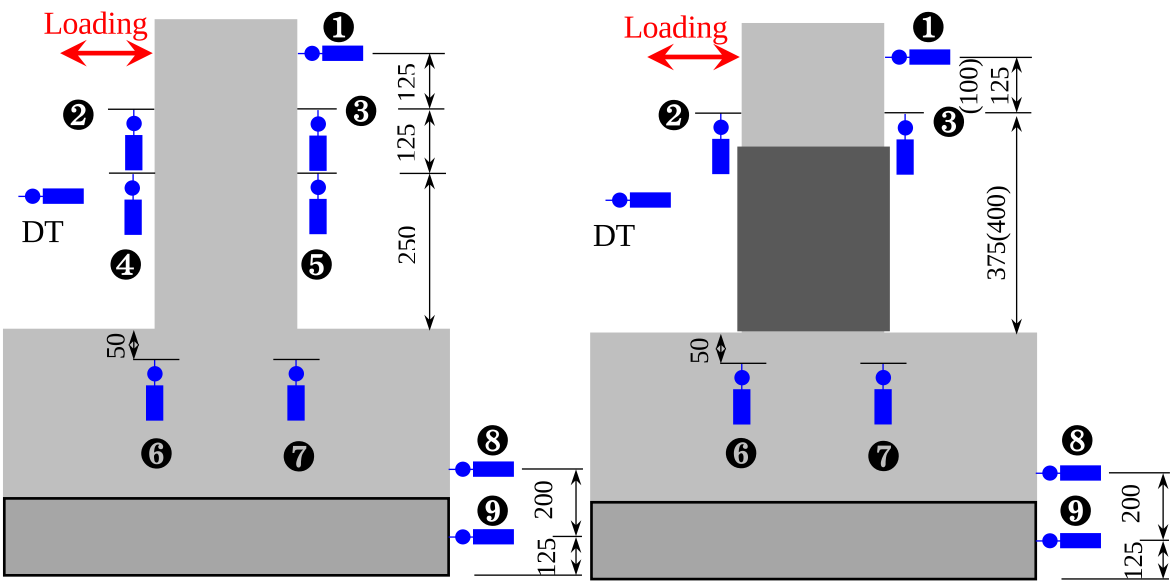

(a) FANUS (b) FATUS

Fig.2- 7 Locations of DTs

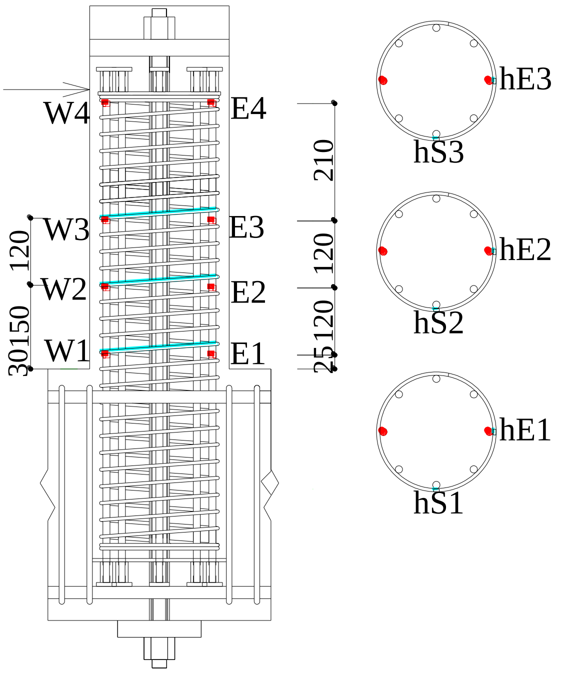

(a) FANUS

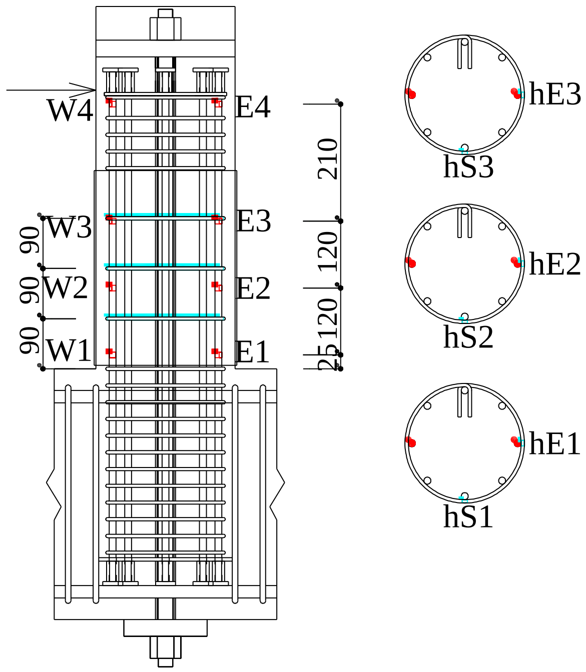

(b) FATUS

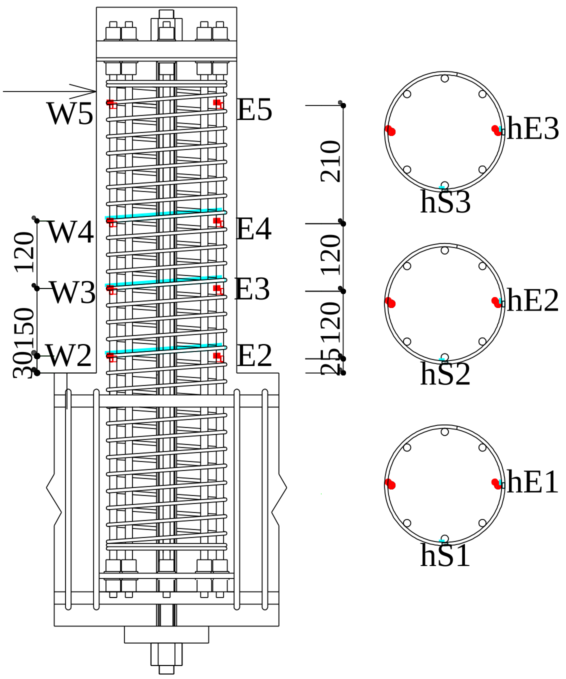

(c) FANSB

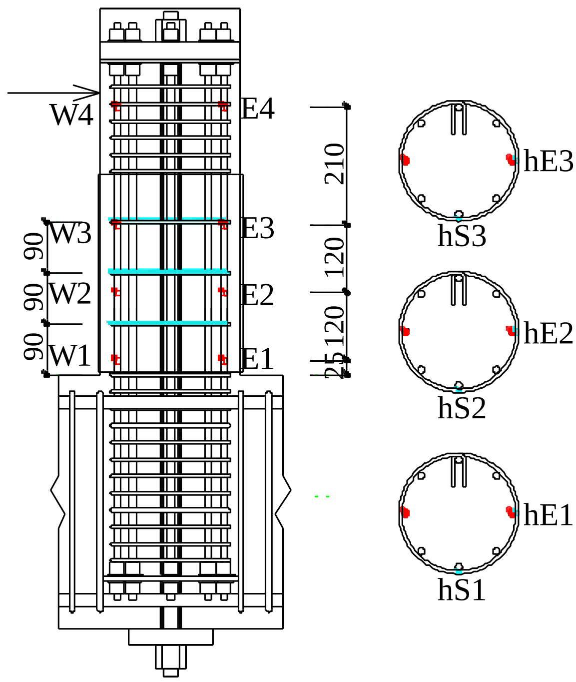

(d) FATSB

Fig.2- 8 Locations of strain gages (Continued)

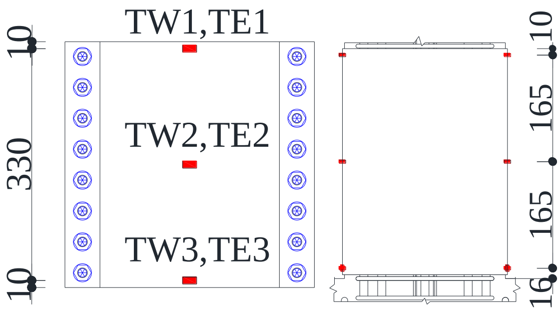

(e) Steel plates

Fig.2- 8 Locations of strain gages

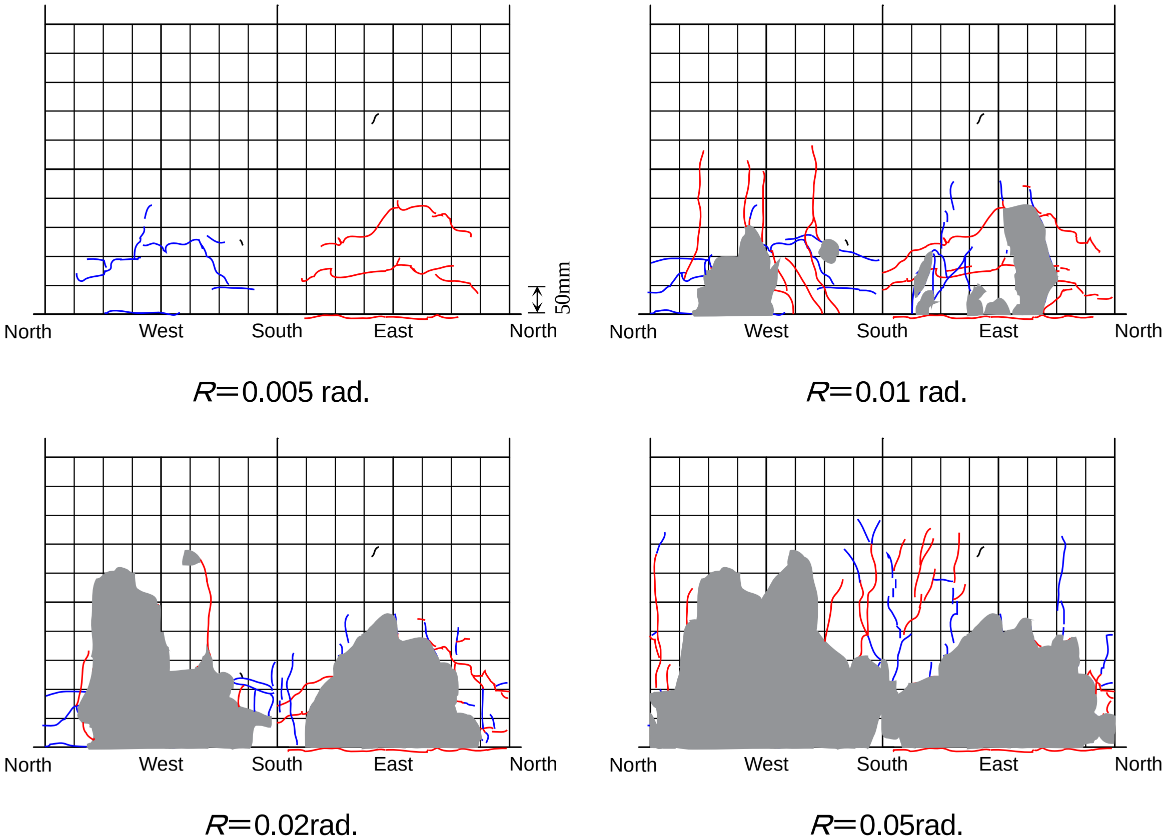

Fig.2-9 (a) Crack patterns of specimen FANSB

During the loading cycle of R=0.005 rad, flexural cracks were observed at the section about 185mm away from column base. The splitting cracks were observed at R=0.075rad, and expanded along with drift level. Flaking of the concrete shell was also observed at R=0.0075 rad, but spalling-off of the cover concrete was not observed until R reached 0.015rad. From R=0.02 rad on, more and more concrete shell spalled off, but the lateral resistance of the specimens still continued increasing until R=0.03rad. Testing was terminated at R=0.05rad, where buckling of SBPDN rebar was observed due to significant spalling-off of concrete shell. The region of spalling-off of cover concrete finally covered the end region with length of 1.0D

– 1.5D.

Fig.2-9 (b) displays the crack pattern of specimen FATSB. The crack pattern was observed after the testing and removing the steel plates. One can see from Fig.2-9 (b) that confinement by steel plates did mitigate the damage degree. Only very subtle flexural cracks and several splitting cracks could be found on the surface.

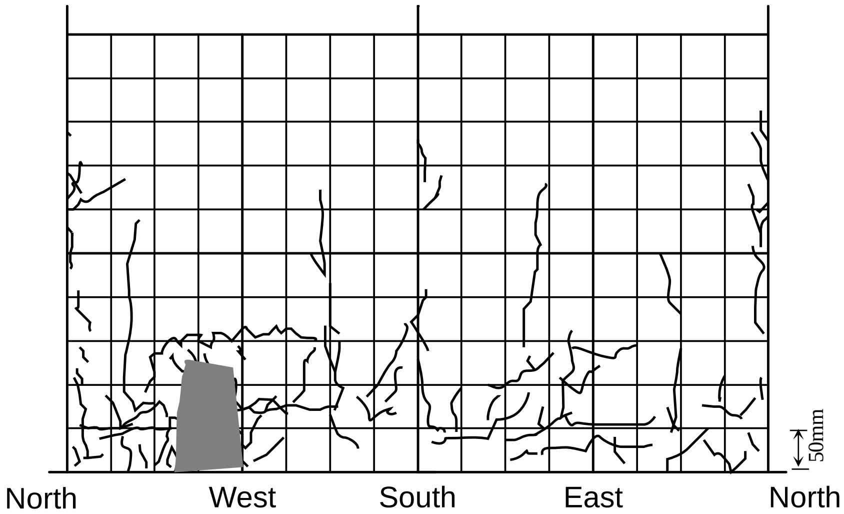

Fig. 2- 9 (b) Crack pattern of specimen FATSB

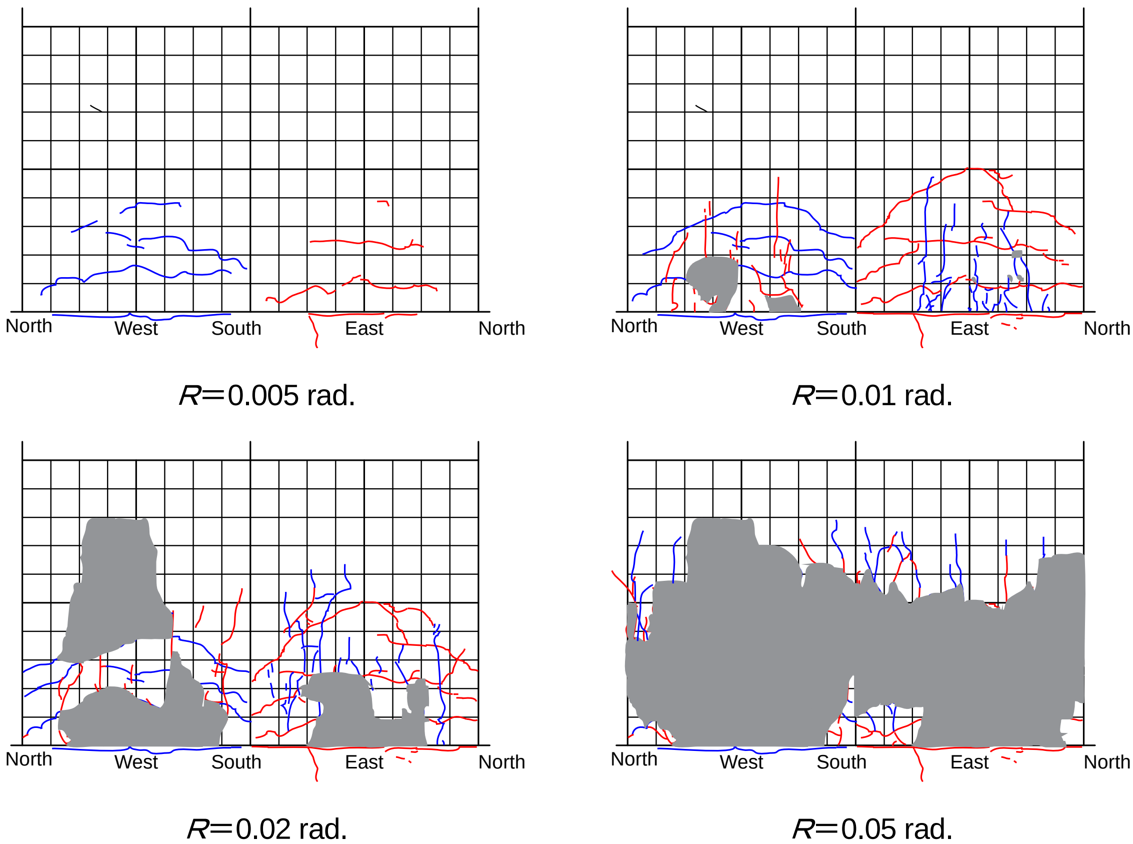

Fig.2-9 (c) Crack patterns of specimen FANUS

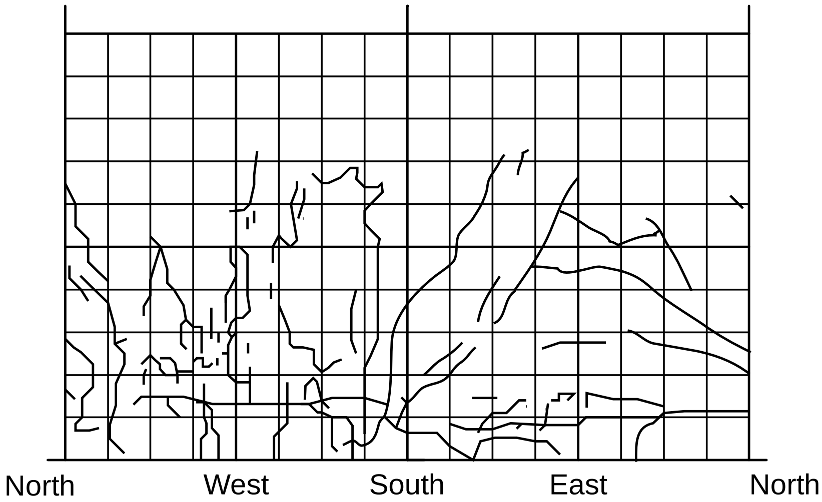

Fig.2- 9(d) Crack pattern of specimen FATUS

Fig.2- 9 Crack pattern of specimens

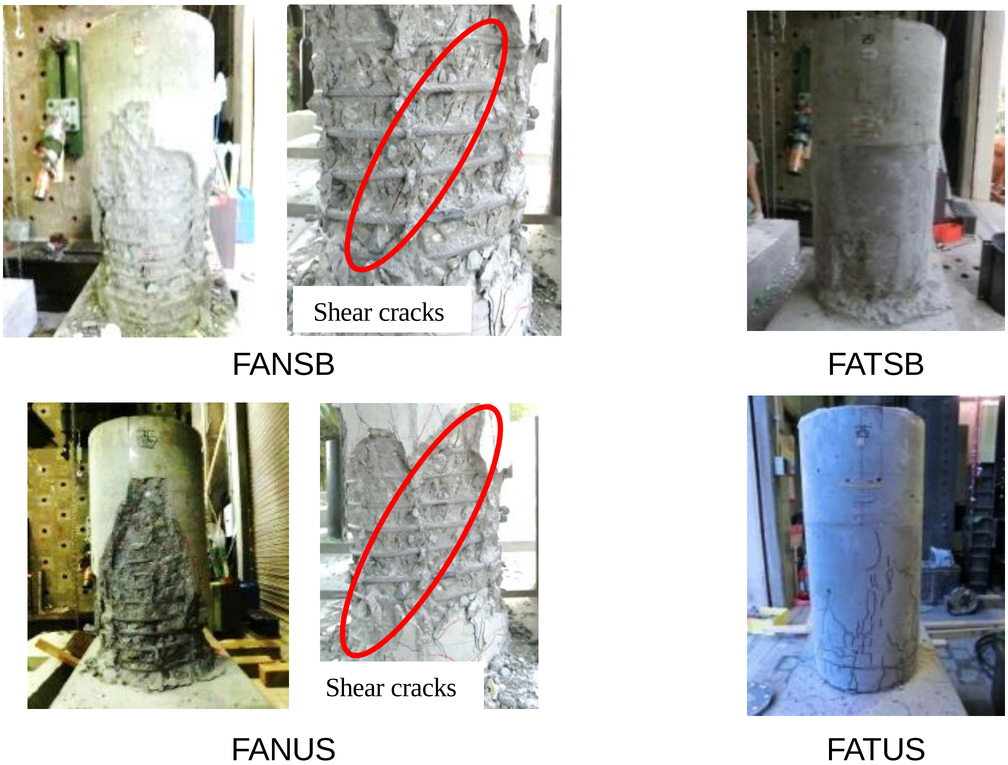

Fig.2- 10 Overall views of test columns after testing

Crack patterns of specimen FANUS is illustrated in Fig.2-9 (c). Flexural cracks were firstly observed at the section 60 mm away from the column base at R=0.0025rad. Due to the high bond strength of USD 685 rebars, flexural cracks were observed at the section 250mm away from the column base when R reached 0.01rad from which on splitting and shear cracks occurred. The spalling-off of cover concrete was firstly observed at R=0.015rad. shear cracks expanded along with drift angle, and at R=0.025 rad in pull direction, the cover concrete spalled off so significantly that spiral and longitudinal rebars were completely exposed. High bond strength of USD 685 rebars caused more severe damages than SBPDN rebars.

The final crack pattern of specimen FATUS is shown in Fig.2-9 (d). While cracks of concrete could not be observed during the testing, swelling of steel plates was verified by hand touch at R=0.03 rad where the specimen reached its maximum lateral resistance (see Fig.2-11). As the specimen FATSB, the loading was applied until R=0.06 rad in the push direction. Fig.2-10 illustrates overall views of all specimens after testing. Confinement by steel plates obviously mitigated damage degree of concrete columns.

2.3.2 Lateral load – drift angle hysteretic responses

The primary test results are listed in Table 2-4, while the lateral load *V* versus drift angle *R* relationships of all specimens are shown in Fig.2-11. The white square, triangle, diamond and circle superimposed in Fig.2-11 represent the testing stages when the flexural crack was firstly observed, when longitudinal rebar reached the yield strength, when spirals reached the yield strain and when the lateral resistance reached its maximum, respectively. The dotted line represents the so-called P-delta mechanism line.

Table 2 - 4 Primary test results of all specimens

Specimen	f'_c (N/mm^2)	Longitudinal rebar		Transverse reinforcement					V_{exp} (kN)	R_{expQ} (%)
		Name	ρ_g (%)	s (mm)	ρ_h (%)	Steel plate	t (mm)	ρ_t (%)		
FANSB	78.7	SBPDN rebar	2.05	30	1.98	No	-	-	230	3.0
FATSB	78.7			90	0.56	Yes	3.2	2.5	313	7.0
FANUS	76.8	USD rebar	2.07	30	1.98	No	-	-	261	2.5
FATUS	73.8			90	0.56	Yes	3.2	2.5	318	3.0

Note: f'_c =concrete compression strength; ρ_g= the ratio of longitudinal rebar; s=the spacing of transverse reinforcement; ρ_h=the volumetric ratio of spirals; V_{exp}= ultimate lateral load; R_{expQ}= drift angle at V_{exp}; t=thickness of steel plate; ρ_t= the volumetric ratio of steel plates.

By comparing the measured V-R curve of specimen FANSB with that tested by Cai et al. [2-2], it can be found that the use of fly ash in large quantities decreased resilience of circular concrete columns confined by spirals. The only difference between these two specimens lies in concrete strength. As compared with concrete strength of 78.7 MPa of specimens FANSB, the concrete strength of the specimen described in reference 2-2 was 47.2 MPa. The lateral resistance of specimens FANSB kept increasing until R=0.035 rad, whereas the V-R curve of the specimen in reference 2-2 kept increasing up to R=0.05rad. And therefore, this decrement in resilience of circular concrete column may be attributed to the inherent brittle feature of the high strength LQFA concrete.

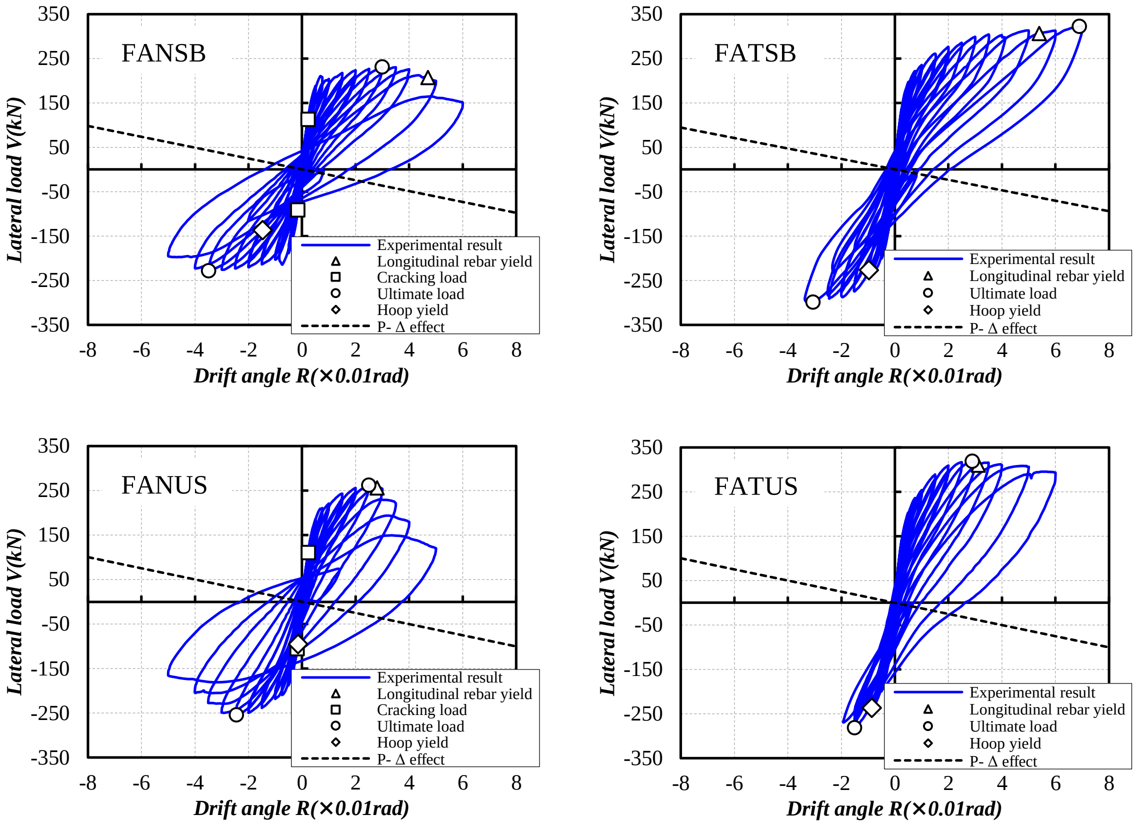

Fig.2- 11 Lateral load V– drift angle R relationships

However, partial confinement by steel plates is apparently effective in enhancing the resilience of circular LQFA concrete columns as shown in Fig.2-11. Confinement by thin steel plates with diameter-to-thickness (D/t) ratio of about 80 did enhance the resilience of LQFA concrete columns from 0.035rad to at least 0.05rad. Steel confinement constrained whole concrete section and prevented the lateral resistance of specimen FATSB from degrading along with drift level due to the spalling-off of concrete shell. This fact implies that combination of LQFA concrete, longitudinal SBPDN rebar and partial confinement by steel plates is a good candidate for developing sustainable and resilient concrete columns.

On the other hand, specimens FANUS and FATUS, both of which were reinforced with USD 685 deformed rebars, reached their peak lateral resistance at the same drift angle of 0.025 rad as shown in Fig.2-11. The lateral resistance of spiral-confined specimen FANUS commenced degrading after R=0.025 rad due to more and more severe spalling-off of cover concrete and the inherent brittle feature of high-strength LQFA concrete. The degradation rate of lateral resistance was larger than that induced by the P-delta effect. Confinement by steel plates could not enhance the resilience of specimen FATUS. It is the yielding of USD 685 rebars at R=0.025 rad that reduced the resilience and confinement effect by the steel plates on high-strength LQFA concrete.

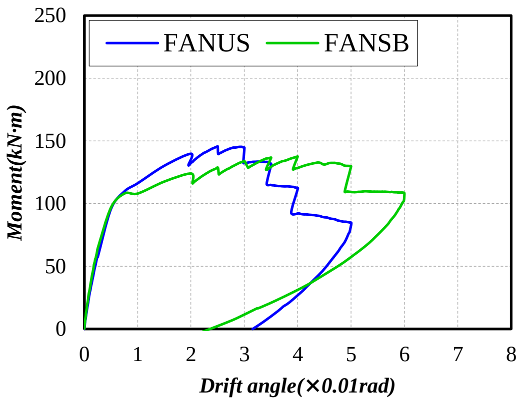

Spiral-confined

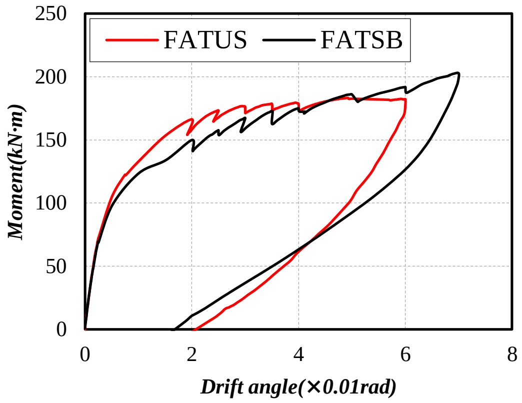

tube-confined

(a) Effect of the type of rebar

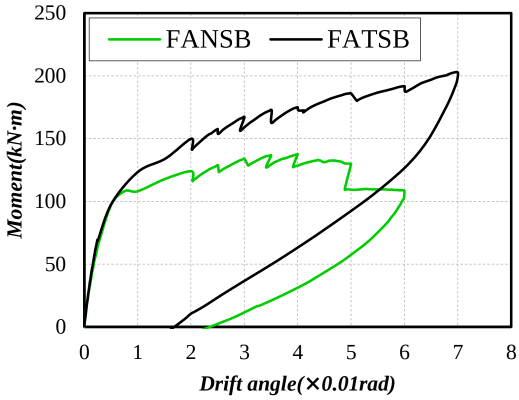

SBPDN rebars

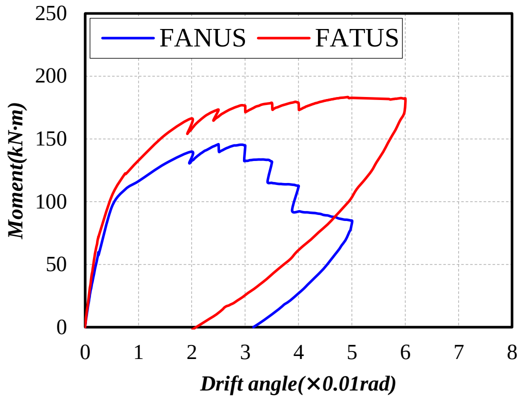

USD 685 rebars

(b) Effect of confinement method

Fig. 2- 12 Effects of main structural factors

As one can see from Fig.2-11, once USD 685 rebars yielded, the lateral resistance by them do not increased further along with strain or drift and tends to maintain at a certain level. From the strain or drift where USD 685 rebars commences yielding on, the P-delta effect, the softening feature of high-strength concrete as well as the spalling-off of cover concrete all contribute to the degradation in the lateral resistance. If the lateral resistance by longitudinal rebars cannot increase any further due to yielding to cover the degradation due to above-mentioned factors, the resilience will be terminated at that drift or strain level. In other words, delaying the yielding of longitudinal rebars is the top priority to ensure sufficient resilience to concrete members.

To better see effects of the type of high-strength longitudinal rebar and the confinement method on overall seismic performance of LQFA concrete columns, the envelope curves in the push direction are compared in Fig.2-12 in form of base moment M versus drift angle R relationships. Moments shown in Fig.2-12 include the moment by lateral force and the P-Δ moment. In addition, the lateral forces measured at each specified drift angle are shown in Table 2-5 for all specimens.

Table 2 - 5 Lateral forces measured at specified drift angle R (×0.01 rad)

Specimen	$V_{exp}(kN)$											
	R=0.25	R=0.5	R=0.75	R=1	R=1.5	R=2	R=2.5	R=3	R=3.5	R=4	R=5	R=6
FANSB	125	187	206	204	206	223	226	230	229	226	199	150
FATSB	134	196	221	235	250	276	285	298	299	302	313	322
FANUS	116	186	210	220	242	256	261	253	220	180	120	-
FATUS	140	203	234	245	288	309	316	318	315	309	305	292

From Fig.2-12 and Table 2-5, the following observations can be made: 1) the type of high-strength longitudinal rebars did not influence the M-R curves of LQFA concrete columns with same concrete strength and steel amount were identical until R=0.0075 rad and 0.005rad when confined by spirals and steel plates, respectively; 2) the higher the bond strength of rebar, the larger the lateral resistance until R=0.03rad or 0.04 rad where high-strength rebar began yielding; 3) confinement by steel plates could greatly enhance lateral resistance at large drift, and hence lead to much larger resilience than confinement by spirals.

2.3.3 Strains measured in steel bars and steel plates

To investigate the reason for the stable increment in the lateral resistance at large drift of the specimens reinforced by ultra-high strength SBPDN 1275/1420 rebars, Fig.2-13 plots strains of longitudinal rebars measured at the section 25mm away from the column bottom. In Fig.2-13, the blue lines and red lines represent the strain at initially tensile and compressive side, respectively. The black dotted line expressed the yield strain of the longitudinal bars.

The strains of SBPDN rebars increased at the same rate as the strains of USD rebars until R=0.0075rad, but the increment rate became less than that of USD rebars after R=0.0075rad, which implies that the SBPDN rebars began to slip from that deformation level. The SBPDN rebars didn’t reach its yield strain in tension till R=0.05rad for specimen FATSB. The SBPDN bars in specimen FANSB reached its yield strain in compression at R=0.04rad, because of the severe spalling-off of the concrete shell. The stable increase in tensile strain contributed to the stable increase in lateral resistance of column till large deformation. For the specimens with USD rebars, however, the tensile strains reached its yield strain at about R=0.03rad, and from then on the lateral resistance commenced degrading.

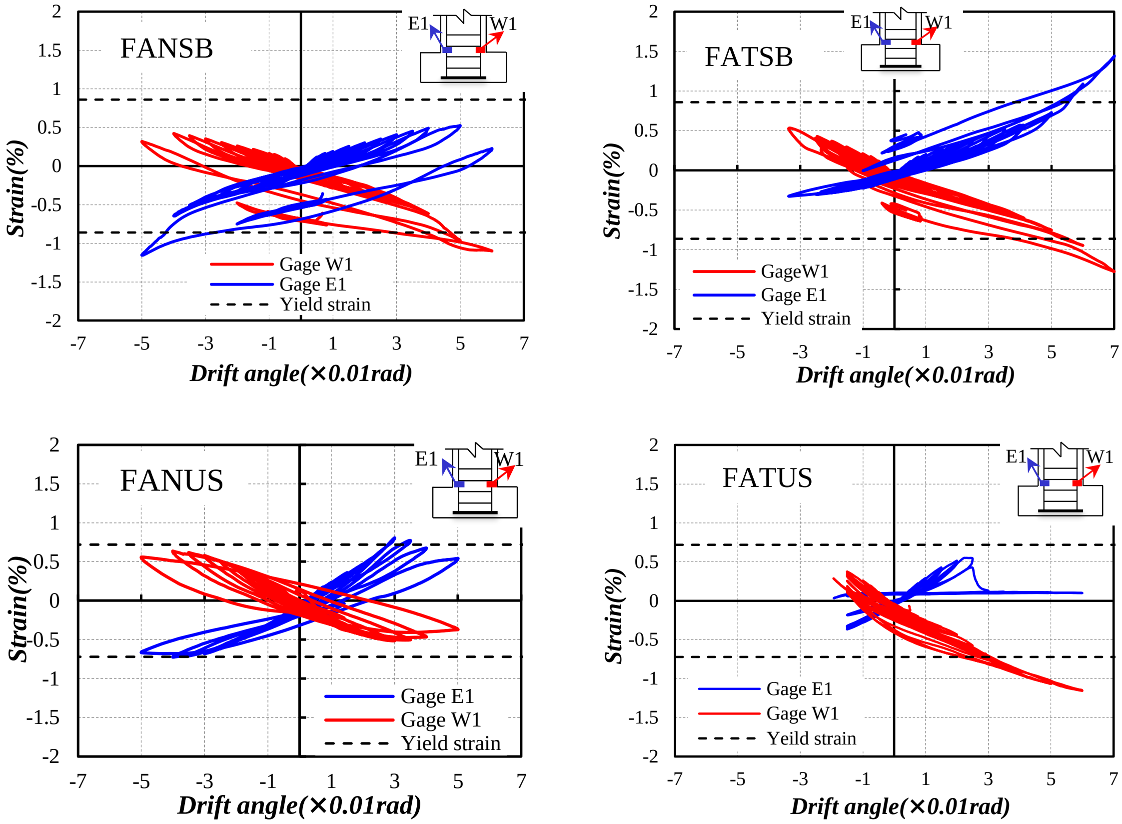

Fig.2- 13 Measured strains of longitudinal rebars

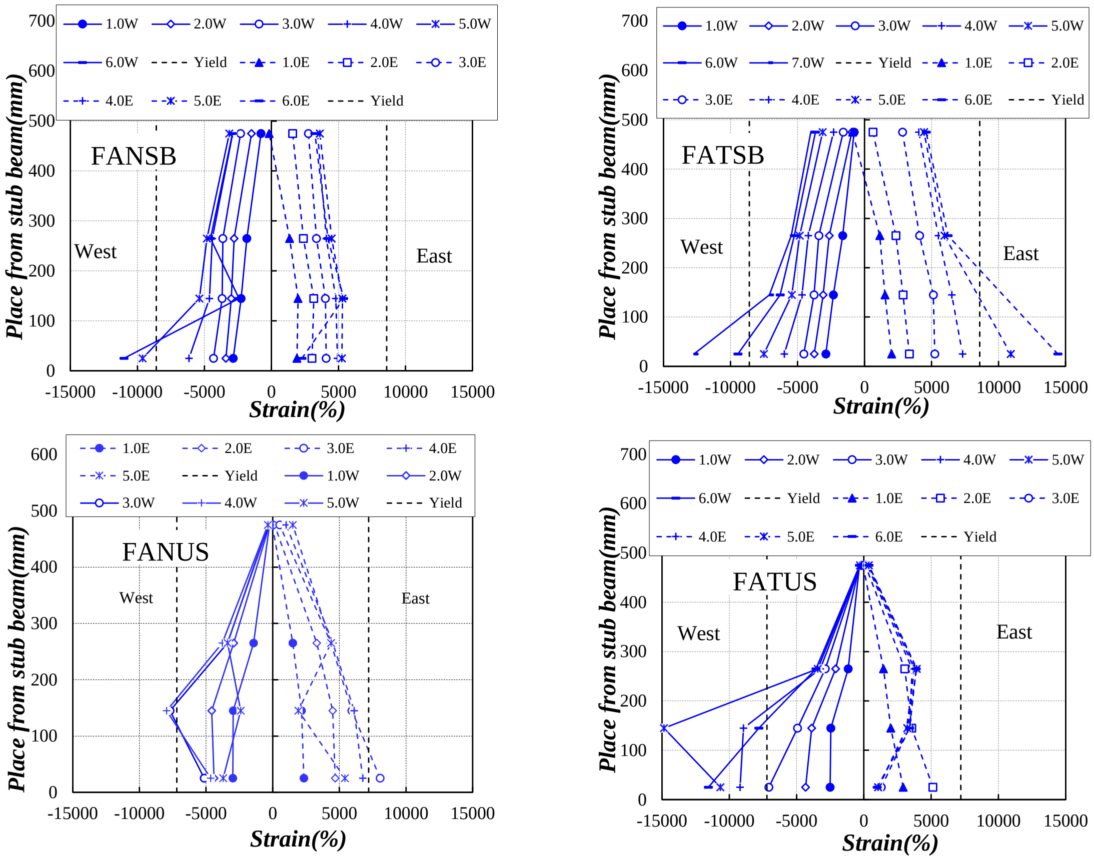

Fig.2- 14 Strain profiles of longitudinal rebar along column height

Fig.2-14 shows strain profiles of longitudinal rebars along the column height measured at specific drift angles. The vertical dotted lines superimposed in Fig.2-14 represent the yield strains. As one can see from Fig.2-14, the strains of USD 685 rebars tended to concentrate within the end region of about 1.0D (D = diameter of column section), while those of SBPDN rebars distributed approximately constant along column height. Low bond strength of SBPDN rebar allowed for the axial strain to be transmitted from the critical region of column to the adjacent region where longitudinal rebars have been conventionally assumed remaining in elastic region. It is this transmission of steel strain that delays the yielding of SBPDN rebars and enables the lateral resistance by SBPDN rebars to keep increasing along with deformation until they yielded.

The circumferential strains of measured at initial compressive side (flange) of spirals and the circumferential and vertical strains on the surface of steel plates are shown in Fig.2-15 and Fig.2-16, respectively, with horizontal line expressing the yield strain of the steels.

Comparing measured circumferential strains of specimens FANSB and FANUS, confined by spirals, one can see that the strains of spirals in specimen FANSB exhibited much slower increment rate along with drift than those in specimen FANUS, and reached yield strain at R=0.03rad. For the two specimens confined by steel plates, FATSB and FATUS, the strains measured at the sections 145mm and 265mm away from column base of specimen FATSB showed larger values at large drift than those measured in specimen FATUS. Transmission of axial strain along column axis in SBPDN rebar avoided concentration of steel strain in the vicinity of column base, distributing strain or deformation of steel to a wider region, which consequently made the concrete in the widened region sustain higher axial stress, resulting in larger circumferential strain in spirals confining the concrete.

The vertical and transverse strains shown in Fig.2-16 were measured at the initial compressive side of column sections 16mm, 141mm and 271mm away from the column base.

From Fig.2-16, one can see that vertical strains were much smaller than circumferential or transverse strains. The vertical strains measured at the bottom end of steel plates exhibited small values till the end of testing, which implies that the steel plates sustain little, if any, axial stress as expected. The largest transverse strains were measured at the top end of steel plates in both specimens, but the absolute vertical strain to transverse strain ratios at each specific drift were about 3.0, which means that the steel plates still provided as little resistance to the axial stress as can be ignored.

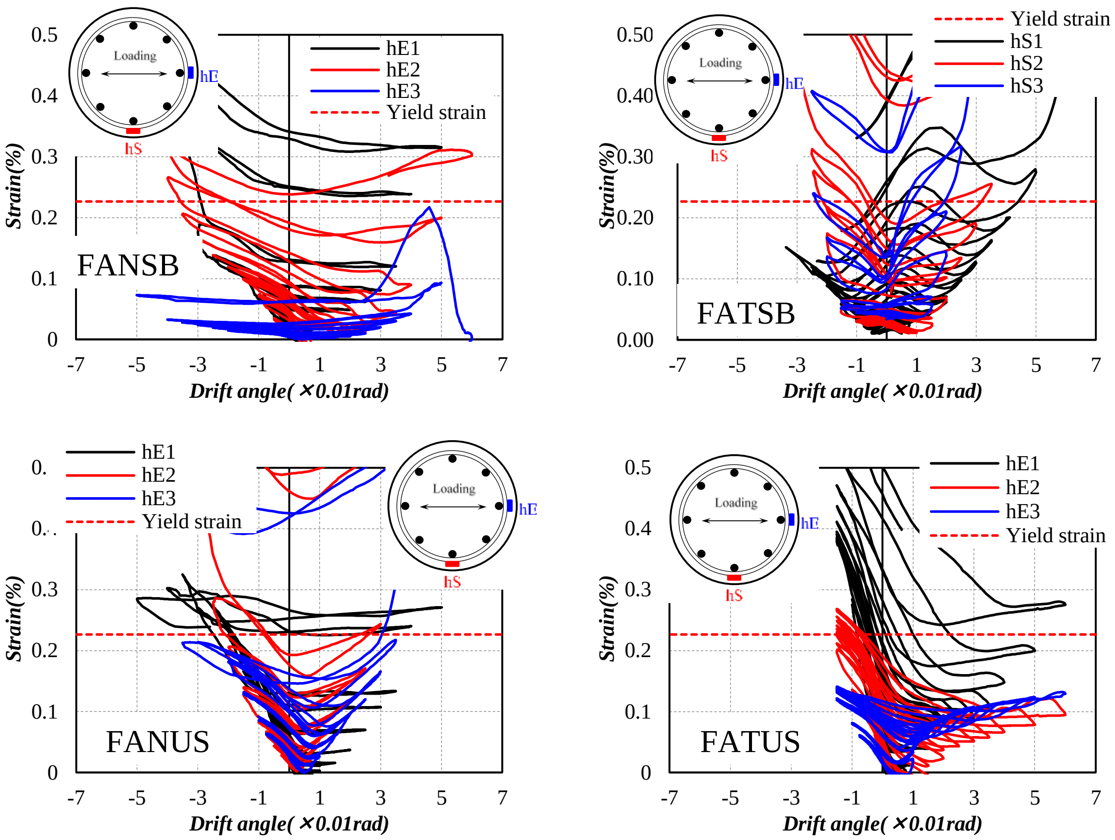

Fig. 2- 15 Circumferential strains of spirals

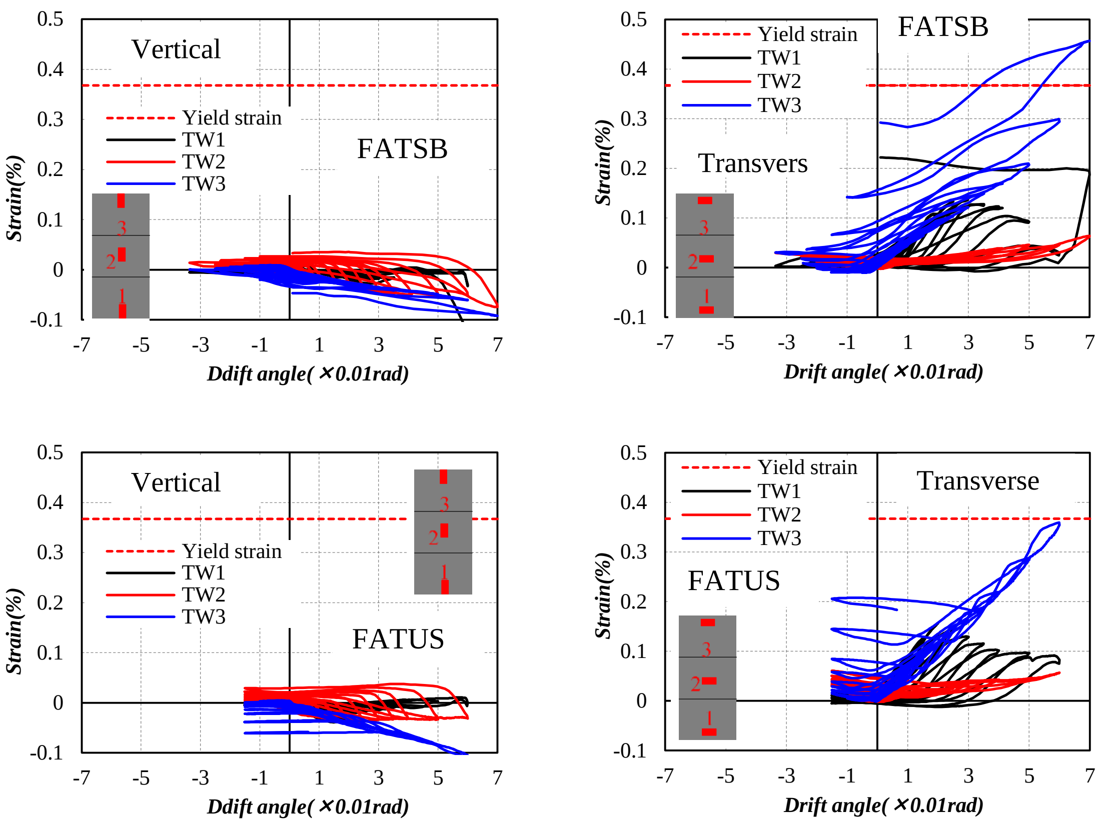

Fig.2- 16 Strains of steel plates

2.3.4 Axial compression load

The relationships between axial compression load and drift angle are shown in Fig.2-17. The total axial compression load consisted of two parts, one of which was provided by vertical hydraulic jack and the other was provided by the post-tensioned PC bar. The latter is obtained by using the measured strains of four gages locating at bottom and up ends of the PC bar.

As can be seen from the figure, the axial deformations of specimens confined only by spirals quickly decreased due to shear failure and spalling of massive cover concrete from drift angle R = 0.04rad and 0.035rad, respectively, for specimen FANSB and FANUS whose failure modes were shear failure. As shown in Fig. 2-18, the axial deformations of these two test columns abruptly increased in shortening after shear failure occurred. This shortening led to the loss of axial load provided by the PC bar. If total axial compression were applied through vertical hydraulic jack, these two specimens might exhibited more brittle response after R=0.04 rad and 0.035rad, respectively, than those shown in Fig. 2-11. On the contrary, the axial deformations of specimen FATSB and specimen FATUS confined by steel plates kept a constant value until the test was end.

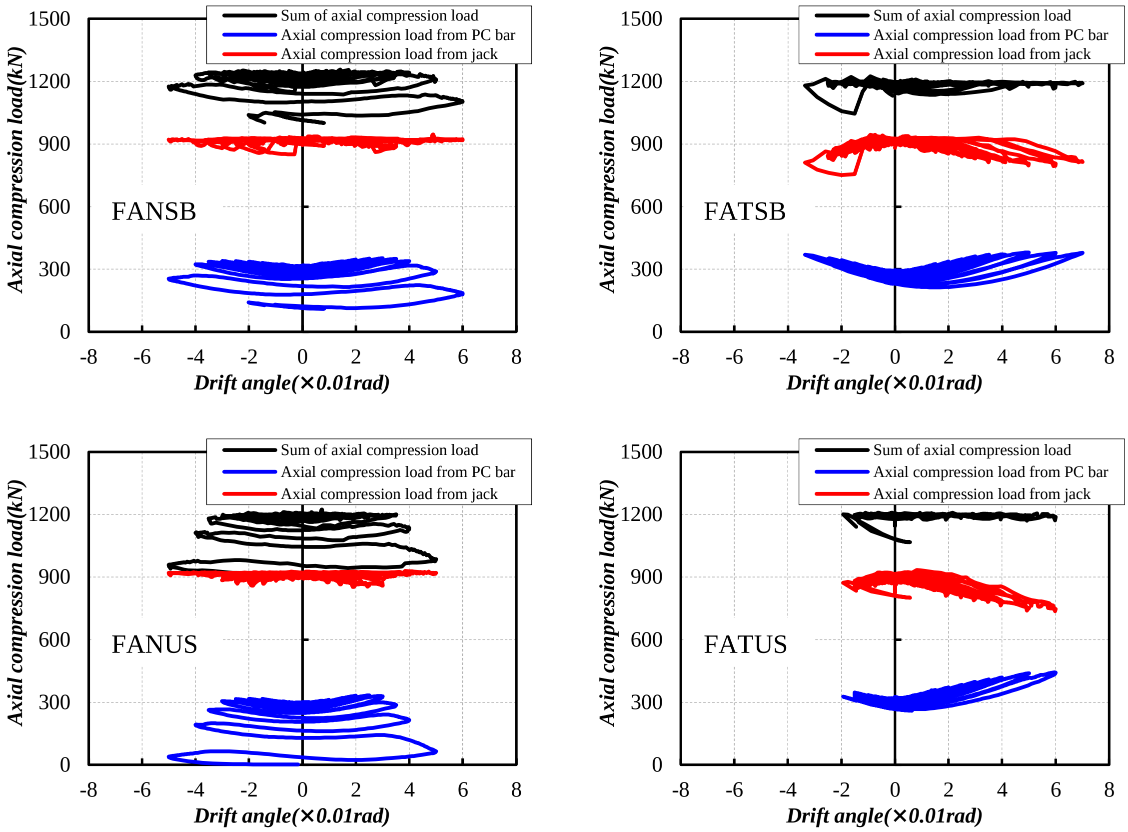

Fig.2- 17 The variation of axial compression load of test columns

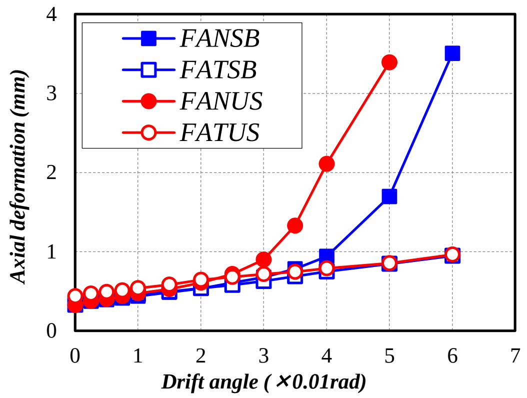

Fig. 2- 18 Axial deformation of test columns

2.3.5 Residual deformations

Residual drift angle has been widely accepted as one of the important indicator for the reparability of concrete components and structures [2.3], and hence will be an important index measuring resilience of LQFA concrete columns. Fig.2-19 shows the measured residual drift angles corresponding to each specific drift level of all specimens. The experimental results shown in Fig.2-19 represent the average of residual drift angles measured in both directions.

No significant difference was observed in the measured residual drift among the specimens with SBPDN rebars and USD 685 rebars until R=0.025rad. From that drift angle on, the residual drift angles of the specimens with USD 685 rebars gradually became larger than those of specimens with SBPDN rebars. Since the USD 685 rebars commenced yielding at R=0.025 rad, it can be said that the yielding of longitudinal rebar triggered the progress of residual drift angle. For specimen FANSB, high bond strength of USD 685 rebar led high stress to the concrete surrounding rebars and made the cover concrete more seriously spalled off along with drift level. This specimen failed in shear at R=0.04 rad, resulting in abrupt increase of the residual drift. Abrupt increase of residual drift angles in specimens with SBPDN rebars was not observed until R exceeded 0.04 rad.

As to the effect of confinement method on the mitigation of residual deformation, one can see from Fig.2-19 that partial confinement of critical regions of columns by steel plates could reduce residual drift of circular LQFA concrete columns, in particular at large drift level. Steel plates constrained all concrete within critical regions and prevented it from spalling off at high compressive strain, and contributing to the mitigation of residual deformation of columns even under relative high axial compression.

Another important observation can also be made from Fig.2-19 about the reparability of LQFA concrete columns reinforced by SBPDN rebars. The use of fly ash in large quantities did lead to high compressive strength of concrete and reduce deformability of it, utilization of the SBPDN bar as longitudinal rebars, however, was apparently effective not only in ensuring stable increase in lateral resistance to LQFA concrete columns, but also in mitigating residual deformation. For the specimens with SBPDN rebars, spiral-confined or steel plate-confined, their residual drift angles corresponding to the peak drift of 0.04 rad were about 0.005 rad. Since the value of 0.005 rad means that the non-reparability probability of the columns is close to zero [2-3], very high reparability of LQFA concrete columns is obvious after experiencing drift twice of the ultimate drift at life safety state.

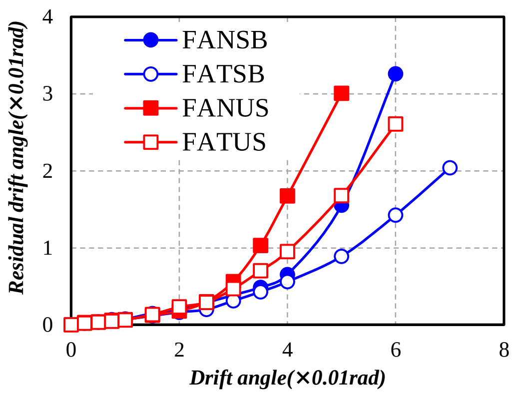

Fig.2- 19 Residual drift angle of specimens

2.3.6 Energy dissipation feature

To understand energy dissipation feature of LQFA concrete columns, equivalent viscous damping coefficient *heq* defined as in Fig.2-20 [2.4], was calculated and compared in Fig.2-21 for all test columns.

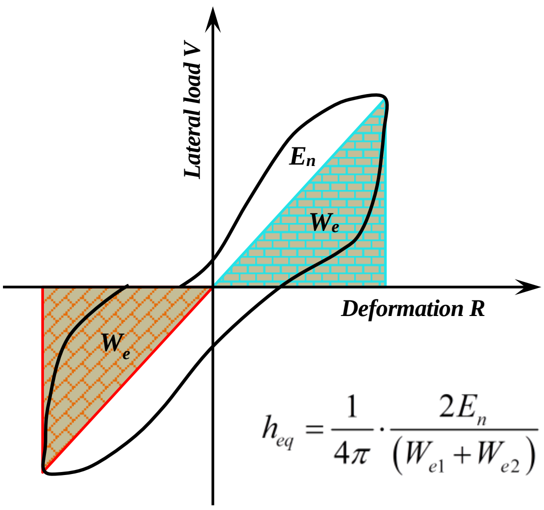

Fig.2- 20 Definition of equivalent viscous damping factor [2.4]

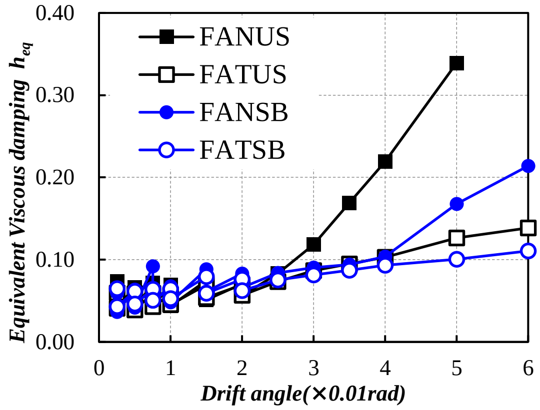

Fig.2- 21 Equivalent viscous damping ratios of LQFA cantilever columns

The experimental results shown in Fig.2-21 indicate that the equivalent viscous damping factors remained approximately constant up to R=0.025 rad., which implies that LQFA concrete columns behaved in a approximately nonlinear elastic manner up to this drift level. In particular, the measured *heq* of specimens with SBPDN rebars maintained slow increase along with drift.

As compared with *heq* of conventional ductile concrete members, the *heq* of concrete columns with high-strength rebars, SBPDN or USD 685, is much small. Considering the fact that higher *heq* means more severe damage, the small *heq* means that LQFA concrete columns with SBPDN rebars is not intended to dissipate energy induced by earthquakes, but to build a robust and resilient skeleton of frame structures, which are expected to be reopened as soon as possible after strong earthquakes. Although resilient concrete structure don't mainly carry the duty to dissipate energy from earthquake, it's still need to evaluate the energy dissipation capacity because it will be the important index to design dampers which will dissipate the most energy in the resilient structure.

2.4 CONCLUSIONS

Four circular concrete cantilever columns were tested to investigate effects of combination of a large quantity of fine fly-ash, ultra-high-strength rebar with low bond strength, and confinement by thin steel plates, on seismic behavior of concrete columns under single-curvature deformation. From the experimental results described in this chapter, the following conclusion can be drawn.

(1) Combination of a large quantity of fine fly-ash, ultra-high-strength rebar with low bond strength, and confinement by thin steel plates is a simple but effective method to create

robust and resilient concrete components. The circular LQFA concrete cantilever columns with SBPDN rebars and under axial compression with axial load ratio of 0.33 showed higher resilience than the columns with USD 685 rebars.

(2) While high compressive strength of concrete due to high fly ash replacement level of 455kg/m^3 reduced deformability or stability of LQFA concrete columns, utilization of SBPDN rebars as longitudinal rebars and proper confinement by spirals could ensure stable increment of lateral resistance up to the drift level of 0.04 rad. Confinement by steel plates in lieu of spirals could further enhance that drift level up to 0.05rad.

(3) Utilization of USD 685 rebars could ensure LQFA concrete columns stable response and higher early lateral resistance until R=0.025 rad. The high bond-strength of USD rebar, however, tended to cause yielding of it earlier than SBPDN rebar, resulting in degradation of lateral resistance of the columns after R=0.025 rad. Even the confinement by steel plates could not enhance this critical drift level.

(4) Residual drift angle, a well-known and adopted indicator for the reparability of concrete components, was primarily dependent upon if the longitudinal rebars yielded. Confinement method exhibited little influence on the residual drift angle. Once longitudinal rebars commenced yielding, tensile or compressive, the residual drift would increase at a much higher rate than that before the yielding, which implies that delay of the yielding of longitudinal rebar is crucial to the resilience of concrete members.

REFERENCES

[2.1] Funato, Y., Sun, Y. P., Takeuchi, T., Cai, G. C., "Modeling and Application of Bond Characteristic of High-strength Reinforcing Bar with Spiral Grooves," Proceedings of the Japan Concrete Institute, V.34, No.2, 2012, pp.157-162.

[2.2] Cai, G. C., "Seismic Performance and Evaluation of Resilient Circular Concrete Columns," Doctoral dissertation, Kobe University, 2014.

[2.3] Japan Road Association (JRA-1996), "Design Specifications of Highway Bridges, Part Ⅲ Concrete Bridge, Part Ⅴ Seismic Design," Japan Road Association, Tokyo, 1996.

[2.4] Jacobsen L. S., "Damping of Composite Structures," Proceedings of 2nd world conference on earthquake engineering, No.2, 1960, pp.1029-1044.

Chapter 3

Seismic Behavior of Circular LQFA Concrete Beam-Columns Reinforced by SBPDN bars and Steel-Plates

3.1 INTRODUCTION

In addition to the strong column-weak beam mechanism, another lateral resistance mechanism for frame structures is the weak column-strong beam mechanism, which has been taken as undesirable one among structural engineer community for the last fifty years. As shown in Fig.3-1, weak column-strong beam mechanism has been often observed at the lowest story of concrete buildings designed by pre-1982 code [3-1], and usually causes too large residual deformation for the damaged buildings not to be repaired, even if they can survive a strong earthquake. On the other hand, if the columns at the lowest story are assigned sufficient resilience or self-centering feature, they can return buildings to original position and promote recovery and re-occupancy after earthquakes.

Based on the test results described in chapter two, combination of LQFA concrete, SBPDN rebars and confinement by steel plates can be presumed to be suitable for the development of resilient columns located at the lowest story and deformed in double curvature. The column under double curvature deformation will be referred to as beam-column hereafter. Objectives of this chapter are listed below:

Fig.3- 1 Damage to the Olive View Hospital in the 1971 San Fernando earthquake (Steinbrugge K. V., NISEE Database) [3-2]

(1) To experimentally verify robustness and resilience of circular LQFA concrete beam-columns with SBPDN rebars and confined by steel plates.

(2) To investigate influence of the method to unite steel plates on the seismic properties of circular LQFA concrete beam-columns.

(3) To study effect of anchoring details of longitudinal SBPDN rebars at the contra-flexure portion of column on the seismic performance of circular LQFA concrete beam-columns.

(4) To clarify if the anchorage length of SNPDN rebars within the beam and column joint affects overall performance of circular LQFA concrete beam-columns.

3.2 EXPERIMENTAL PROGRAM

3.2.1 Description of test columns

In order to achieve the goals aforementioned, four 1/3 scale circular column specimens simulating columns in weak column-strong beam mechanism were fabricated and tested under combined constant axial compression and reversed cyclic lateral load. All specimens had diameter of 250mm and shear span of 500mm. Outlines of specimens are given in Table 3-1, and reinforcement details and dimensions of specimens are illustrated in Fig.3-2.

Experimental variables were uniting method of steel plates, anchorage details of SBPDN rebars at the middle of column and anchorage length of SBPDN rebars within loading stubs. Two types of connecting methods were adopted to unite steel plates into circular steel tube to confine test columns. According to the uniting method, the steel tubes formed are referred to as “bolted tube” and “welded tube”, respectively, hereafter.

Table 3 - 1 Outlines of test columns

Specimen	f'_c (N/mm^2)	*a/D*	*n*	Steel plate *t* (mm)	Steel plate *D/t*	Steel plate uniting method	Tie plate	Anchorage length (mm)
CFABY26	70	2	0.33	1.6	156	Bolt	Yes	260
CFAWY26						Weld	Yes	260
CFABN26						Bolt	No	260
CFABY13						Bolt	Yes	130

Note: f'_c: target concrete strength; *a/D*: shear span ratio; *n*: axial load ratio; *t*: the thickness of steel plate; *D*: the diameter of column section.

The bolted tube was made by at first bending flat steel plates into semicircular shape with wing of 30mm in width, and then connecting two pieces of the semicircular plates through bolts and nuts along the column height (See Fig.3-2). The welded tube was formed by welding two pieces of the semicircular plates together.

Of the four specimens, three were confined by bolted tube and one was confined by welded tube to verify if the bolted tube could provide the same confinement effect to concrete as the welded tube. Thickness of the steel plates was 1.6 mm to give a diameter-to-thickness (D/t) ratio of 156 to steel tubes. Circular hoops having spacing of 90 mm were adopted just to keep longitudinal SBPDN rebars in location. Clearances of 6 mm were provided between tube ends and faces of loading stubs in order for the tubes to only provide lateral confinement to concrete rather than directly sustain the axial stresses induced by bending and axial load.

Longitudinal steel in each specimen consisted of eight ultra-high strength SBPDN rebars with nominal diameter of 12.6 mm. These SBPDN rebars were placed uniformly around the perimeter of column section with cover concrete of 30 mm. Each SBPDN rebar was connected via an internally threaded pipe at the middle of column height as shown in Fig. 3-2, and both ends of it was further anchored to end steel plates of 6 mm in thickness by nuts to stop the slippage. Since the rebars in a beam-column under seismic loading will be pushed at one end but pulled at the other end simultaneously, they tend to slip mostly in the vicinity of contra-flexure section. To avoid negative effect of this slippage, for specimens CFABY26, CFAWY26 and CFABY13, each SBPDN rebar was also tied to a steel tie plate by nuts at the middle of column to prevent the slippage of SBPDN rebar at the contra-flexure section. No steel tie plate was adopted in specimen CFABN26 to investigate necessity of the tie plate at the middle of column.

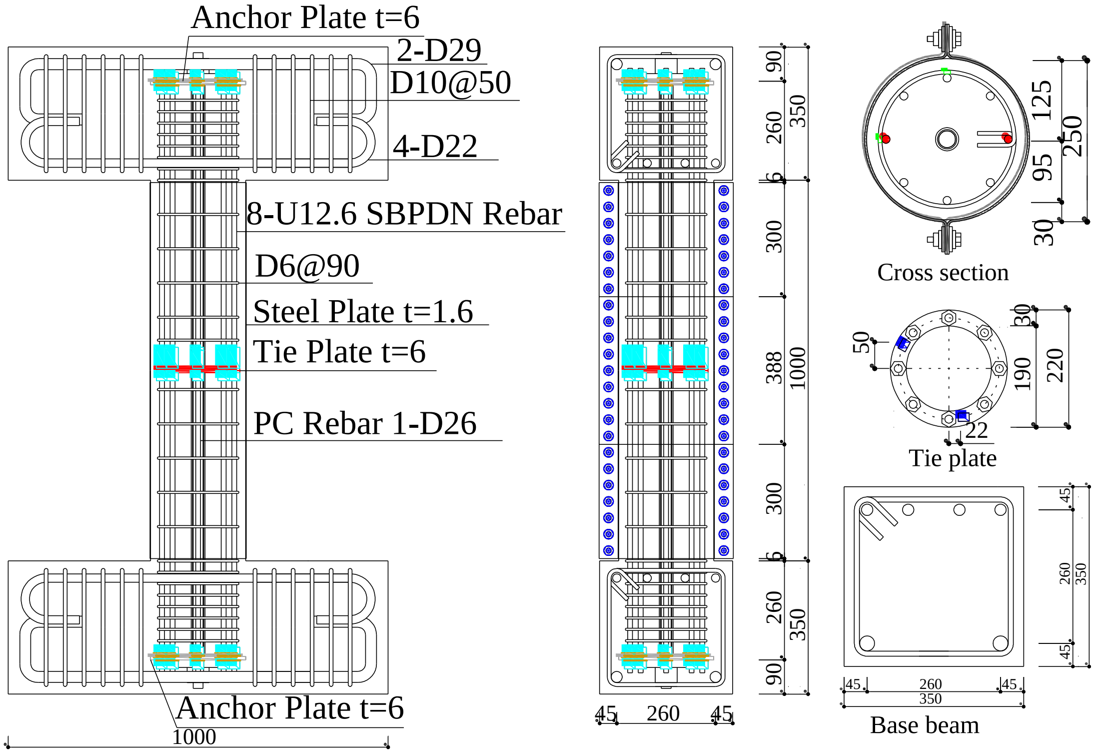

(a) Test beam-column CFABY26

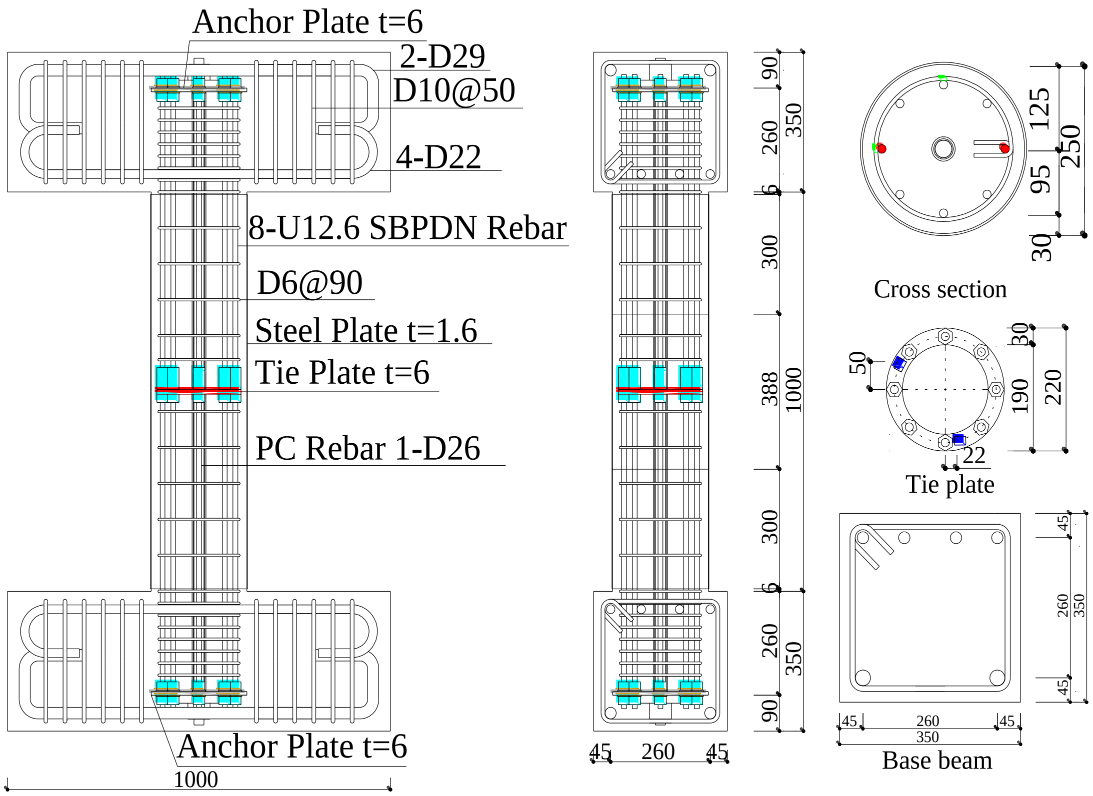

(b) Test beam-column CFAWY26

Fig.3 - 2 Details of test columns (Continued)

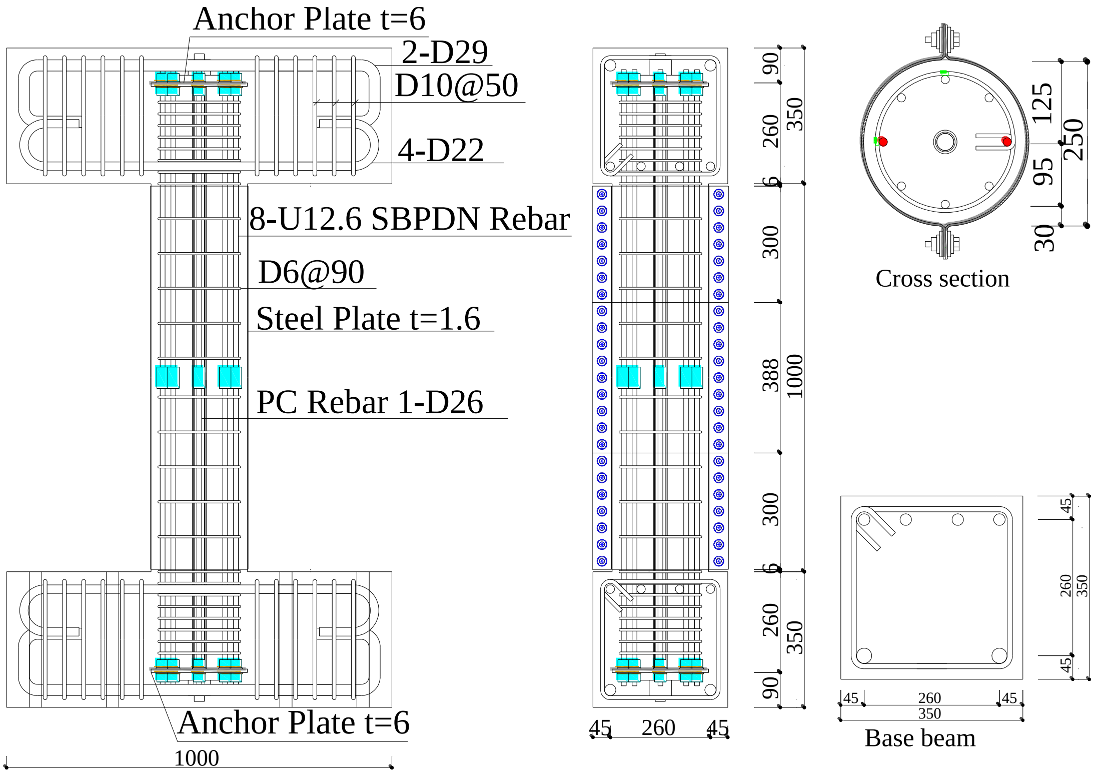

(c) Test beam-column CFABN26

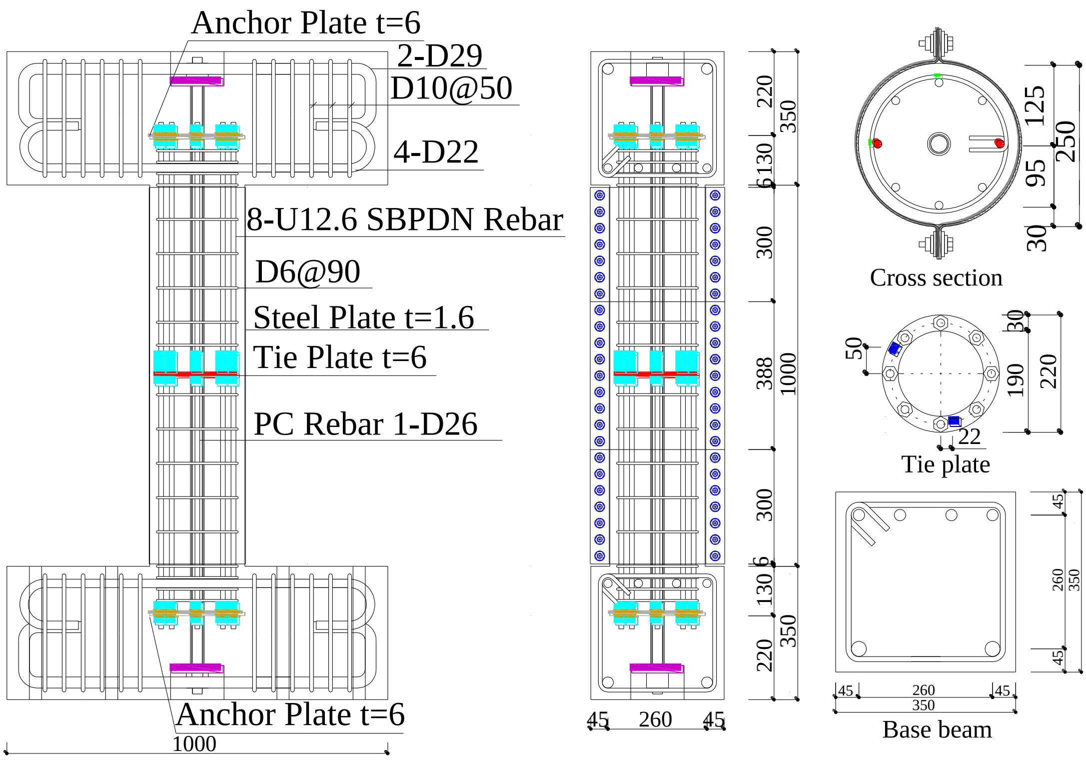

(d) Test beam-column CFAB13

Fig.3 - 2 Details of test columns

Due to the capacity limitation, about 1/3 of the total axial compression was provided via a PC bar. As shown in Fig.3-2, a hole with diameter of 35 mm was provided in the center of column to place the PC bar whose diameter was 26 mm.

The anchorage length into loading stubs for each SBPDN rebar in specimens CFABY26, CFAWY26 and CFANY26 was 260 mm, while that in specimen CFABY13 was 130 mm. The difference in anchorage length was mainly designed to investigate effect of anchorage length on seismic capacities of the columns.

3.2.2 Material properties

Ready-mix LQFA concrete with targeted compressive strength of 70MPa was used to make the specimens. Table 3-2 shows mix proportion of the LQFA concrete. As one can see from Table 3-2, up to 455kg of fly ash was used to replace fine aggregate in per unit volume of concrete. Normal weight coarse aggregate with a maximum size of 20mm and Portland cement were used in concrete. The specimens were cured in the forms with their tops covered by wet burlaps for four weeks after casting and then were air-cured after removing of forms. The 28-day strength and the actual strength of LQFA concrete at the 35-day before testing are shown in Table 3-2 and Table 3-4 along with primary test results, respectively.

The SBPDN rebar had a yield strength of 1377 MPa and a bond strength of 3.0 N/mm^2. As shown in Table 3-3, the thin steel plate used to confine test columns had a yield strength of 273 MPa, while the yield strength of D6 circular hoop was 394 MPa. The values shown in Table 3-3 represent the average of three standard test coupons.

Table 3 - 2 Mix proportion of concrete

Fly Ash (kg/m^3)	W/C	Water (kg/m^3)	Cement (kg/m^3)	Fine Aggregate		Coarse Aggregate (kg/m^3)	Admixture (kg/m^3)	f_c' (MPa)
				Sand (kg/m^3)	Crushed Sand (kg/m^3)			
455	0.65	185	285	334	146	833	5.92	61

Table 3 - 3 Mechanical properties of the steels

Name	Type	f_y (N/mm^2)	f_u (N/mm^2)	E_s (N/mm^2)	ε_y (%)	*Elongation* (%)
SBPDN bars	SBPDN 1275/1420	1377	1463	215000	0.84**	9.9
PL1.6	SS400	273	522	201000	0.34**	40.0
D6	SD295A	394	522	197000	0.21	26.5

Note: f_y=yield stress; f_u=ultimate stress; E_s= young modulus; ε_y= yield strain; ε_y=0.34%**, ε_y=0.84%** are obtained according to the 0.2% offset method.

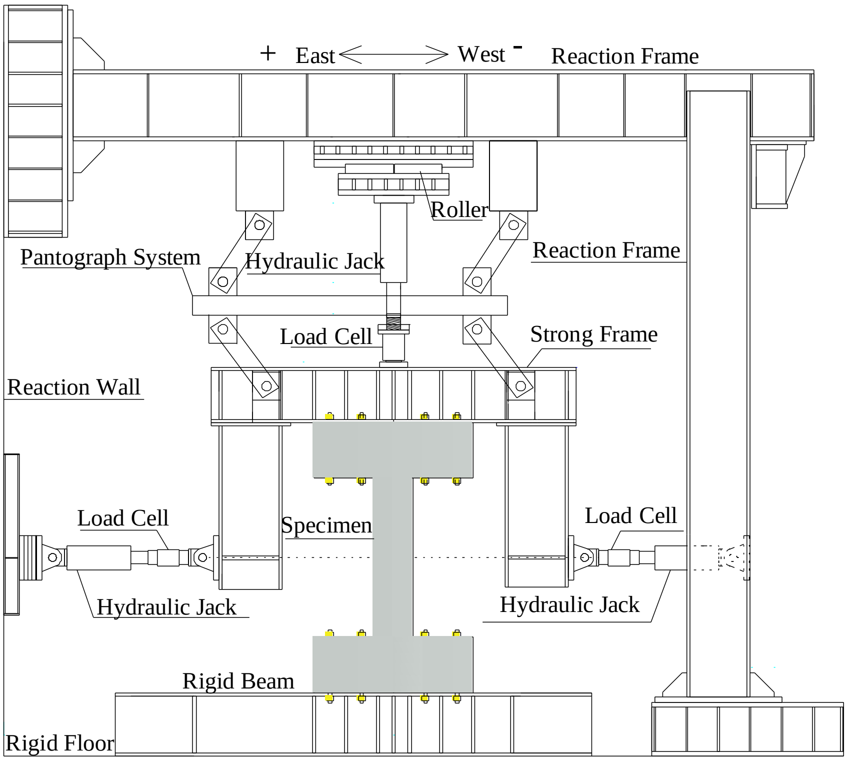

Fig.3 - 3 Schematic view of test setup (unit: mm)

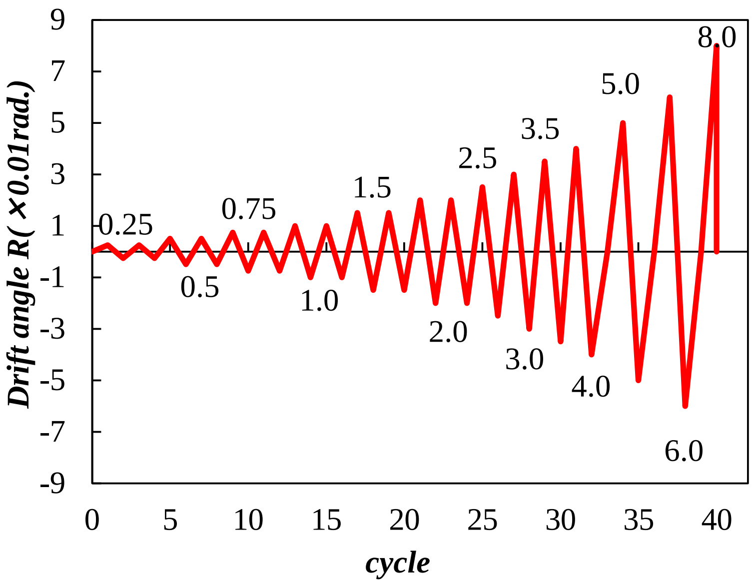

Fig.3 - 4 Loading program

3.2.3 Test setup

The test setup is illustrated in Fig.3-3, which consisted of a steel loading beam assembly. Two hydraulic jacks with capacities of 500 kN in push and 300 kN in pull for reversed cyclic lateral load, and one hydraulic jack with capacity of 1 MN for axial compression. The bottom rigid steel beam was fixed to the reaction floor by post-tensioned PC bars. The 1 MN hydraulic jack was connected to the loading frame via a roller so that the jack could move freely in the horizontal direction.

The reversed cyclic lateral load was controlled by drift angle R that is defined as $R=\Delta/L$, where Δ is the lateral displacement measured by a Linear Variable Differential Transformer (LVDT), and L is the shear span of specimens. Two complete cycles were applied at each targeted drift angle until R reached 0.02rad, and only one cycle was performed at each following drift. The loading program is shown in Fig.3-4.

3.2.4 Instrumentation and measurement

As illustrated in Fig.3-5, in addition to the LVDT for measuring the relative lateral displacement, a total of sixteen displacement transducers (DTs) were used to measure the axial deformation and the slippage of the loading stubs.

Sixteen strain gages were used to measure the strains of SBPDN rebars placed at compressive and tensile sides of column section as shown in Fig.3-6. In addition, eight strain gages were

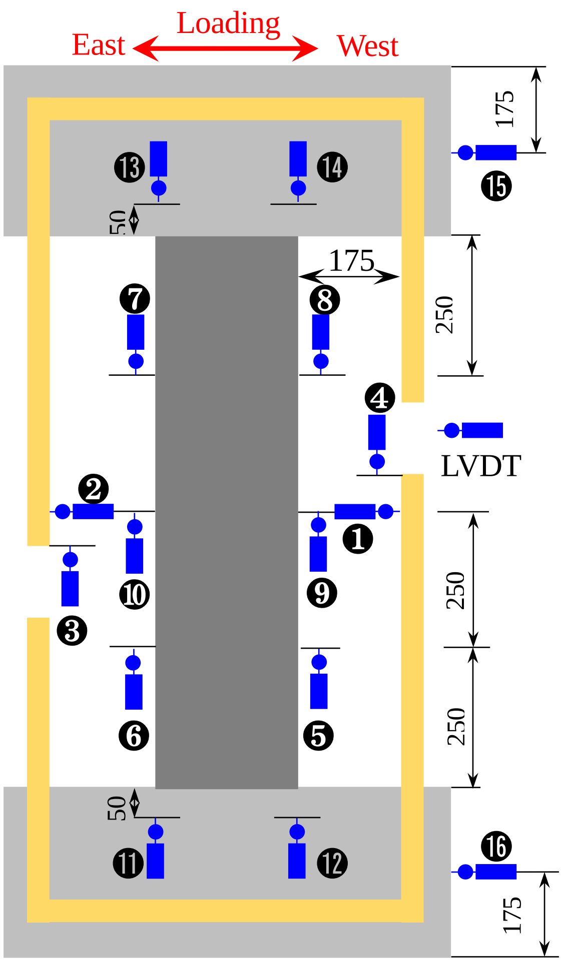

Fig.3 - 5 Locations of LVDT and DTs

used to measure the strains of circular hoops and six bi-axial strain gages were embedded on the compressive and tensile surfaces of steel tubes. Locations of the strain gages are also shown in Fig.3-6.

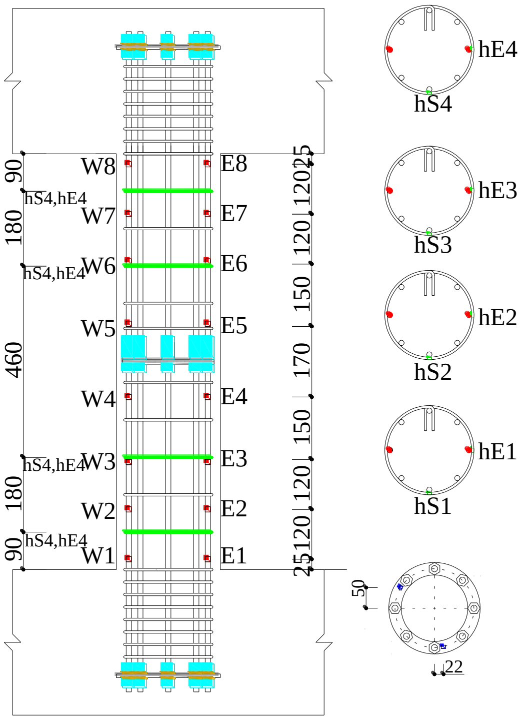

(a) CFABY26

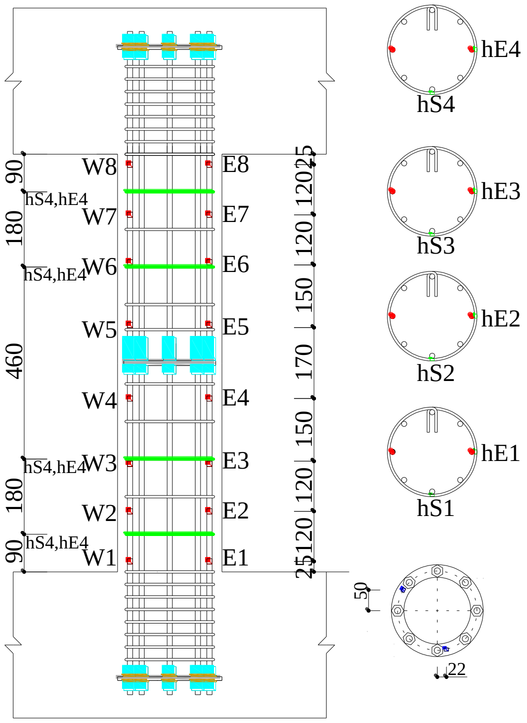

(b) CFAWY26

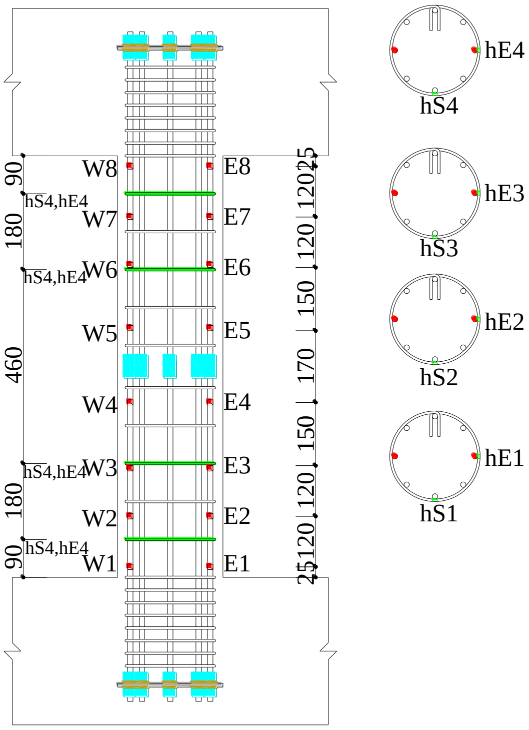

(c) CFABN26

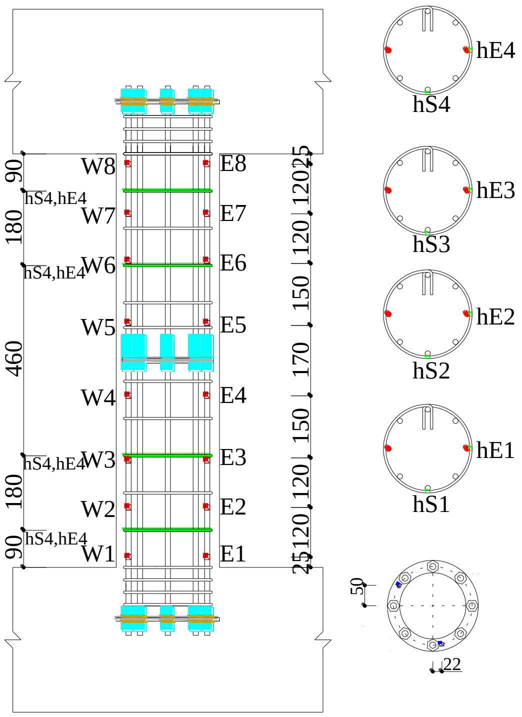

(d) CFABY13

Fig.3 - 6 Locations of strain gages

3.3 TEST RESULTS AND OBSERVATIONS

3.3.1 Observed behavior of the test beam-columns

Fig.3-7 shows crack patterns of all specimens. The crack patterns were observed after testing and removing the steel plates because all specimens were wrapped by steel plates, which hindered observation of cracks during loading. The only exception of cracks was the flexural cracks in the vicinity of top and bottom portions of the test beam-columns.

Flexural crack was observed at the clearance of 6mm between the ends of steel plates and loading stubs in all specimens at R=0.0025rad, while flaking or spalling-off of concrete was at first observed at R=0.01 rad. Lateral expansion of steel plate was clarified when R approached about 0.03 rad. As shown in Fig.3-7, damage in three specimens confined by the bolted tube was effectively mitigated by the steel plate-confinement. However, for specimen CAFWY26, the welding portion near the top end of the welded tube began rupturing at R=0.04 rad. During pushing the specimen to the next drift level, the welding portion completely ruptured when R became close to 0.05 rad, triggering brittle shear failure and loss of the gravity-sustaining capacity. The bolted tubes provided a more secure confinement effect to LQFA concrete than the welded tube, which implies that careful attention must be paid to the welding portion when thin steel plates are intended to confine concrete columns.

3.3.2 Lateral load—drift angle hysteretic responses

The lateral load versus drift angle hysteretic relationships of all specimens are shown in Fig.3-8, in which the white triangles, circles and diamonds represent the testing stages of yielding of SNPDN rebar, maximum load, and yielding of transverse hoops, respectively. Table 3-4 shows primary test results including the measured maximum lateral load V_{exp} and the corresponding drift angle R_{exp}. The values of the measured V_{exp} in Table 3-4 express the average of the maximum lateral loads in push and pull directions.

Table 3 - 4 Primary experimental results of specimens

Specimen	f'_c (N/mm^2)	P (kN)	P_{PC} (kN)	n	Steel plate t (mm)	Steel plate D/t	Steel plate uniting method	V_{exp} (kN)	R_{exp} (0.01rad)
CFABY26	65	1040	263	0.33	1.6	156	Bolted	300	4.97
CFAWY26	70	1178	215	0.34			Welded	312	4.96
CFABN26	65	1050	340	0.33			Bolted	257	3.48
CFABY13	72	1130	320	0.33			Bolted	287	5.00

Note: P: axial load provided by hydraulic jack; P_{pc}: axial load provided by PC bar; n: axial load ratio
V_{exp}: the measured maximum lateral force; R_{exp}: the drift angle at V_{exp}.

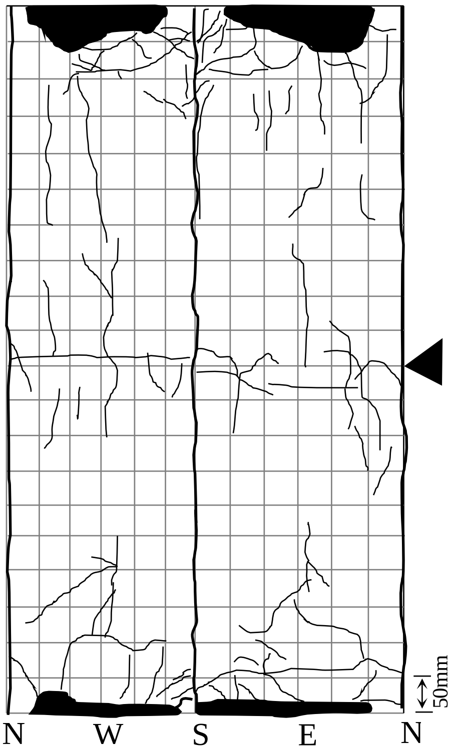

(a) CFABY26

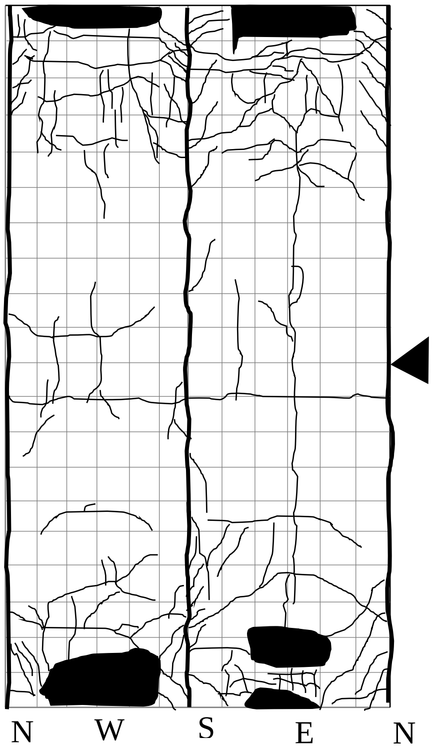

(b) CFABN26

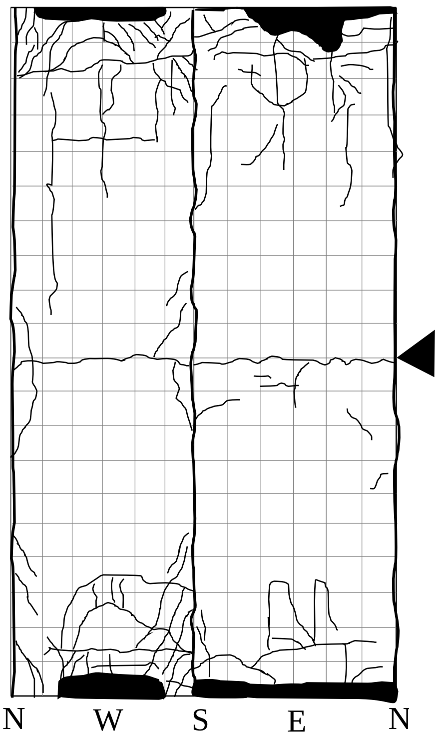

(c) CFABY13

(d) CFAWY26

Fig.3 - 7 Failure patterns of test beam-columns

As apparent from Fig.3-8, the lateral resistances of the specimens with their SBPDN rebars anchored via a tie plate at the middle of column increased stably along with drift until R reached 0.05rad. In these specimens (CFABY26, CFAWT26 and CFABY13), the maximum lateral resistance was measured soon after SBPDN rebars reached the yield strain. On the other hand, specimen CFABN26, whose SBPDN rebars were not anchored to tie plate at the middle of column reached its maximum lateral resistance at R= 0.035rad, and then gradually degraded in lateral resistance with drift level until R reached 0.08rad. The SBPDN rebars did not reach the yield strain till the end of testing, which implies necessity of anchorage of SBPDN rebars at the middle of column to ensure higher resilience to LQFA concrete columns than R=0.035 rad.

To better see effect of experimental variables on seismic behavior of LQFA concrete columns, the envelope curves in the push direction are compared in Fig.3-9. To minimize the P-delta effect, the envelope curves are compared in terms of moment M - drift angle relationships. At first, from Fig.3-9 (a) one can see that the bolted steel tube could provide the same confinement effect to high-strength concrete as the welded tube. The difference between lateral resistances of specimens CAFBY26 and CAFWY26 can be attributed to the difference of concrete strengths. Since the tubed steel tube may rupture at the welding portion at large drift, the uniting steel plates by bolts and nuts can be a good alternative to provide sufficient and secure confinement to brittle high-strength concrete.

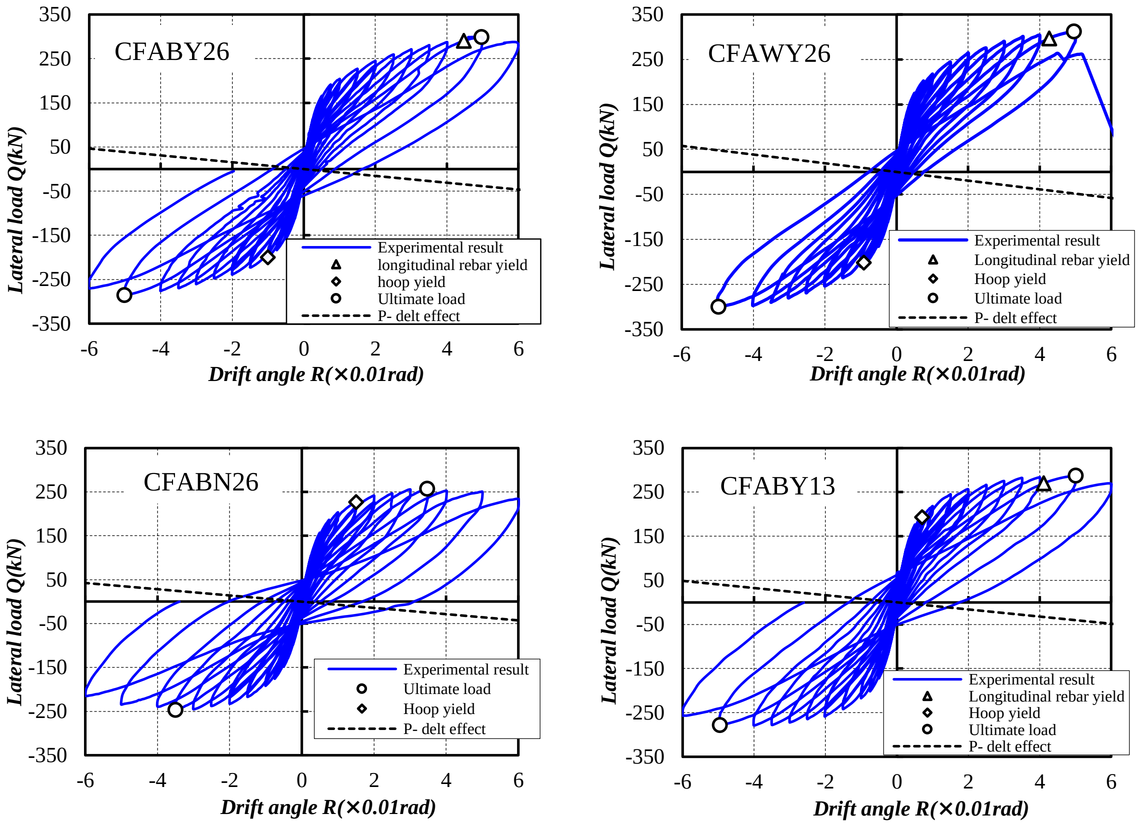

Fig.3 - 8 Lateral load – drift angle relationships of specimens

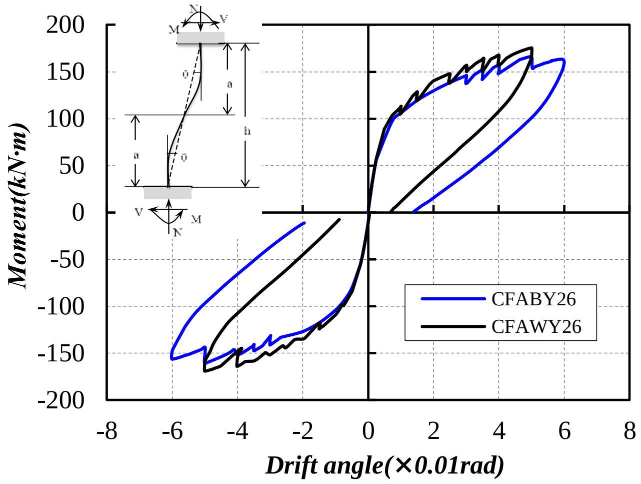

(a) Effect of uniting method of steel plates

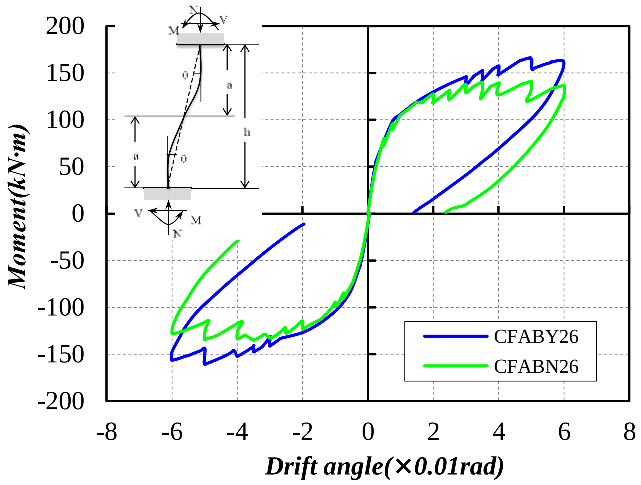

(b) Effect of anchorage detail of SBPDN at middle of column

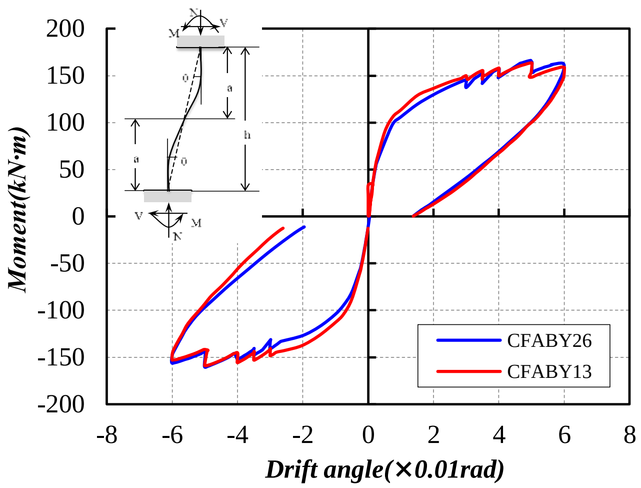

(c) Effect of anchorage length within loading stub

Fig.3 - 9 Effects of experimental variables on seismic behavior of specimens

Necessity of anchorage by tie plate for SBPDN rebars near the contra-flexure section of column can be obviously observed from the comparison shown in Fig.3-9 (b). The lateral resistance of specimen CFABN26 stopped stably increasing at R=0.035rad. Slippage of SBPDN rebars near the contra-flexure portion prevented the steel strain from further increasing and hindered SBPDN rebars in sustaining higher lateral force.

As to the effect of anchorage length within loading stub, one can see from Fig.3-9 (c) that the shorter anchorage length did not induce negative influence on the seismic performance of LQFA concrete columns.

3.3.3 Measured strains of SBPDN rebars

Fig.3-10 shows strains of SBPDN rebars for all specimens measured at the section 20mm away from the column bottom. The blue lines and red lines represent the strain at initially tensile and compressive side, respectively. The dotted horizontal lines express the yield strain of SBPDN rebar.

As shown in Fig.3-10, the strains of longitudinal SBPDN rebars of three specimens with tie plate at the middle of column height stably increased along with drift angle, and reached the yield strain when drift angle R approached 0.05rad. The measured strains of SBPDN rebars in specimens CFABN26 also exhibited stable increase until R=0.04 rad. However, increment of the steel strains slowed down from that drift level on, and the measured strains did not reach the yield strain until R=0.08 rad. This can be attributed to the commencement of slippage of SBPDN rebars in specimen CFABN26 in which no tie plate was used at the contra-flexure section.

Fig.3-11 plots the strain profile along the column height of SBPDN rebars at several specific drift angles. As one can see from Fig.3-11, the steel strain of SBPDN rebars tended to distribute along the column height rather than concentrated within the limited critical end regions as conventional deformed rebars did. The low bond strength of SBPDN rebar promoted the transmission of strain from the critical end section towards the contra-flexure section. This transmission of steel strain mitigates the progress of the strains of SBPDN rebars at the end sections and delay the yielding of them.

3.3.4 Measured strains of circular hoops

Fig.3-12 shows the strains of transverse hoops 90mm, 270mm, 730mm and 910 mm away from the column bottom section. The horizontal dotted lines represent the yield strain of steel. Detail of the locations of strain gages can be found in Fig.3-6. All measured strains shown in Fig.3-12 express circumferential strains of hoops.

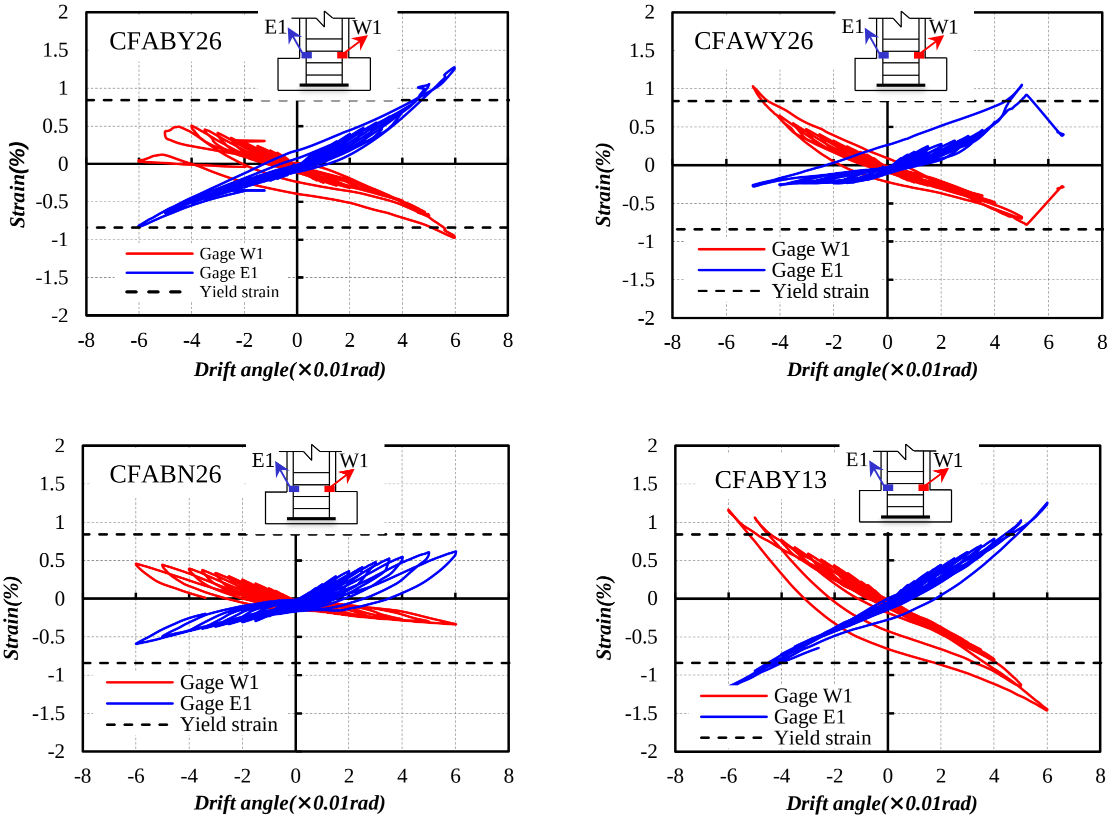

Fig.3 - 10 Measured strains of longitudinal SBPDN rebasr

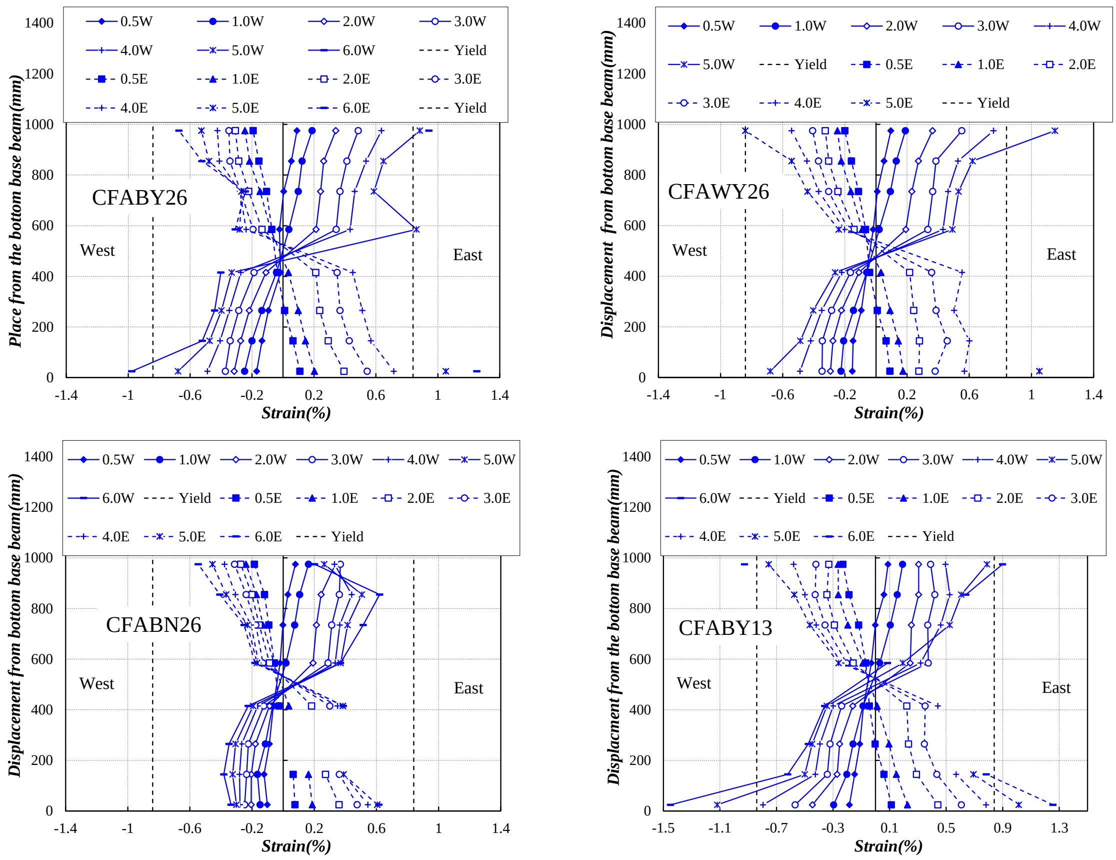

Fig.3 - 11 Strain profiles of SBPDN rebars along column height

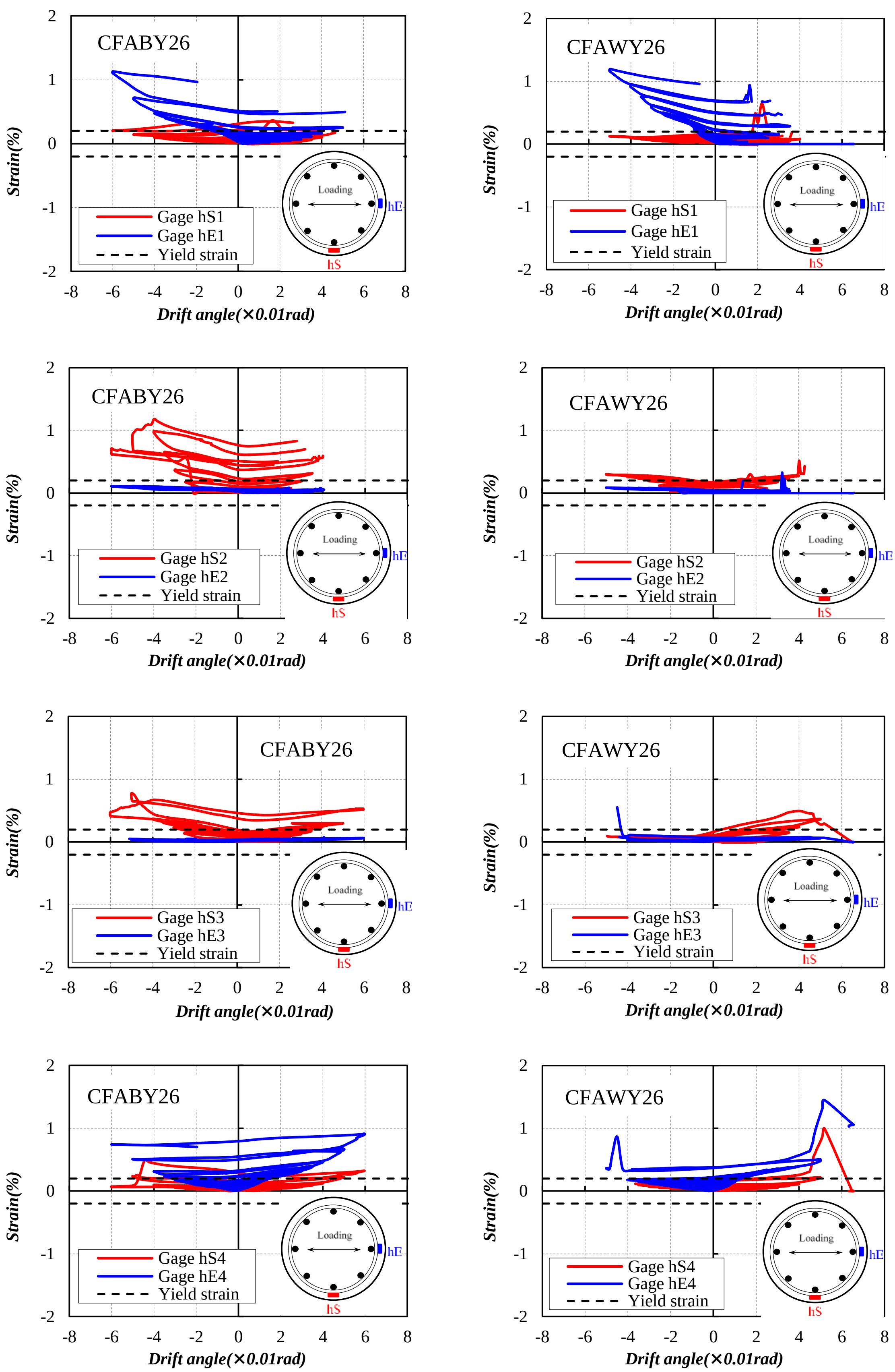

Fig.3-12 Measured strains of hoops (Continued)

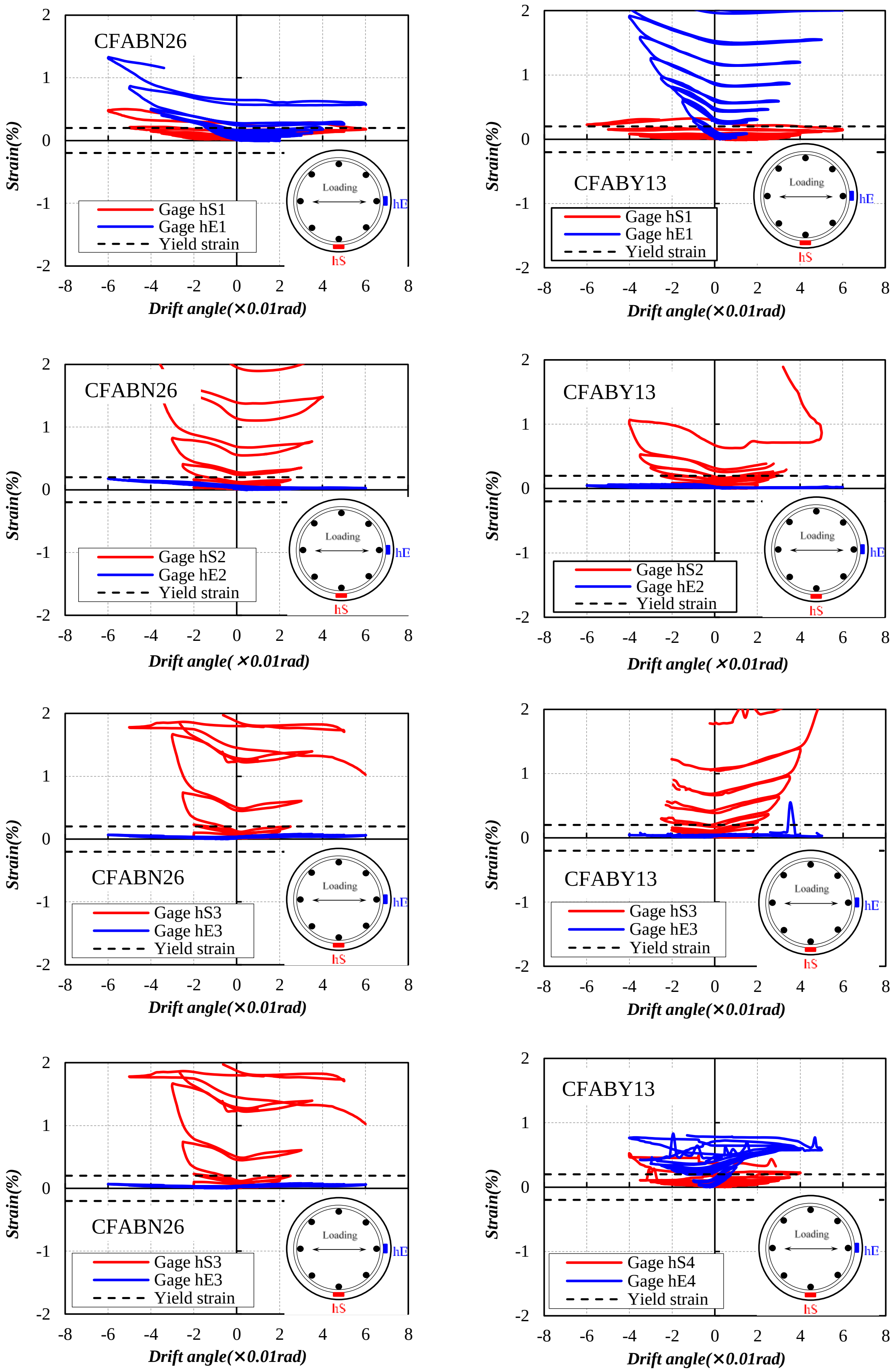

Fig.3 - 12 Measured strains of hoops

It can be seen from Fig.3-12 that the circumferential strains measured at the extreme tensile and compressive sides of column section closer to the top and bottom ends were larger than those at the web sides at the same section, while those at the web sides exhibited larger values at the sections closer to the column middle. These facts clarified that circular hoops at the sections close to column ends primarily confined concrete and circular hoops at the sections away from column ends mainly resisted the shear force.

Strains of steel plates

Fig.3-13 shows examples of the strains measured on the surface of the steel plates used to confine the columns. The dotted horizontal lines represent the yield strain. At the ends of steel plates, circumferential strains exhibited large value, while the axial strains were very small, which implies that the steel plates did provide lateral confinement to LQFA concrete located at extreme compressive edge of the critical end sections of column as expected.

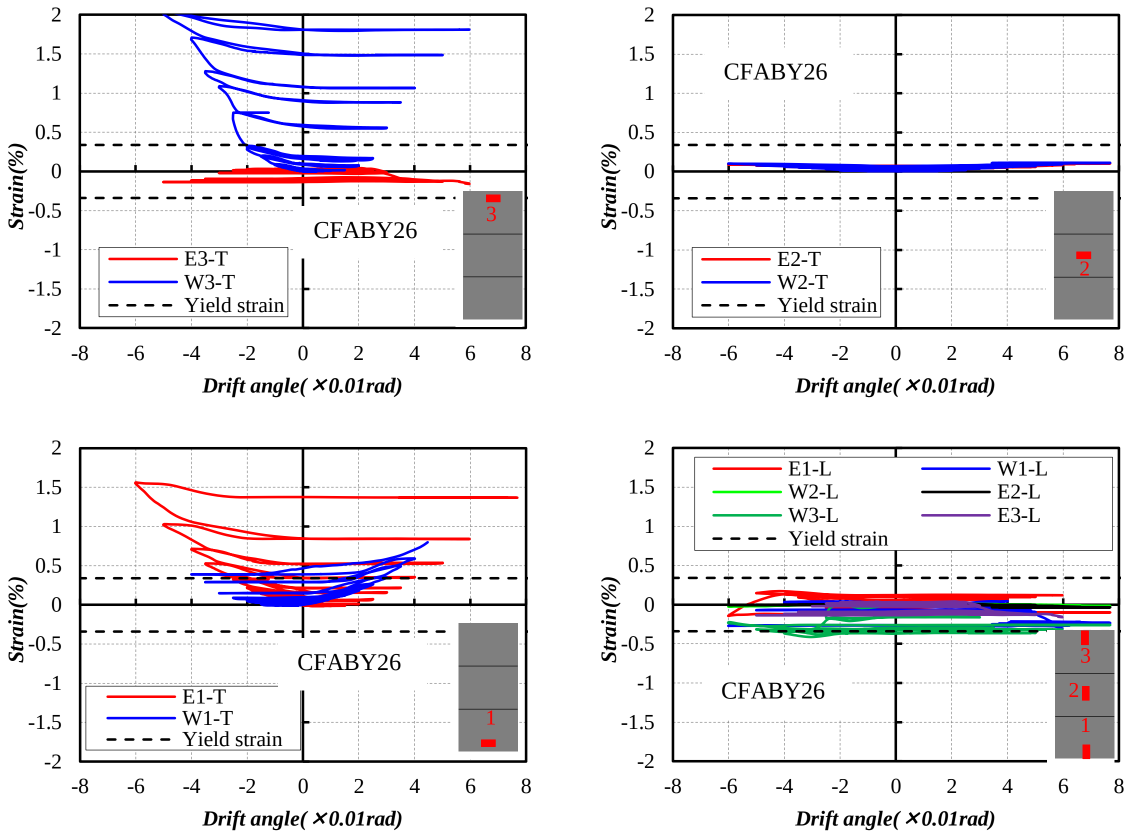

Fig.3 - 13 Measured strains on the surface of steel plates

3.3.4 Residual deformation

Fig.3-14 shows experimental results of residual drift angles corresponding to each target drift angles. The experimental drift angles shown in Fig.3-14 represent the average of residual drift angles in both directions.

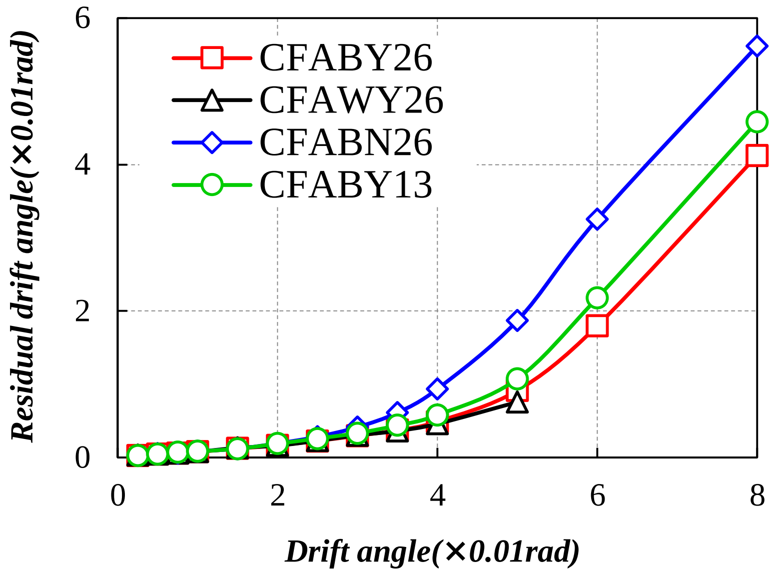

Fig.3 - 14 Residual deformations of test beam-columns

As obvious from Fig.3-14, the residual drift angles of all specimens were very small until R=0.03 rad. The ratios of the residual drift to the experienced peak drift were about one-tenth before R reached 0.03 rad. After R=0.03 rad, however, residual drift of specimen CFABN26 exhibited sharper increase than the others. This can be attributed to the slippage of SBPDN rebars in specimen CFABN26, which did not utilize the tie plate to anchor SBPDN rebars at the middle of column height.

It is interesting to note that the residual drift angle of specimen CFABY13 increased at a faster rate than specimen CFABY26 from R=0.03 rad on. The shorter anchorage length within the loading stub, which is intended to simulate the beam-column joint of frame structures, seemed to have caused a little faster development of steel strain in SBPDN rebars, leading to the little higher increasing rate of residual drift angle.

No significant difference between the measured residual drift angles of specimens CFABY26 and CFAWY26 was observed until the latter failed abruptly in shear, which verifies again that the bolted steel plates could provide more secure confinement effect to high strength LQFA concrete columns than the welded steel tube.

3.3.5 Energy dissipation capacity

Based on the same reason stated in chapter two, the energy dissipation capacity of test columns in this chapter is still to be discussed. The equivalent viscous damping coefficient *heq* are shown as in Fig.3-25. Like the cantilever columns tested in chapter two, the measured *heq* maintained nearly a constant of about 0.07 until R reached 0.03 rad. For the beam-columns with tie plate at the middle of column height, the *heq* kept this small value until the yielding of SBPDN rebars.

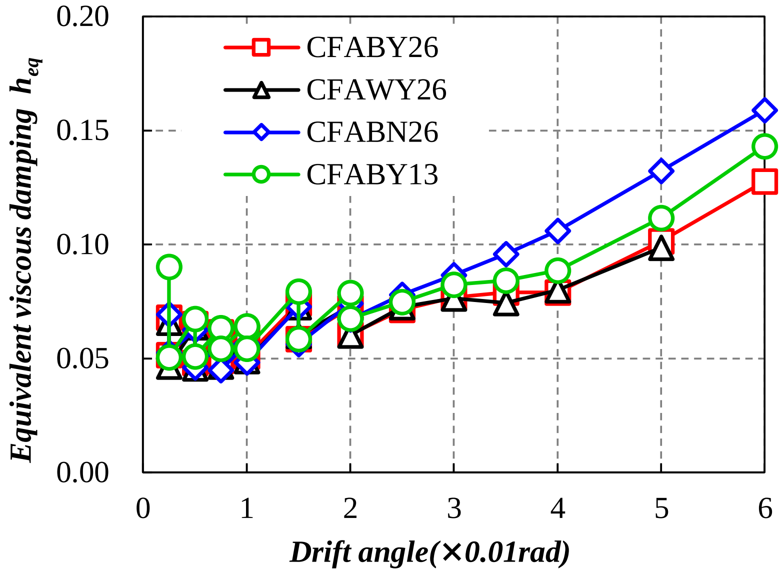

Fig.3 - 15 Measured equivalent viscous damping heq

3.4 CONCLUSIONS

Four circular columns were fabricated and tested to investigate robustness and resilience of circular LQFA concrete beam-columns reinforced with SBPDN rebars and confined by thin steel plates. From the experimental results described in this chapter, the following concluding remarks can be made.

(1) Combination of a large quantity of fly-ash, ultra-high strength rebar with low bond strength and confinement by thin steel plates is a simple and effective method to make sustainable and resilient concrete beam-columns.

(2) While compressive strength of LQFA concrete was beyond 70MPa, combination of SBPDN longitudinal rebar and partial confinement by thin steel plates could ensure circular LQFA concrete beam-columns sufficient resilience until drift angle reached 0.05rad even when the columns were under relatively high axial compression with axial load ratio of 0.33.

(3) Uniting steel plates by bolts and nuts to form a steel tube could provide high strength concrete the same confinement effect as the welded steel tube. When using thin steel plates to confine high-strength concrete, the bolted tube can work more reliably that the welded tube, which has a risk of rupture near the welding portion at large deformation.

(4) To ensure LQFA concrete beam-columns a resilience up to 0.05 rad, the tie plate should be embedded at the contra-flexure section of column to anchor SBPDN rebars and reduce their slippage.

(5) Shorting the anchorage length of longitudinal bar within beam-column joint had little influence on the overall seismic performance of LQFA columns.

REFERENCES

[3.1] Architectural Institute of Japan (AIJ). "AIJ standard for Structural Calculation of Reinforced Concrete Structures," Architectural Institute of Japan, 1982, Tokyo.

[3.2] Bertero V. V. 2000. Introduction to Earthquake Engineering. National Information Service for Earthquake Engineering, Structural Engineering Slide Library: Set J, NISEE-2000-01. http://www.eerc.berkeley.edu/ebooks/. July, 10, 2016.

Chapter 4

Shear Behavior and Ultimate Shear Capacities of LQFA Concrete Beams

4.1 INTRODUCTION

As described in previous two chapters, circular concrete columns made of LQFA concrete hardly failed in shear due to the high compressive strength of concrete. This fact coincides with the investigation conducted by Kim et al. [4.1]. On the basis of analysis of numerous and previous studies, Cai et al. have developed a complete shear strength model for circular concrete columns [4.2]. However, the compressive strength of LQFA concrete is beyond the scope of their model.

In order to promote the use of LQFA concrete in actual buildings located at earthquake-prone zones such as Japan and China, knowledge and information on the shear behavior of LQFA concrete members are indispensable. In particular, as illustrated in Fig.4-1, if there is not a sound shear behavior and strength model for a LQFA concrete column, the column may fail unexpectedly and prematurely in shear when drift reaches a certain level.

Based on the above-mentioned backgrounds, the following items are taken as objectives of this chapter.

1） Acquirement of basic information on the shear behavior of LQFA concrete members.

2） Development of a complete shear capacity model applicable to both circular and square concrete columns. The proposed model is supposed to cover higher concrete strength than previous models.

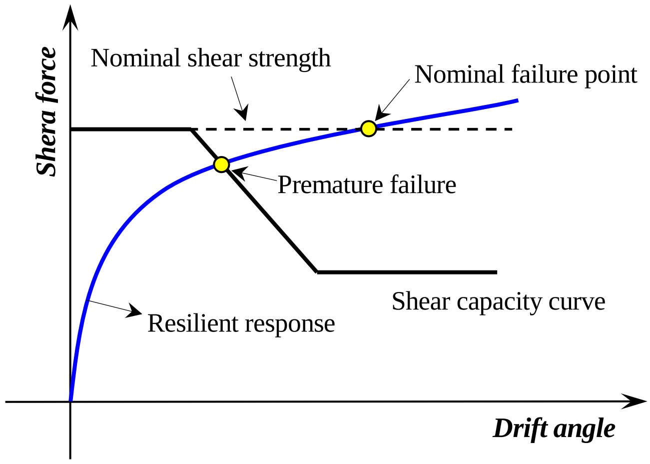

Fig.4- 1 Relationship between resilient response and shear capacity

4.2 EXPERIMENTAL INVESTIGATION

4.2.1 Outlines of specimens

Since high strength concrete columns with compressive strength over 50 MPa hardly failed in shear [4.1], to obtain experimental information on the shear behavior of LQFA concrete components, bending-shear test were conducted on twenty prismatic LQFA concrete beams. Tables 4-1 lists the experimental variables and predicted ultimate capacities of all specimens, while Fig.4-2 show reinforcement details and dimensions.

All specimens had a rectangular section with overall depth of 250mm and width of 150mm, and were reinforced longitudinally with SBPDN rebars in order for these specimens to fail in shear. The experimental variables were the shear span ratio *a/d* (*a* and *d* are shear span and effective depth of beam section, respectively), the steel ratio of transverse reinforcement (p_w) and the steel amount of SBPDN rebars (p_t). As shown in Fig.4-2 and Table 4-1, the shear span ratio *a/d* varied from 1.0 to 4.0. The tensile steel consisted of two SBPDN rebars with diameter of 12.6 mm or two SD345 deformed D13 rebars for twenty three specimens to give a steel ratio of about 0.76%, and only one specimen had three SBPDN rebars as its tensile steel to investigate effect of the steel amount on shear properties of LQFA concrete members. The steel ratio of stirrup varied widely from 0% to 0.76%.

The specimens were divided into two series. The first series (S1 series) consisted of eight specimens which were made and tested in 2013 to obtain basic information on the shear behavior of LQFA concrete beams. The second series (S2 series) also included twelve specimens which were fabricated and tested in 2015 to investigate ultimate shear strength, chord rotation and variation of the shear strength along with chord rotation (or drift ratio).

Table 4- 1 Experimental variables and predicted failure mode of test specimens

Series (year)	specimen	a/d	Shear reinforcement		Predicted strength and failure mode			
			s (mm)	p_w (%)	Q_A (kN)	Q_{my} (kN)	Q_A/Q_{my}	Failure mode
S1 (2013)	No. 1	1.0	220	0.19	221	323	0.68	Shear
	No. 2		110	0.38	230		0.71	
	No. 3		55	0.76	243		0.75	
	No. 4	2.0	220	0.19	127	161	0.78	
	No. 5		55	0.76	149		0.91	
	No. 6	2.5	220	0.19	109	129	0.84	
	No. 7		110	0.38	116		0.89	
	No. 8		55	0.76	129		0.99	
S2 (2015)	No. 9	1.5	-	0	120	205	0.58	
	No. 10		110	0.38	150		0.73	
	No. 11	2.0	220	0.19	112	154	0.72	
	No. 12		110	0.38	121		0.78	
	No. 13		110	0.38	130	231	0.57	
	No. 14		55	0.76	134	154	0.87	
	No. 15	2.5	-	0	76	123	0.61	
	No. 16		110	0.38	106		0.86	
	No. 17	3.0	-	0	61	102	0.59	
	No. 18		110	0.38	91		0.87	
	No. 19	4.0	-	0	61	77	0.78	
	No. 20		110	0.38	91		1.17	Flexure

The theoretical flexural strength (Q_{my}) and shear strength (Q_A) are calculated using the design equations prescribed in JBDPA standard [4.3] for concrete members without fly ash. As one can see from Table 4-1, the predicted Q_A of nineteen specimens were smaller than the calculated Q_{my}, which means that these beams were designed to fail in shear. Specimen No.20 had a calculated Q_A larger than the calculated Q_{my}. This specimen was intended to clarify if the JBDPA shear strength equation is applicable to LQFA concrete beams with *a/d* ratio larger than

3.0, the application upper limit on the shear span ratio of the equation.

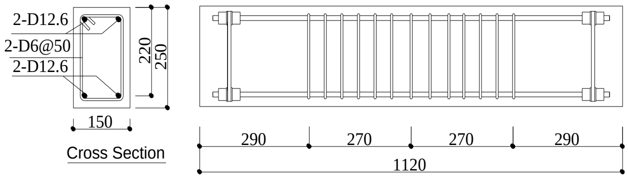

(a) Test beam in series I with shear span ratio of 1.0

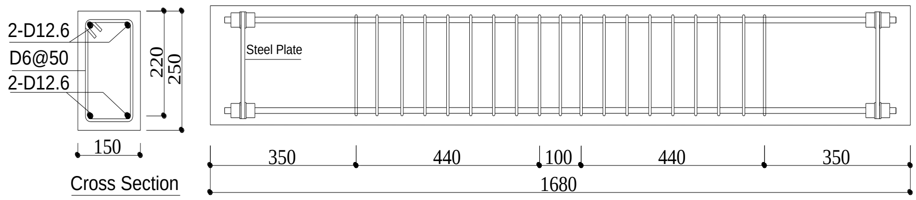

(b) Test beam in series S1 with shear span ratio of 2.0

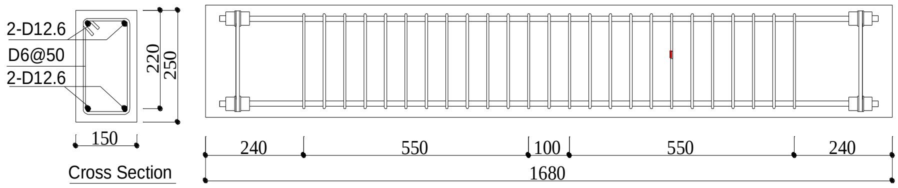

(c) Test beam in series S1 with shear span ratio of 2.5

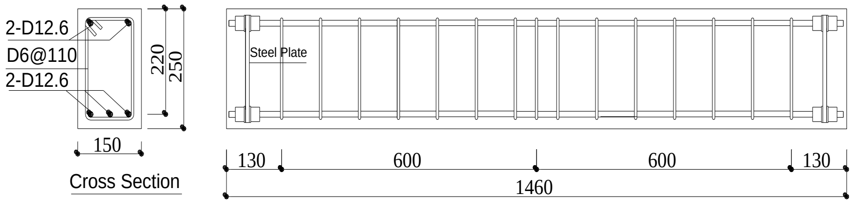

(d) Test beam with stirrups in series S2

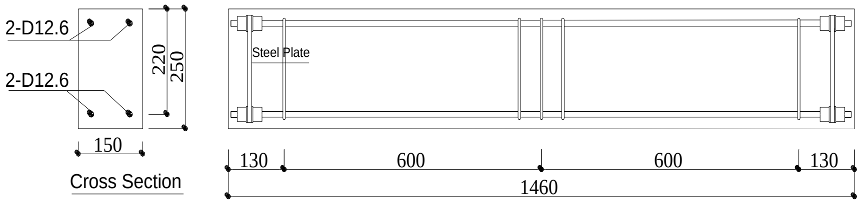

(e) Test beam without stirrup in series S2

Fig.4- 2 Reinforcement details and dimensions of specimens

Two batches of ready-mixed LQFA concrete with the *W/C* ratio of 65 % were used to make the specimens. Table 4-2 shows mix proportions of concrete. The water content and the cement content per unit volume of concrete were 185 kg/m^3 and 285 kg/m^3, respectively. The values of 65 % and 185 kg/m^3 represent the JASS 5-prescribed upper or lower limits on the *W/C* ratio and the water content, respectively, while the value of 285 kg/m^3 is close to the lower limit on the cement content (270 kg/m^3) of structural concrete [4.4].

The specimens were cured in the forms with their tops covered by wet burlaps for four weeks after casting and then were air-cured after removal of the forms. The actual compressive strengths of concrete cylinder (100mm in diameter and 200mm in height) for the S1 and S2 series of specimens were 76 MPa and 64 MPa, respectively. The two concrete strengths represent the average of over nine standard concrete cylinders tested during the loadings of the test beams with average testing ages of 276 days and 45 days, respectively. Fig.4-3 shows the strength gains of the two batches of LQFA concrete along with the formula proposed by Matsufuji et al. [4.5] to predict the strength gain due to both time and fly ash content. It is obvious from Fig.4-3 that the strength gains of the two batches of LQFA concrete agreed fairly well with the formula by Matsufuji et al.

Table 4- 2 Mix proportions of concrete

Series	Fly Ash (kg/m^3)	W/C	Water (kg/m^3)	Cement (kg/m^3)	Fine Aggregate		Coarse Aggregate (kg/m^3)	Admixture (kg/m^3)
					Sand (kg/m^3)	Crushed Sand (kg/m^3)		
I	455	0.65	185	285	334	146	833	5.92
Π	455	0.65	185	285	325	141	833	7.40

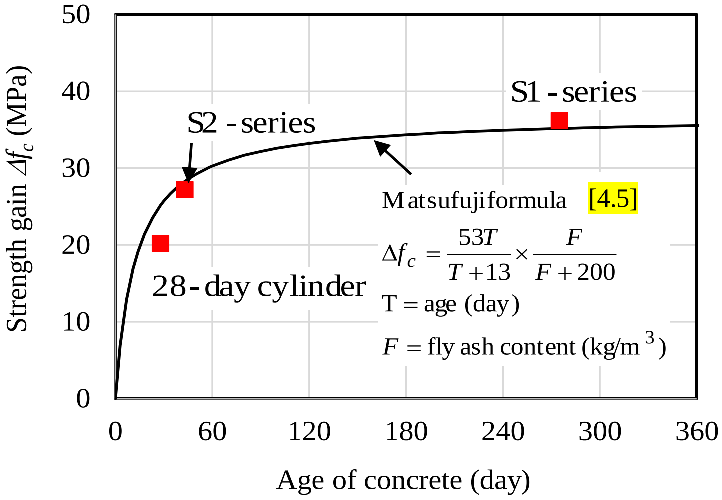

Fig.4- 3 Measured strength gains of LQFA concrete (FA=455 kg/m^3)

Table 4- 3 Mechanical properties of the steels

Notation	Elastic modulus E_s (GPa)	Yield strength f_{sy} (MPa)	Yield strain ε_{sy} (%)	Tensile strength f_{su} (MPa)	Elongation ratio (%)
D6	190 (191)	426 (384)	0.23 (0.22)	517 (510)	25.9 (28.3)
D12.6	215 (209)	1423* (1358*)	0.86* (0.85*)	1499 (1458)	9.7 (9.9)
PL9	188 (207)	327 (356)	0.19 (0.20)	479 (445)	41.5 (43.8)

Note: *obtained by 0.2% offset strain rule; the values in parentheses are those used in 2015

As one can see from Fig.4-2, each SBPDN rebar was anchored to steel plates (PL9) at both ends by nuts to prevent the rebar from premature slippage. D6 deformed bar was used as shear reinforcement in form of a single rectangular stirrups. Mechanical properties of the steels used are listed in Table 4-3, and the numerical values shown in Table 4-3 represent the average of three standard test coupons.

4.2.2 Test set-up and instrumentations

Loading apparatus is shown in Fig.4-4. A universal testing machine with capacity of 2MN was used to apply the vertical load (P) at the mid-span of each specimen simply supported. A total of five displacement transducers (DTs) were used to measure the vertical displacement at the mid-span and the locations shown in Fig.4-4. Five strain gauges (G1 through G5) were embedded to measure the strains of longitudinal tensile rebar, six or more gauges (through NG to SG) were used to measure the strains of shear reinforcements as shown in Fig.4-4.

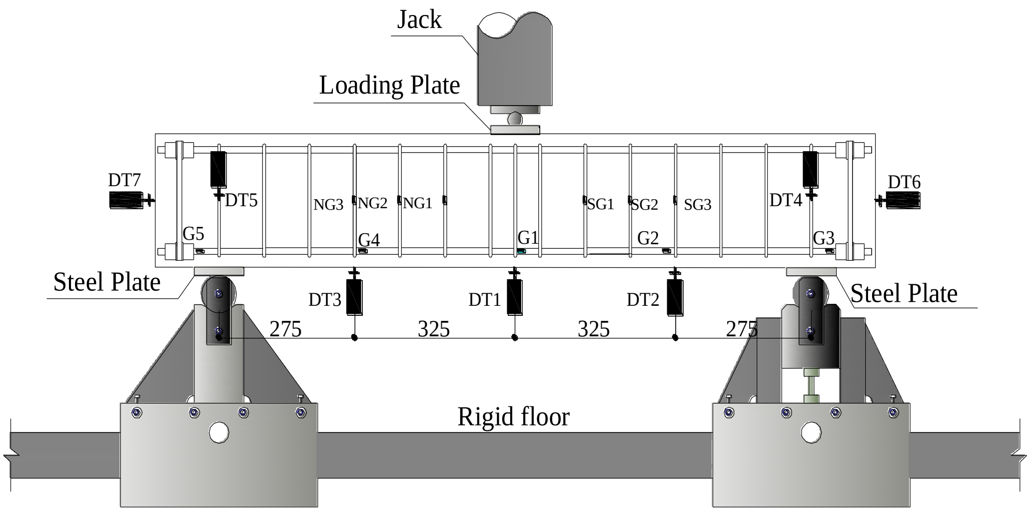

Fig.4- 4 Schematic view of test setup (unit: mm).

4.2.3 Test results and discussions

Fig.4-5 shows the crack patterns of S2-seriese specimens observed after testing. As obvious from Fig.4-5, all specimens exhibited typical crack patterns observed in concrete beams failing in shear. Regardless of different shear span ratio, shear failure of LQFA concrete beams occurred along one primary diagonal shear crack, penetrating the beam by about 45-degree with respect to the beam axis.

Fig.4-6 shows the measured vertical load (*P*) versus chord rotation *R* relationships, while Fig.4-7 displays the relationships between the steel strain (ε_s) at mid-span of tensile rebar and *R* of all specimens, respectively. The chord rotation *R* is the ratio of the vertical displacement $\triangle$ (see Fig.4-9) at the mid-span to the shear span *a*. Each graph in Figs.4-6 and 4-7 includes test results of specimens with the same *a/d* ratio. The horizontal chain lines in each graph represent the predicted flexural load (P_{my}) obtained by doubling the calculated Q_{my}, and the yield strain (ε_{sy}), respectively. The peak shear resistance and corresponding chord rotation in P-R relations will be referred to as ultimate shear strength and ultimate chord rotation, respectively, hereafter.

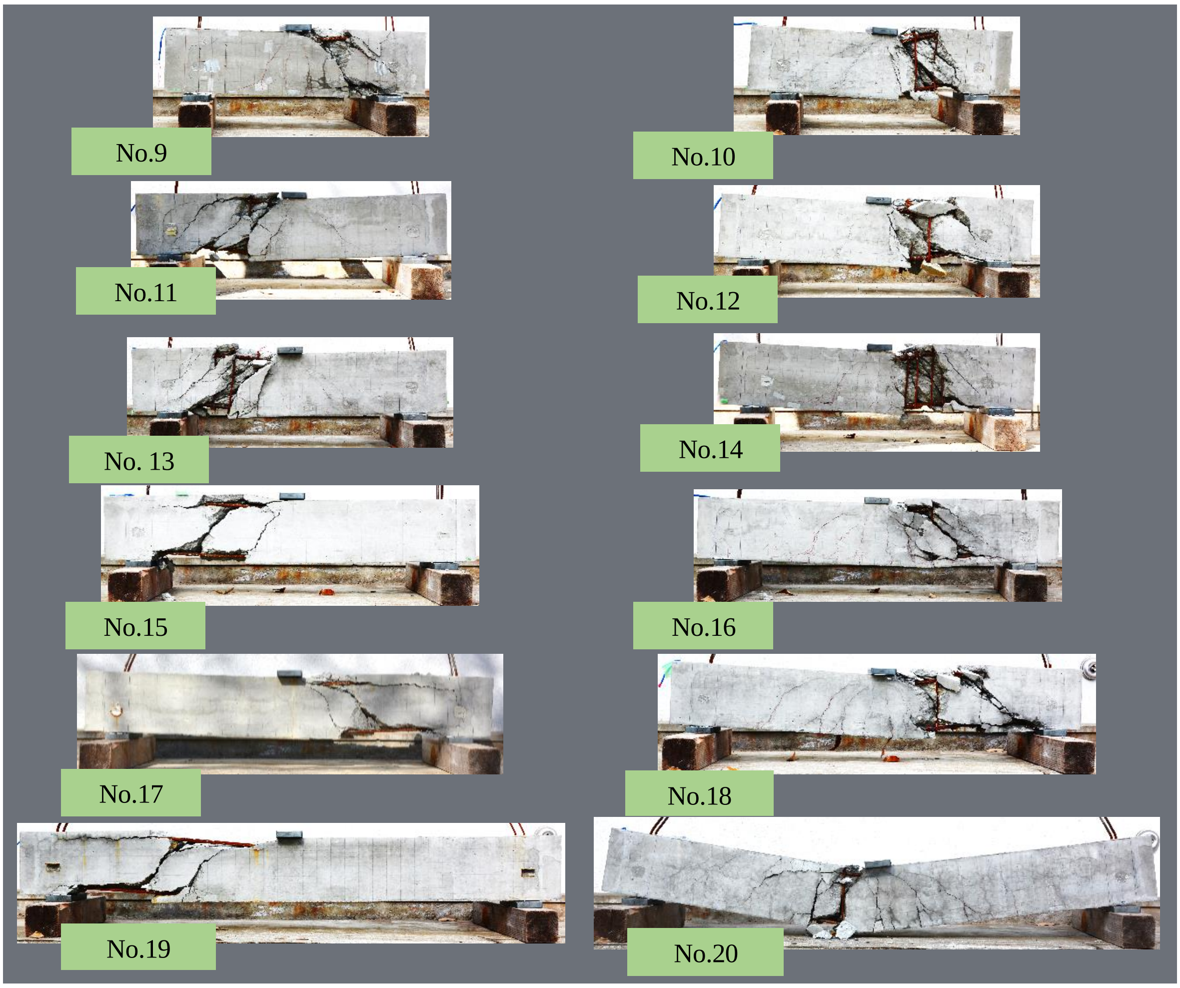

Fig.4- 5 Cracking patterns of Series 2

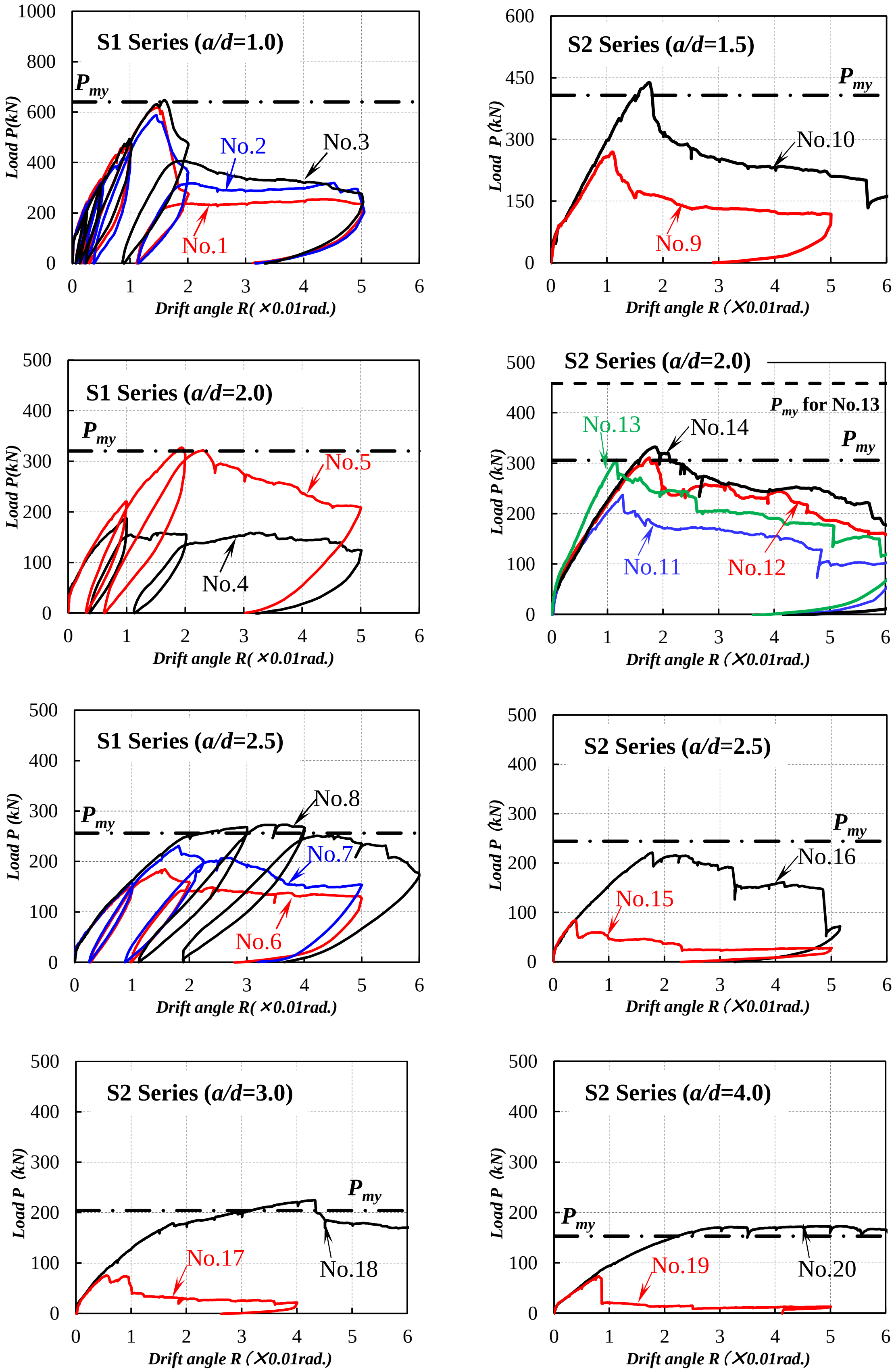

Fig.4- 6 Measured load versus chord rotation relationships

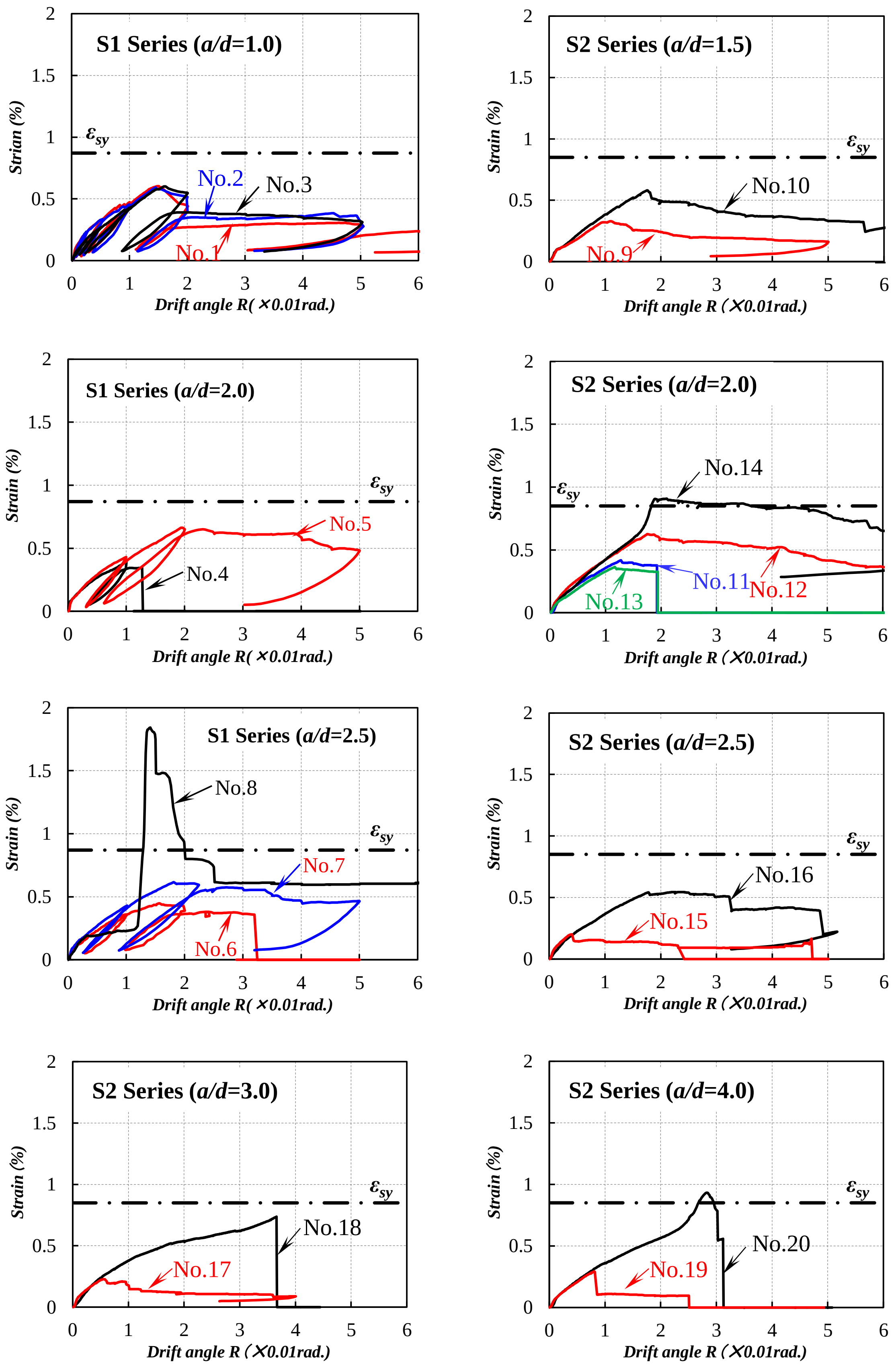

Fig.4- 7 Measured steel strain versus chord rotation relationships

A specimen is generally judged failing in flexure if the measured steel strain reached the yield strain ε_{sy} (See Fig.4-7) at or before the specimen reached its V_{uexp}. Specimens No. 8, No. 14 and No. 20 are judged failing in flexure following this general rule. Specimen No. 18 is also judged failing in flexure while its measured steel strain did not reach the yield strain. This judgement was based on the fact that the strain gage had prematurely broken at R=3.64 % before this specimen reached its V_{uexp} at R=4.31 % (see Fig.4-6). Considering that the measured V_{uexp} exceeded the calculated P_{my} and the ductile post-peak behavior, it can be said that this judgement is reasonable and acceptable.

As apparent from Fig.4-6, short LQFA concrete beams (specimens No.1 through No.3) with the *a/d* ratio of 1.0 exhibited typical shear resistance by the so-called arch action. The three specimens reached ultimate shear strength at nearly the same chord rotation despite the big difference in the amount of stirrup among them. The shear reinforcement enhanced the residual shear resistance at large chord rotation, but exhibited little, if any, significant influence on the ultimate shear strength and chord rotation of short LQFA concrete beams.

Short shear span rendered the external load (*P*) to be transferred to the support through a compressive strut, which connects the loading point with the support. The compressive strut was crushed before the tensile rebars reached the yield strains (see Fig.4-6), which implies that mechanical properties of concrete dominated the ultimate shear strength and chord rotation of short beams.

Most of the specimens with the *a/d* ratio varying between 1.5 and 2.5 failed in shear as designed along a diagonally cracked plane, which extended from the vicinity of the loading point downward by about 45-degree with respect to the beam axis. Increasing the steel amount of stirrups led to higher ultimate shear strength, larger ultimate chord rotation more ductile post-peak behavior of LQFA concrete beams. The concrete outside the diagonally cracked plane provided extra confinement to the concrete in the cracked plane, delaying the extension of the shear crack and rendering the stirrups to effectively resist shear force. On the other hand, by comparing the P-R relationships of the specimens No.12 and No.13 in Fig.4-6, one can see that increasing tensile rebar did not enhance the shear strength, but conversely degraded the post-peak ductility of LQFA concrete beams.

In the case of specimens with the *a/d* ratio larger than 3.0, the specimens (No. 18 and No. 20) with stirrup exhibited ductile flexure behavior till large deformation. These two specimens did not fail till the chord rotation reached 6.0 %.

Four specimens without stirrup (No. 9, No. 15, No. 17 and No. 19) all failed in shear along an about 45-degree shear crack. Comparing their measured P-R relationships, one can see that the ultimate shear strength of LQFA concrete beam without stirrup nonlinearly decreased along with the *a/d* ratio but converged to the shear resistance attained at the *a/d* ratio of 3.0. This can be attributed to that the long shear span reduced stiffness of the beam and deteriorated the extra confinement by the concrete adjacent to the shear crack.

4.3 EVALUATION OF ULTIMATE SHEAR CAPACITYIES OF LQFA CONCRETE MEMEBRS

To conduct reliable ultimate capacity design of LQFA concrete members, a complete shear capacity model will be developed. The proposed shear capacity model defines the relationship between the shear resistance versus drift angle (or chord rotation) as shown in Fig.4-8. This new model is intended to cover both circular and rectangular concrete members made of general concrete and/or LQFA concrete. The proposed model also covers higher strength concrete than the model by Cai et al. [4.2].

As shown in Fig.4-8, the proposed shear capacity curve can be completely determined by four parameters. These parameters are, 1) the nominal ultimate shear strength (Q_u), the ultimate chord rotation or drift ratio (R_u), the degradation slope of shear resistance (K_d) and the residual shear resistance (Q_r) at large deformation.

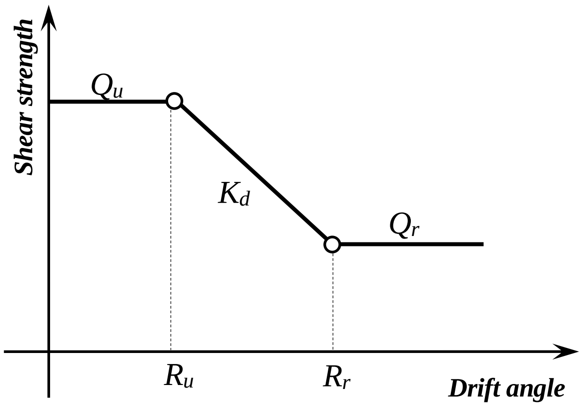

Fig.4- 8 Outline of the proposed shear capacity curve

This section will deal with the nominal shear strength and corresponding chord rotation or drift ratio. The mathematical expressions for the other two parameters and overall model will be presented in the next section.

Table 4- 4 Primary test results and comparisons with the calculated results

Series (Year)	Specimen	Experimental results			Calculated results and comparisons					
		Q_{uexp} (kN)	R_{uexp} (%)	Failure mode	Q_A (kN)	Q_{uexp}/ Q_A	Q_{ucal} (kN)	Q_{uexp}/ Q_{ucal}	R_{ucal} (%)	R_{uexp}/ R_{ucal}
S1 (2013)	No. 1	309	1.46	Shear	221	1.40	261	1.18	1.45	1.01
	No. 2	295	1.45	Shear	230	1.28	288	1.02	1.53	0.95
	No. 3	324	1.60	Shear	243	1.33	341	0.95	1.96	0.82
	No. 4	94	0.99	Shear	127	0.74	117	0.80	1.29	0.77
	No. 5	164	1.94	Shear	149	1.10	198	0.83	2.31	0.84
	No. 6	92	1.58	Shear	109	0.84	87	1.06	1.19	1.33
	No. 7	116	1.82	Shear	116	1.00	106	1.09	1.52	1.20
	No. 8*	137	3.38	Flexure	129	-	(162)	-	(2.37)	-
S2 (2015)	No. 9	135	1.10	Shear	120	1.13	143	0.94	1.22	0.90
	No. 10	220	1.75	Shear	150	1.47	192	1.15	1.72	1.02
	No. 11	119	1.28	Shear	112	1.06	110	1.08	1.27	1.01
	No. 12	156	1.75	Shear	121	1.29	136	1.15	1.61	1.09
	No. 13	153	1.17	Shear	130	1.18	136	1.13	1.01	1.16
	No. 14*	166	1.86	Flexure	134	-	(185)	-	(2.26)	
	No. 15	42	0.40	Shear	76	0.55	52	0.81	0.68	0.59
	No. 16	110	1.77	Shear	106	1.04	102	1.08	1.50	1.18
	No. 17	38	0.56	Shear	61	0.62	40	0.95	0.61	0.92
	No. 18*	113	4.31	Flexure	91	-	(90)	-	(1.60)	-
	No. 19	37	0.81	Shear	61	0.61	40	0.93	0.88	0.92
	No. 20*	87	4.75	Flexure	91	-	(89)	-	(2.19)	-

Note: Q_A = the calculated shear strength by JBDPA equation (Eq. (4-1)) [4.3]

Q_{ucal} = the calculated shear strength by the proposed equations (Eqs. (4-7) and (4-8))

* The calculated ultimate shear capacities for specimens failing in flexure are shown for reference.

Before deriving formulae to evaluate Q_u and R_u, the measured shear strength of LQFA concrete beams is compared with the calculated results by JBDPA equation in Table 4-4. The JBDPA equations to evaluate the ultimate shear strength (Q_A) and the yield flexural strength (Q_{my}) for general concrete beams are written as follows [4.3]:

$$Q_A = \left[\frac{0.094 k_u p_{te}^{0.23} \left(f_c^{'} + 17.6 \right)}{a/d + 0.12} + 0.85 \sqrt{p_w \cdot f_{wy}} \right] bj \tag{4-1}$$

$$Q_{my} = \frac{0.9 a_t f_{sy} d}{a} \tag{4-2}$$

where k_u is the factor accounting for the size effect on the concrete strength and taken as 1.0 as the effective depth of beam section (d) is less than 150mm, decreasing along with d to its lower limit of 0.72 when d reaches and exceeds 400mm; p_{te} is the tensile steel ratio in percentage; p_w is the steel ratio of stirrups; f_c' is the compressive strength of concrete; j is the distance between centroids of the stresses in the beam section and approximately taken as $7d/8$; a_t is the cross-sectional area of tensile steels; and f_{sy} and f_{wy} are the yield strength of tensile rebar and stirrups, respectively.

As obvious from Table 4-4, sixteen specimens failed in shear as designed, but four specimens failed in flexure. Besides the specimen No. 20, three specimens (No. 8, No. 14 and No. 18) also failed in flexure contrary to design. In addition, there is a big difference between the measured Q_{uexp} and the predicted Q_A by JBDPA equation, which tends to underestimate the contribution by stirrup but overestimate the contribution by concrete.

These observations imply urgency and necessity to develop a more refined equation for the ultimate shear strength of LQFA concrete members. Furthermore, to author's knowledge, no explicit formula is recommended for the ultimate deformation of concrete members failing in shear in current design codes.

4.3.1 Nominal shear strength

As shown in Fig.4-5, regardless of different shear span ratio, shear failure of LQFA concrete beams occurred along one primary diagonal shear crack, which penetrated the beam section by about 45-degree with respect to the beam axis. Therefore, it is reasonable to assume that the shear force is primarily resisted by the concrete and the stirrups along and across the primary diagonal shear failure plane, which is abbreviated as diagonal plane hereafter.

The equation to predict nominal shear strength of LQFA concrete members can be derived by considering the equilibrium of the forces acting on the diagonal plane as shown in Fig.4-9. In deriving the equation, three basic assumptions are made; 1) the diagonal plane has an inclination of 45-degree with respect to the member axis, 2) the LQFA concrete across the diagonal plane follows Mohr-Coulomb failure criterion (see Fig.4-10), and 3) the tensile rebars will internally balance the compressive rebars crossing the diagonal plane.

The equilibriums of forces along X and Y directions can be expressed in form of

$$\sum Y = Q + \sigma_{cf}\frac{A_g}{\sin\theta}\sin\theta - \tau_{cf}\frac{A_g}{\sin\theta}\cdot\cos\theta - A_w f_{wy}\frac{d\cot\theta}{s} = 0 \tag{4-3}$$

$$\sum X = N - \sigma_{cf}\frac{A_g}{\sin\theta}\cdot\cos\theta - \tau_{cf}\frac{A_g}{\sin\theta}\cdot\sin\theta + (F_t - F_c) = 0 \tag{4-4}$$

Where Q and N are the shear force to sustain and the axial load applied, respectively, (N); τ_{cf} and σ_{cf} are the shear stress along the diagonal plane and the normal stress perpendicular to the diagonal plane, respectively, (=N/mm^2); A_g is the gross sectional area of member, (mm^2); d is the effective depth of the member section, (mm); s is the spacing of stirrups, (mm); θ is the inclination of the diagonal plane with respect to the member axis; A_w is the total cross-sectional area of stirrup, (mm^2); f_{wy} is the yield strength of stirrup, (=N/mm^2); F_t and F_c are the forces sustained by the tensile and compressive rebars, respectively, (N).

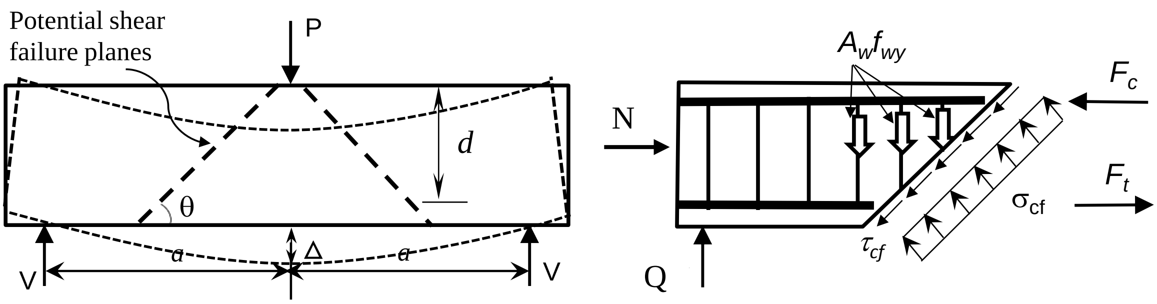

(a) Loading condition (b) Forces acting on the diagonal plane

Fig.4- 9 Conception of shear resistance mechanism

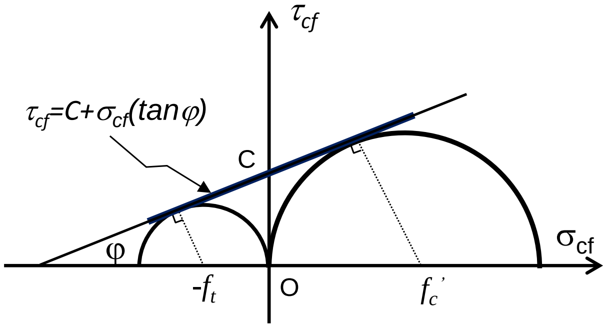

Fig.4- 10 Mohr-Coulomb failure criteria for LQFA concrete

Denoting the ratio of compressive strength (f_c') to tensile strength (f_t) of the concrete as m, and following the assumption that the concrete tensile strength can be approximated as about one-fifteenth of the compressive strength for high strength concrete [4.5], the Mohr-Coulomb failure criterion of LQFA concrete can be simplified as follow:

$$\tau_{cf} = \frac{1}{2\sqrt{m}} \cdot f_c^{'} + \frac{m-1}{2\sqrt{m}} \sigma_{cf} = 0.129 f_c^{'} + 1.807 \sigma_{cf} \tag{4-5}$$

Substituting Eq. (4-5) into Eq. (4-3) and Eq. (4-4), and following the first and the third basic assumptions, the nominal shear strength can be derived as the shear force when LQFA concrete reaches the Mohr-Coulomb failure criterion in form of

$$\begin{aligned} Q_u &= Q_{cu} + Q_{su} = (0.092 + 0.287n) f_c^{'} A_g + \frac{A_w f_{wy} d}{s} \\ &= (0.092 + 0287n) f_c^{'} A_g + \frac{A_w f_{wy} d}{s} \end{aligned} \tag{4-6}$$

where n is the axial load ratio. The assumption that tensile strength of high strength concrete can be taken as one-fifteenth of compressive strength can be verified by test results of standard cylinder of LQFA concrete as shown in Table 4-5, where the splitting strength and compressive strength of eight pairs of LQFA concrete cylinders are listed. The value of 15.5 in parenthesis expresses the average m excluding the No. 5 pair of cylinders.

Table 4- 5 Test results of LQFA concrete cylinders

No.	1	2	3	4	5	6	7	8	Mean
f_c'(MPa)	56.0	63.7	64.3	64.0	66.2	63.4	62.4	76.5	
f_t(MPa)	3.6	3.8	4.2	4.7	3.2	3.7	4.4	4.6	
f_c'/f_t	15.8	16.6	15.4	13.6	22.2	17.1	14.3	16.6	16.4 (15.5)

Further considering the deterioration of the strength of cracked concrete along the diagonal plane as well as the size effect on the concrete strength, the formula to calculate ultimate shear strength can be written as:

$$Q_u = (0.092 + 0287\, n) f_c^{'} A_g + \frac{A_w f_{wy} d}{s} \tag{4-7}$$

In Eq. (4-7), v_c is the strength reduction factor of concrete. According to the previous study on the ultimate shear strength of general concrete members [4.2], v_c is primarily affected by the concrete strength and the shear span ratio, an indirect but more appropriate factor measuring the size effect [4.6].

Fig.4-11 shows the relationship between the measured v_c and the *a/d* ratio of the specimens failing in shear. The experimental v_c was obtained by at first subtracting the shear resistance V_{su} by the stirrups (see Eq.(4-7)) from the measured shear strength V_{uexp} to obtain the shear force resisted by concrete (V_c) and then dividing the V_c by $0.092 f_c' A_g$. From the results shown in

Fig.4-6, Eq. (4-8) can be derived to evaluate the strength reduction factor v_c.

$$v_c = e^{\left(-0.01 f_c^{'}\right)} \times \begin{cases} 0.35 + 0.39(a/d - 3.0)^2, & a/d \le 3.0 \\ 0.35, & a/d > 3.0 \end{cases} \quad (f_c^{'} \text{ in MPa}) \tag{4-8}$$

Eq. (4-8) is superimposed in Fig.4-11. The correlation coefficient between the measured v_c and the calculated ones by Eq. (4-8) is as high as 0.918, which implies high accuracy of Eq. (4-8).

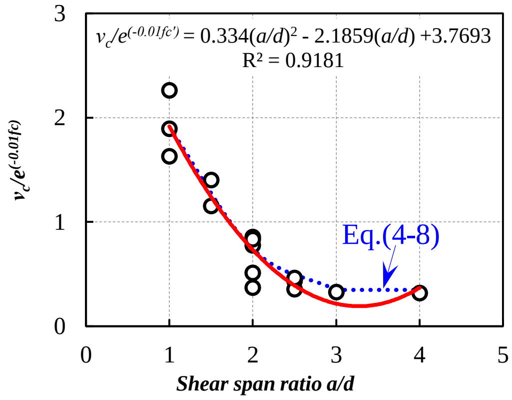

Fig.4- 11 Experimental strength reduction factors

4.3.2 Ultimate chord rotation or drift ratio

According to the study by Ang et al. [4.7], the shear strength degradation of general concrete members is mainly caused by the deterioration of the shear resistance by concrete. Therefore, among many potential factors, the steel ratio p_w of stirrup and the lateral confinement index I_c ($=p_w f_{wy}/f_c^{'}$) have been well presumed to be the main factors influencing ultimate chord rotation or drift ratio of concrete members because both factors strongly affect material property of the concrete.

Fig.4-12 shows the relationships between the experimental R_{uexp} and several structural factors, including the steel ratio p_w, the index I_c and the factor β. The factor β represents the ratio of the measured shear strength (Q_{uexp}) to the calculated flexural strength (Q_{my}), and is a factor representing the margin of the shear resistance over the flexure resistance of concrete members. Fig.4-12 also shows influence of the *a/d* ratio, which strongly affects the ultimate shear strength (Q_{cu}) of the concrete as shown in Eqs. (4-7) and (4-8).

As apparent from Fig.4-12, the *a/d* ratio exhibits little correlation with R_{uexp}. Both p_w and I_c show relatively strong correlation with R_{uexp}. The factor β, however, exhibits much stronger correlation with R_{uexp} than the others. Based on the results in Fig.4-12, Eq. (4-9) can be derived to calculate ultimate deformation of LQFA concrete members failing in shear.

$$R_u = (2.04\beta - 0.19) = 2.04\frac{Q_u}{Q_{my}} - 0.19 \ge 0.4 \quad (in\,\%) \tag{4-9}$$

Where 0.4% is the smallest measured peak drift ratio in all test beams failing in shear. This value is close to 0.5%, which is the peak drift of general concrete members failing in shear, and it is reasonable to recommend this value as the lower limit of the calculated peak strain for LQFA concrete members failing in shear.

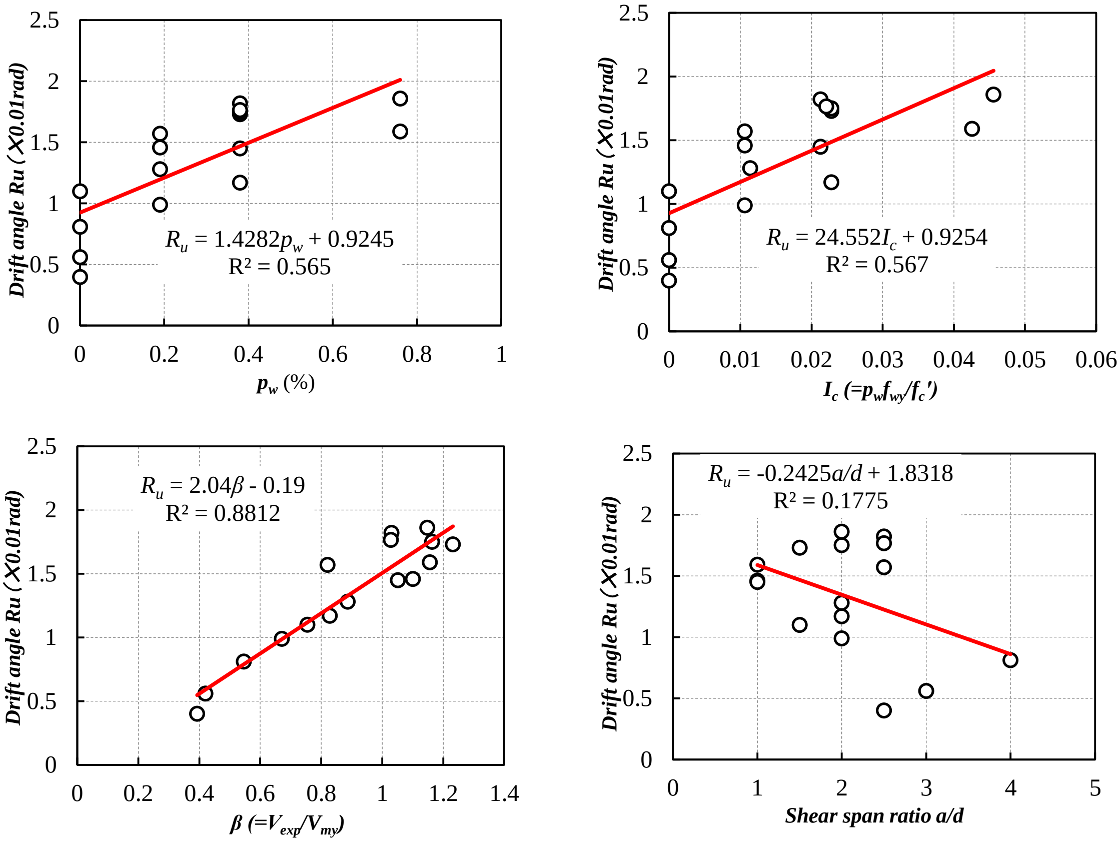

Fig.4- 12 Measured ultimate chord rotations

4.3.3 Verification of the proposed equations

To verify accuracy of the proposed equations, the experimental Q_{uexp} and R_{uexp} of sixteen specimens failing in shear are compared with the calculated Q_{ucal} by Eq. (4-7) and Eq. (4-8) and the calculated R_{ucal} by Eq. (4-9) in Fig.4-13 along with the statistics in terms of the ratio of the experimental result to the calculated one. The calculated Q_{ucal} and R_{ucal} are also listed in Table 4-4. The calculated Q_{ucal} and R_{ucal} of the specimens failing in flexure are listed in Table 4-5 by parentheses only for reference and are not included in Fig.4-13.

As obvious from Fig.4-13 and Table 4-4, the calculated Q_{ucal} exhibits very good agreement with the measured Q_{uexp}, and the Q_{uexp}/Q_{ucal} ratio has a mean value of 1.01, and a standard deviation of 0.13. While scattering is observed between the measured R_{uexp} and the calculated R_{ucal}, the experimental/calculated ratio exhibits a mean value of 0.95 and a standard deviation of 0.24. Considering the instability of peak chord rotation due to the near-zero stiffness, these two statistical results indicate that Eq. (4-9) is reliable and accurate enough for practice.

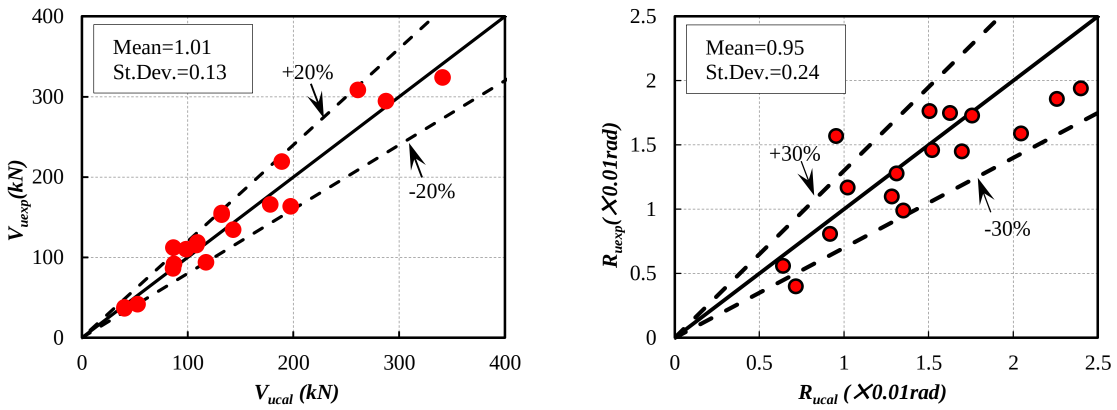

(a) Nominal shear strength (b) Ultimate chord rotation

Fig.4- 13 Comparisons between the experimental results and the calculated ones

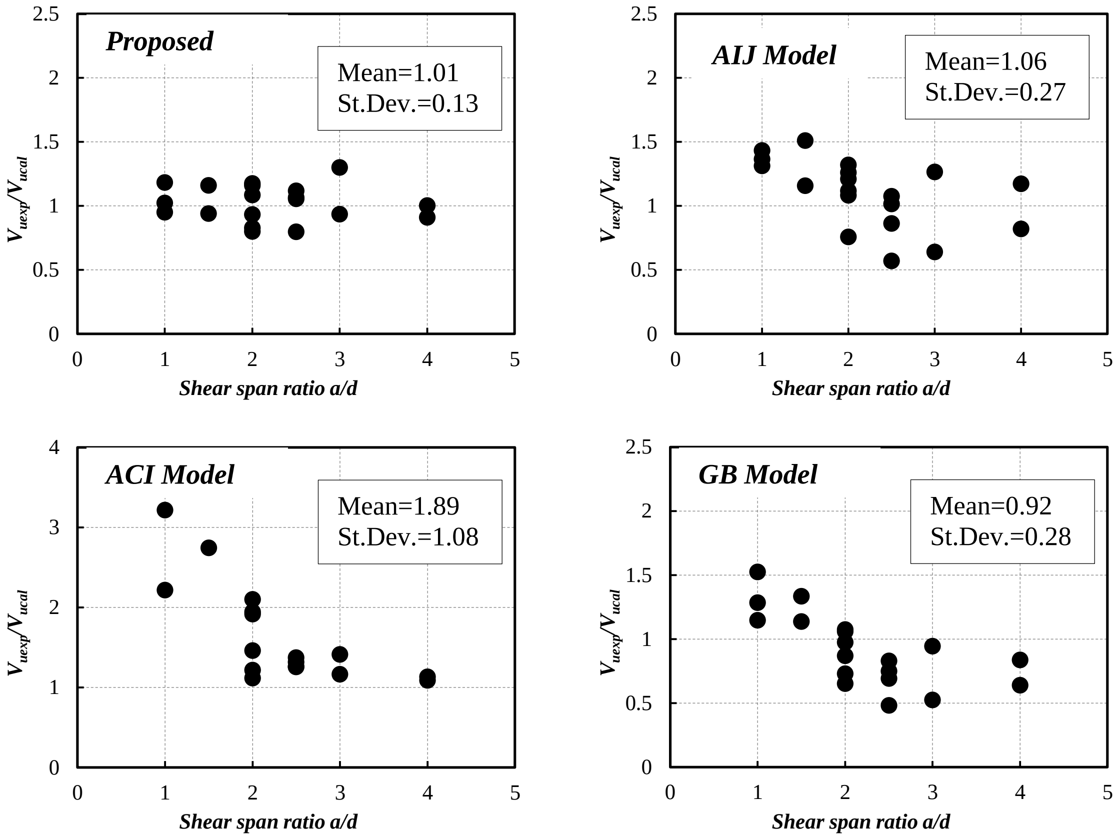

Fig.4- 14 Comparison of accuracy of current shear strength models

To further verify accuracy of the proposed shear strength equations, Fig.4-14 compares the measured Q_{uexp} with the calculated shear strengths Q_{ucal} by four representative models. The other three models are the AIJ equation (AIJ model), the equation prescribed in ACI code [4.8] (ACI model), and the equation recommended in Chinese code [4.9] (GB model) for general concrete beams. The AIJ equation is equivalent to the JBDPA equation.

4.4 OVERALL SHEAR CAPACITY MODEL

Study on the shear capacity curve can trace back to the work by Ang et al. [4.7], who experimentally and analytically demonstrated that shear strength of concrete columns tended to degrade along with deformation and proposed a shear capacity curve for circular concrete columns. Since the pilot work by Ang et al., many researchers and institutes have proposed several shear capacity curve models for general concrete members. The representative models includes those by the California Department of Transportation's (Caltrans) model (1995) [4.10], by the University of California, San Diego (UCSD) [4.11], by University of Southern California (USC) [4.12], and the University of California, Berkeley (UCB) [4.13].
Details of these models can be found in reference [4.2] and will not be given here.

All the previous models, however, define the shear strength as a function of displacement ductility. This definition hinders their application in actual seismic design of concrete columns because of the ambiguity and arbitrariness of the yielding displacement that is indispensable in defining the displacement ductility. Furthermore, because the previous models were all intended for circular columns, a new shear capacity model which can cover both circular and rectangular concrete members is desirable.

Since the Q_u and R_u have been defined by Eq. (4-7) and Eq. (4-9), respectively, this section will be devoted to the development of equations to obtain the degradation slope K_d and the residual shear resistance Q_r (see Fig.4-11).

4.4.1 Shear strength degradation slope K_d

Fig.4-15 shows the relationships between the shear resistances (Q_c and Q_s) and chord rotation for the specimens that failed in shear and without stirrups. The V_s shown in Fig.4-15 was obtained on the basis of the measured strain of stirrups and the assumption that the stirrup was a perfectly elasto-plastic material. The Q_c of these specimens then was calculated by subtracting the measured V_s from the measured shear force. For the four specimens without stirrups, the Q_c is equal to the measured shear force and will not be shown.

As obvious from Fig.4-15, the shear resistance by stirrups maintained nearly constant after beams reached their peak resistances, while the shear resistance by concrete exhibited significant degradation after the peak resistances along with deformation. This can be attributed to the inherent degradation of the concrete strength along with deformation.

From the relationships between Q_c and chord rotation R shown in Fig.4-15, the experimental results of K_d can be obtained by using the best-fit method. Fig.4-16 displays relationships

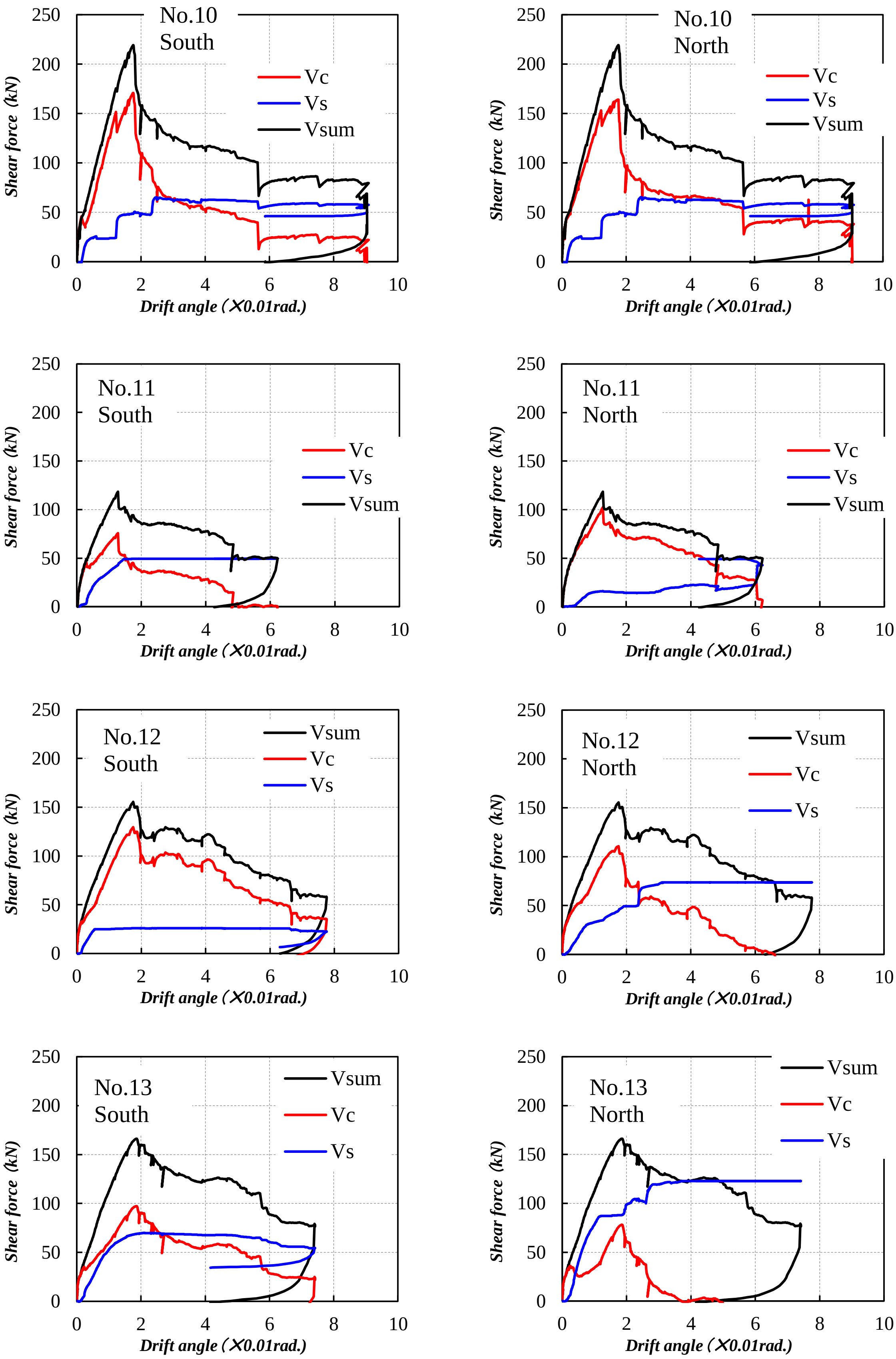

Fig.4-15 Shear resistances by concrete and stirrups (to be continued)

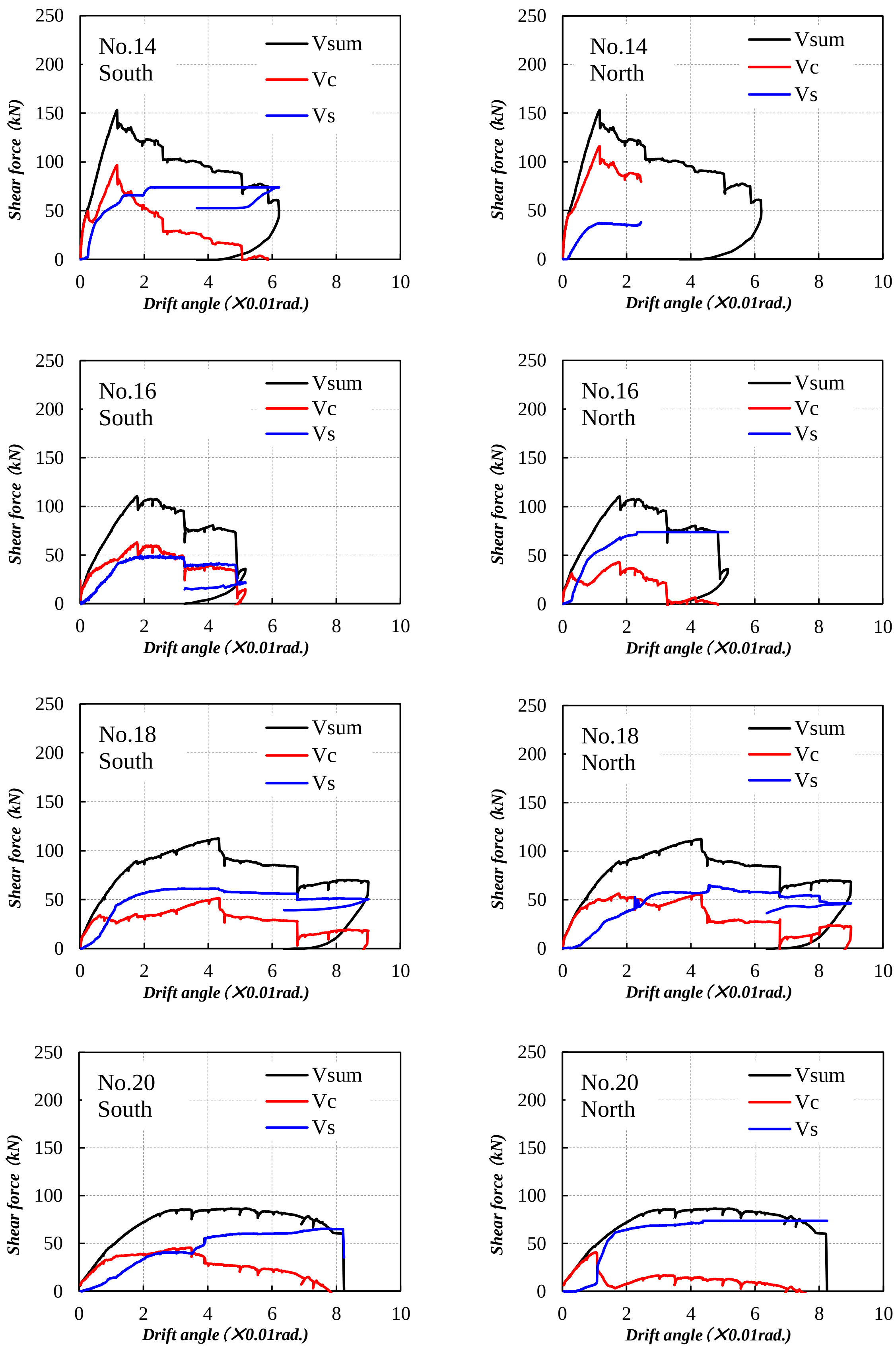

Fig.4- 15 Shear resistances by concrete and stirrups

between the measured K_d and several structural factors, including shear span ratio (a/d), confinement index ($p_w f_{wy}$) , and integrated factor γ ($=a/d*p_t f_y/f_c$). The factor γ is intended to express influence of the so-called dowel effect by longitudinal steel on the shear resistance by concrete.

As one can see from Fig.4-16, the factor γ strongly affects the shear strength degradation slope of LQFA concrete beams that failed in shear. The confinement index had a little, influence on the degradation slope K_d.

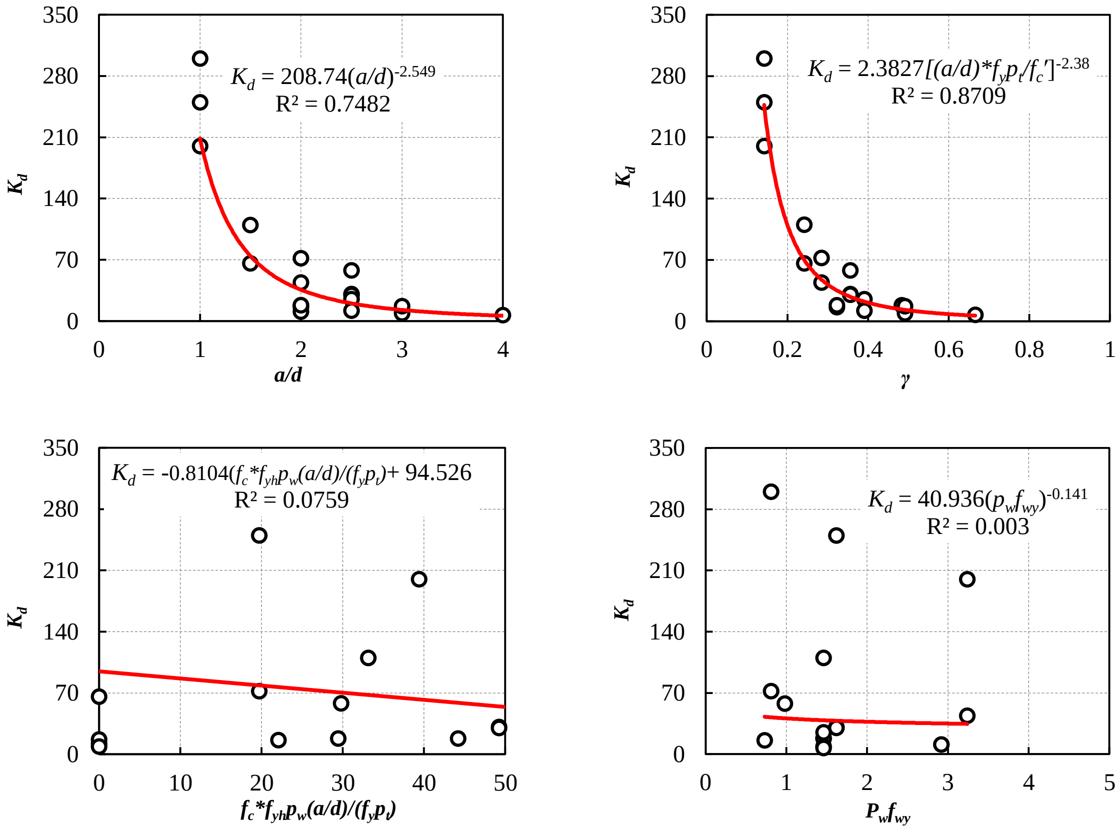

Fig.4- 16 Relationships between measured K_d and main factors

Based on the results shown in Fig.4-16, the following equation cab be derived to evaluate the degradation slope.

$$K_d = 2.84 \cdot \left(\frac{a}{d} \frac{p_t f_y}{f_c'} \right)^{-2.26} \tag{4-10}$$

Herein, K_d is shear strength degradation slope, (*N/rad, rad in %*); a/d is shear span ratio; p_t is the ratio of tension longitudinal bar; f_y is the yielding strength of longitudinal bar, (N/mm^2); f_c' is compressive strength of LQFA, (N/mm^2).

4.4.2 Residual shear capacity Q_r and corresponding deformation R_r

As shown in Fig.4-16, transverse stirrups maintained their shear resistance until large deformation, but the shear resistance by concrete exhibited significant degradation. While the shear resistance by concrete in several specimens maintained a little value at large deformation, but this residual capacity is so little as to be ignored as compared with the constant shear resistance by stirrups. For simplicity, the residual shear capacity of LQFA concrete members can be obtained by Eq. (4-11).

$$Q_r = Q_{su} \tag{4-11}$$

After determining the residual shear capacity Q_r by Eq. (4-11), the corresponding chord rotation or drift ratio R_r can be simply obtained as the abscissa of the intersection point of the degrading straight line and the horizontal line expressed as follow:

$$R_r = R_u + \frac{Q_u - Q_r}{K_d} = R_u + \frac{Q_{cu}}{K_d} \tag{4-12}$$

4.4.3 Complete shear capacity curve

After determining four critical parameters and denoting the shear resistance at a given drift level R as Q_n, the complete shear capacity curve can be defined as follows:

$$Q_n = \begin{cases} Q_u, & R \le R_u \\ Q_u + K_d\left(R - R_u\right), & R_u < R \le R_r \\ Q_r, & R > R_r \end{cases} \tag{4-13}$$

where Q_u, R_u, Q_r, K_d and R_r are given by Eq. (4-7), Eq. (4-9) through Eq. (4-12), respectively.

4.4.4 Verification of the proposed model

Fig.4-17 shows comparisons between the experimental *Q-R* curves and the predicted ones by Eq. (4-13) for LQFA concrete beams describes in this chapter. From Fig.4-17, one can see that the calculated shear capacity curves agree fairly well with the measured ones.

To further clarify applicability and accuracy of the proposed model, Eq. (4-13) is applied to predict the failure mode of the circular LQFA concrete columns reported in the previous two chapters of this paper. When applying the proposed model to the circular concrete columns, it should be noted that the flexural strength Q_{my}, which is necessary in the calculation of the ultimate drift ratio R_u by Eq. (4-9), is to be calculated by the method proposed by Sun et al. [4.14]. In addition, the circular steel tubes used to confine concrete will be taken as circular stirrups with a spacing of zero without limitation on p_w, which has been assigned an upper limit of 1.2% for conventional stirrups in current Japanese code. The calculated shear capacity curves of circular columns by Eq. (4-13) are compared with the measured *Q-R* relationships in Fig.4-18. Two calculated curves are depicted in Fig. 4-18 for the columns confined by steel plates. One is obtained without limitation on p_w, and the other with the upper limitation of 1.2% on p_w.

For the three specimens (FANUS, FANSB) which were described and failed in shear failure at large deformation, the calculated shear capacity curves trace the envelope curves of hysteretic behavior of them with relatively high accuracy. In particular, in the case of specimens FANUS and FANSB, both of which were confined by conventional circular stirrups, the calculated shear capacity curves predicted the ultimate drift ratio and the degradation slope very well. For the other circular LQFA concrete columns in which shear failure did not occur till the end of tests, the calculated shear capacity curves Eq. (4-13) are all beyond the envelope curves until large drift ratio without intersecting with them.

From above-mentioned observations, it can be said that the proposed shear capacity curve is sufficiently accurate to predict if and when LQFA concrete members, circular and/or rectangular, fail in shear. This model obviously enables structural engineers to conduct reliable and reasonable design for sustainable and resilient concrete members.

Table 4- 6 Calculations of shear strengths of test columns

Specimen	f_c' *(mm)*	Transverse reinforcement				V_{Exp} *(kN)*	V_{Cal}*(kN)*		R_u*(%)*	
		p_w *(%)*	*t* *(mm)*	P_{w+t} *(%)*	P_{w+t} *(1.2%)*		P_{w+t} *(%)*	P_{w+t} *(1.2%)*	P_{w+t} *(%)*	P_{w+t} *(1.2%)*
FANSB	79	0.85	-	0.85	0.85	230	318	318	2.55	2.55
FATSB	79	0.28	3.2	2.78	1.2	313	825	495	4.43	2.58
FANUS	77	0.85	-	0.85	0.85	261	318	318	2.70	2.70
FATUS	74	0.28	3.2	2.78	1.2	318	821	491	5.07	2.95
CFABY26	65	0.28	1.6	1.55	1.2	300	530	463	3.19	2.76
CFAWY26	70	0.28	1.6	1.55	1.2	312	538	471	3.34	2.90
CFABN26	65	0.28	1.6	1.55	1.2	257	530	463	3.19	2.76
CFABY13	72	0.28	1.6	1.55	1.2	287	538	470	3.20	2.78

Note: p_w is ratio of shear reinforcement; *t* is thickness of steel plates; p_{w+t} is ratio of transverse reinforcement considering effect of steel plates $=p_w+2t/(D+2t)$; p_{w+t} (1.2%) is the the upper limitation of transverse reinforcement for specimens confined by steel plates; V_{Exp} is experimental shear strengths of test columns; V_{Cal} is calculated shear strengths of test columns; R_u is shear strength degradation starting point;

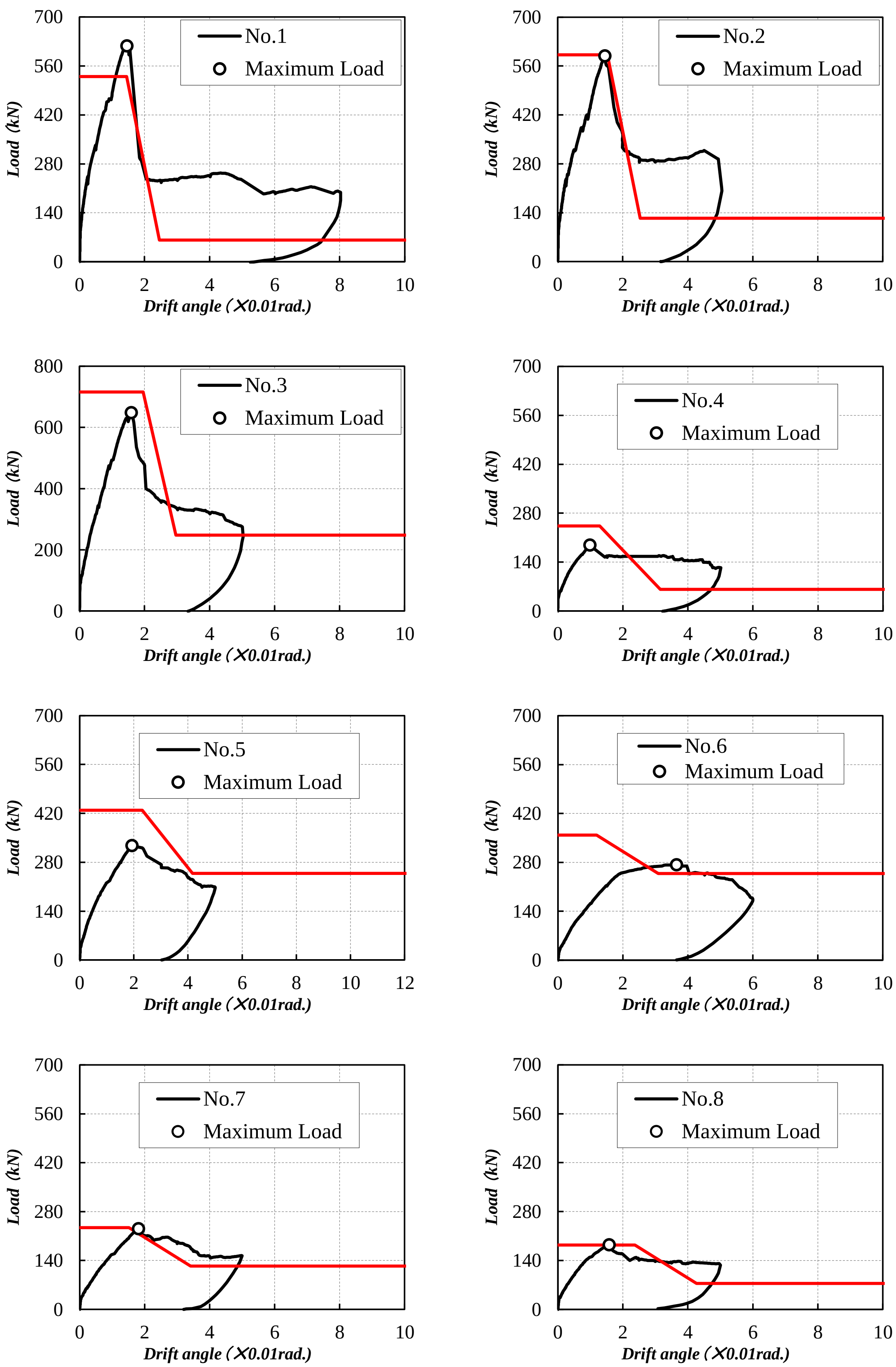

Fig. 4-17 Comparison results of rectangular LQFA concrete beams(Continued)

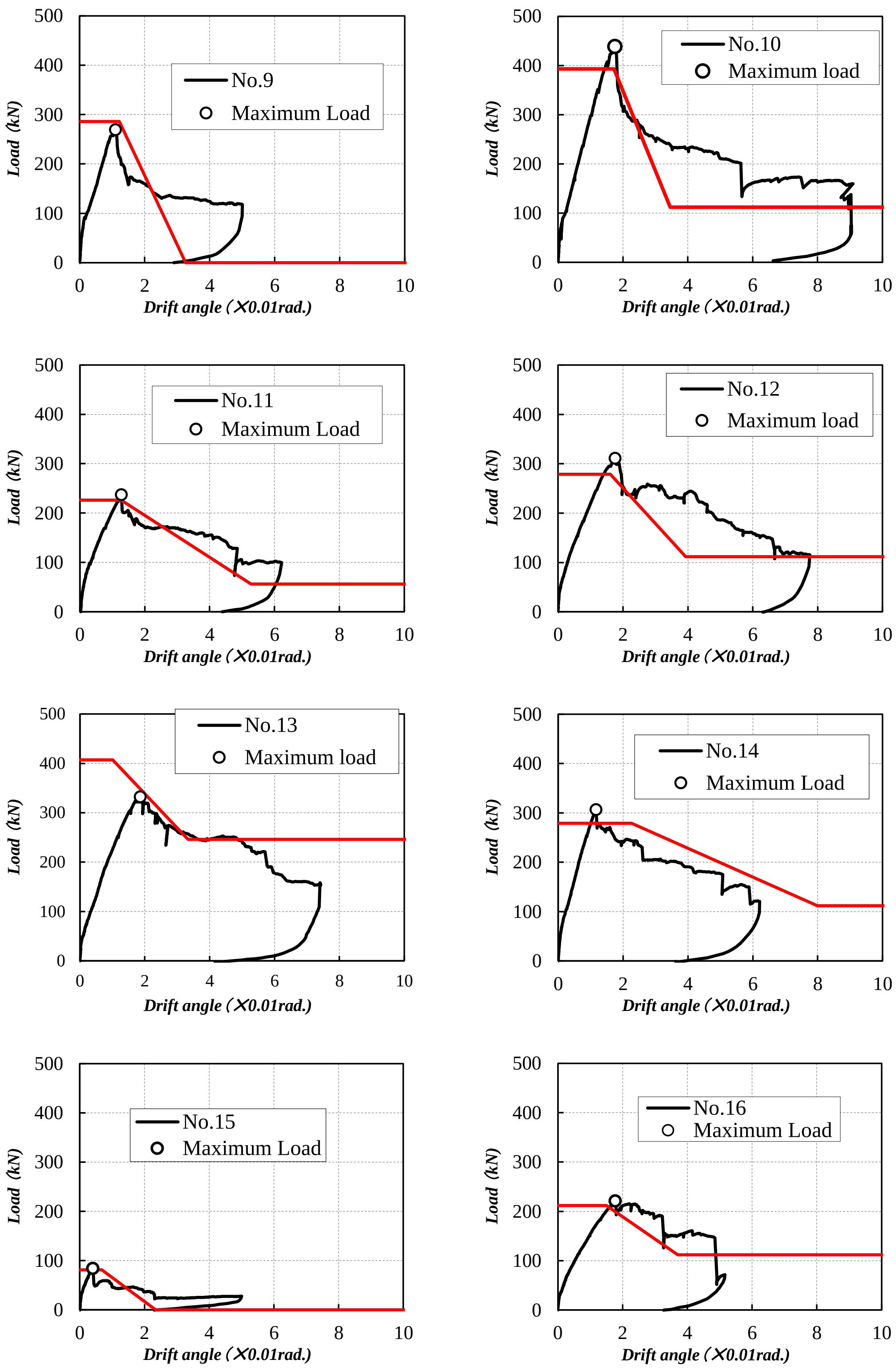

Fig.4-17 Comparison results of rectangular LQFA concrete beams(Continued)

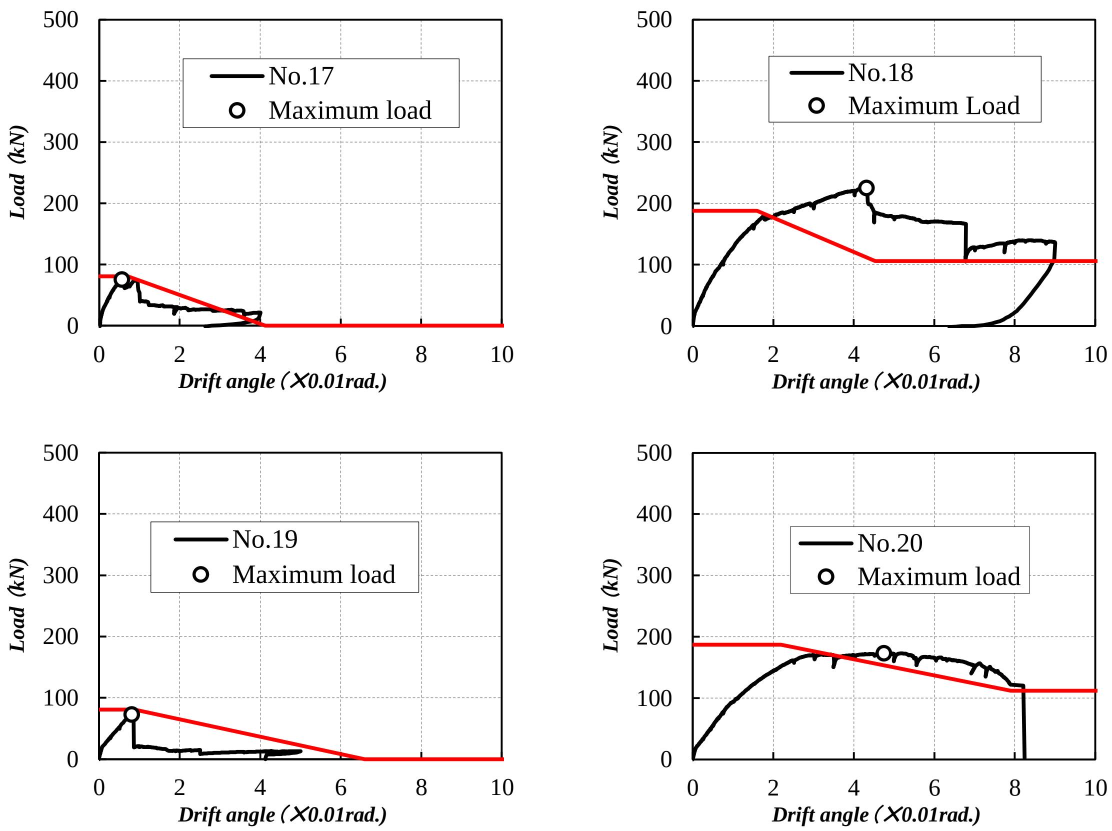

Fig.4- 17 Comparison between the calculated shear capacity curves and the experimental results of rectangular LQFA concrete beams

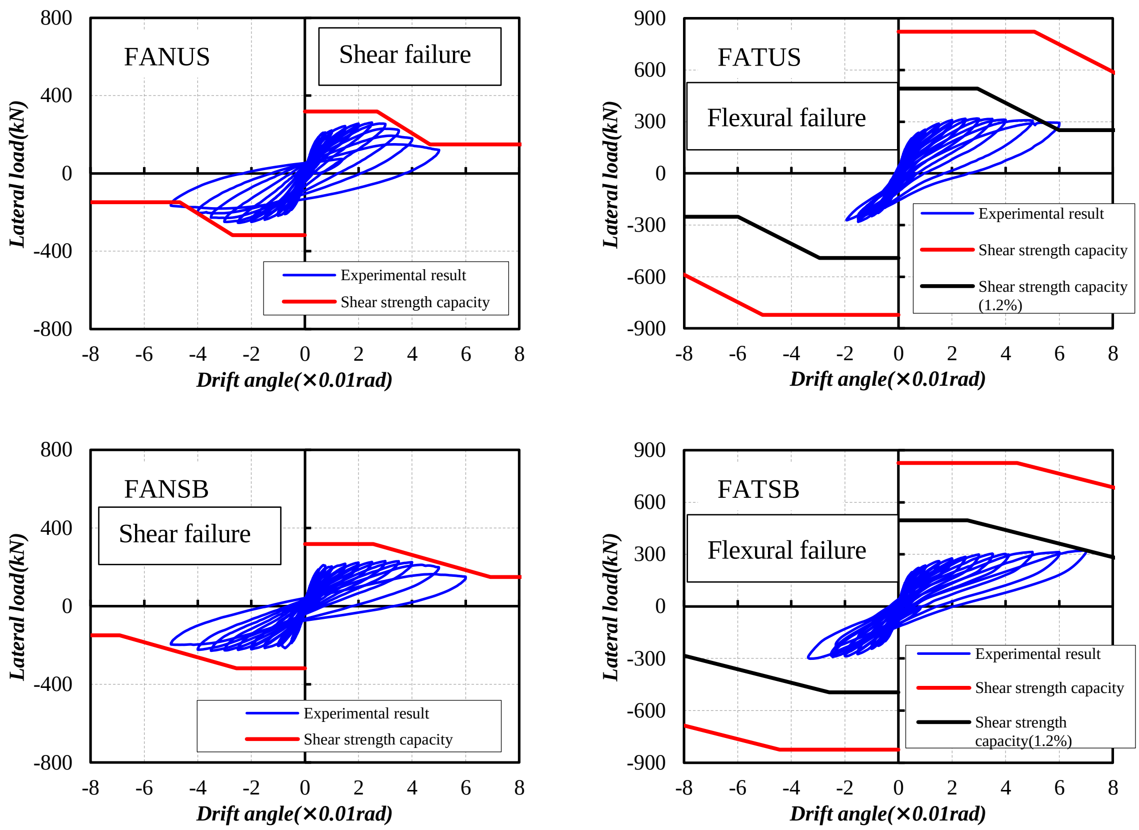

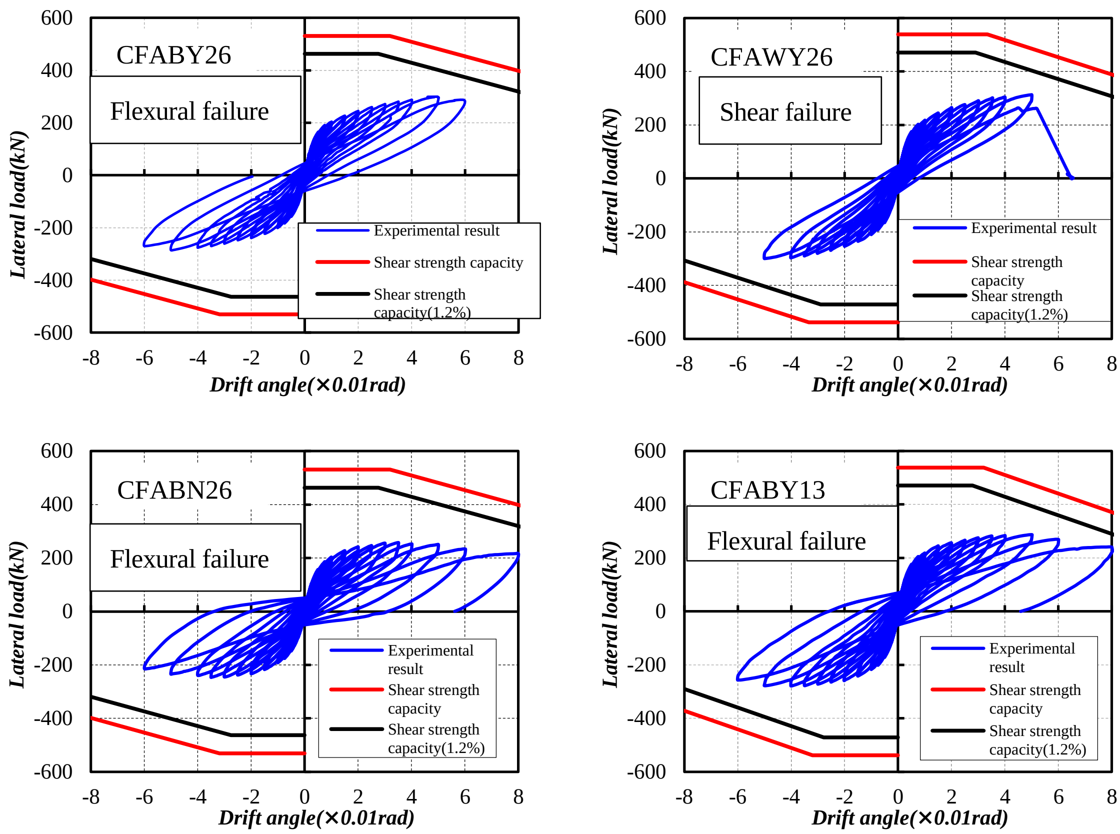

Fig.4- 18 Comparison between the calculated shear capacity curves and the experimental results of circular LQFA concrete columns

4.5 CONCLUSIONS

Twenty concrete beams were tested under combined shear and bending in order to obtain basic information on the shear behavior of LQFA concrete beams with emphasis placed on the evaluation of ultimate shear strength and deformability. The fly ash was used to primarily replace fine aggregate and the replacement level of fly ash was 455 kg/m^3 for all specimens. Based on the test results, a complete shear capacity model were developed to trace the variation of shear resistance of LQFA concrete members along with deformation (chord rotation or drift ratio). From the experimental and analytical works described in this chapter, the following conclusions can be drawn:

1) While the compressive strength of LQFA concrete was beyond 70 MPa, shear failure of LQFA concrete beam occurred along a primary diagonal plane by about 45-degree with respect to the beam axis as observed in general normal-strength concrete beams despite the difference in the shear span and the steel ratio of stirrups.

2) The shear resistance by the concrete in LQFA concrete beams was strongly affected by the shear span (*a/d*) ratio, a factor indirectly accounting for the so-called size effect of structural member on the concrete strength. For the short LQFA concrete beams with the *a/d* ratio of 1.0, the ultimate shear strength and chord rotation depended more upon the shear span ratio than the steel ratio of stirrups. Increasing the steel ratio of stirrup from 0.19% to 0.76% only brought about 10% increment in ultimate shear strength and chord rotation. On the other hand, for the LQFA concrete beams with the *a/d* ratio larger than 1.5, the ultimate shear strength and chord rotation increased significantly along with the steel amount of stirrup.

3) Based on the equilibrium of the forces acting on the diagonal shear plane and Mohr-Coulomb criteria for LQFA concrete, equations (Eq. (4-7) and Eq. (4-8)) were developed to predict the ultimate shear strength of rectangular and circular LQFA concrete members, including beams and columns. These equations can reasonably and accurately account for effect of the shear span ratio on the shear resistance by LQFA concrete, and give more accurate prediction of the measured shear strength than the equations prescribed in current design codes. The ratio of the experimental/calculated shear strength has a mean value of 1.02, and a standard deviation of 0.14.

4) The ultimate chord rotation or drift ratio of LQFA concrete members exhibited very strong correlation with the factor β, which is the ratio of the calculated shear strength to the calculated flexural strength. A linear equation (Eq. (4-9)) was proposed to predict the ultimate deformation. The proposed equation gives a relatively accurate prediction of the measured results. The ratio of the experimental/calculated deformation has a mean value of 0.99, and a standard deviation of 0.21.

5) On the basis of test results of LQFA concrete beams which failed in shear, a complete shear capacity curve for LQFA concrete members was developed. The proposed model defines the shear resistance of LQFA concrete members as a multi-linear function of drift ratio or chord rotation, and hence can trace the change or degradation of shear strength along with deformation. The predicted shear capacity curves exhibited fairly good agreement with the measured results of both rectangular LQFA concrete beams and circular LQFA concrete columns, which implies reliability and accuracy of the proposed model.

6) Due to their simplicity and accuracy, the proposed equations enable structural engineers to conduct reasonable and reliable shear design of LQFA concrete members, promoting the application of LQFA concrete to building structures and contributing to reducing environmental burden by concrete industry.

REFERENCES

[4.1] Kim, J., Zhu, H. J., Tani, M., Okada, A., "Accuracy Verification of Ultimate Strength Calculation Formula of Circular RC Columns, " Proc. of JCI, V.33, No.2, 2011, pp. 193-198.[In Japanese]

[4.2] Cai, G. C., "Seismic Performance and Evaluation of Resilient Circular Concrete Columns," Kobe University, 2014.

[4.3] Architectural Institute of Japan (AIJ). "AIJ standard for Structural Calculation of Reinforced Concrete Structures," Architectural Institute of Japan, Toukyou.

[4.4] Architectural Institute of Japan, "Japanese Architectural Standard Specification 5 – Construction of Reinforced Concrete Structures," AIJ; Maruzen, Tokyo, 2005. [in Japanese]

[4.5] Matsufuji, Y., Koyama, T., Funamoto, K., Ito, K., "Mix Proportion Principle of Concrete Containing Large Quantity of Coal Ash with Constant Cement Content," Concrete Research and Technology, Japan Concrete institute 2001; V.12, No.2, 2001, pp.51-60.

[4.6] Sun, Y. P., Miyake, Y., "Proposed Calculation Formula of Ultimate Shear Strength of RC Circular Cross-section Column, " Proc. of JCI, V.27, No.2, 2005, pp. 229-234. Ghee, A. B., Priestley, M. J. N., and Paulay, T., "Seismic Shear Strength of Circular Reinforced Concrete Columns," ACI Structural Journal, V.86, No.1, 1987, pp. 45-59.

[4.7] ACI Committee 318, "Building Code Requirements for Structural Concrete (ACI 318-08) and Commentary. ACI," American Concrete Institute, Farmington Hills.

[4.8] GB50010-2010. "Code for design of concrete structures," China Academy of Building Research, Beijing.

[4.9] Caltrans. (1995) "Memo to Designers Change Letter 02," California Department of Transportation, Sacramento, Calif., March.

[4.10] Priestley, M. J. N., Verma, R., and Xiao, Y., "Seismic Shear Strength of Reinforced Concrete Columns," Journal of Structural Engineering, ASCE, Vol. 120, No. 8, August, 1994, pp. 2310-2329.

[4.11] Xiao, Y., and Martirossyan, A., "Seismic Performance of High-Strength Concrete Columns," Journal of Structural Engineering, ASCE, V. 124, No. 3, 1998, pp. 241-251.

[4.12] Sezen, H. and Moehle, J. P., "Shear strength model for lightly reinforced concrete columns." Journal of Structural Engineering, ASCE, Vol.130, No.11, 2004, pp.1692-1703.

[4.13] Sun, Y.P., and Sakino K., "Simplified design method for ultimate capacities of circularly confined high-strength concrete columns," ACI special publication 193, 2000, pp. 571-586.

Chapter 5

Modeling of Capacity Curve of Circular LQFA Concrete Columns Reinforced by SBPDN Rebars

5.1 INTRODUCTION

Tests described in chapters two and three have indicated that combination of LQFA concrete, SBPDN rebars and steel plate jacketing is very effective in making sustainable and resilient concrete columns. Since the LQFA concrete columns exhibit stable increment in lateral resistance till large drift level, current seismic design methodology, for example, the ultimate capacity design method recommended in Japanese construction laws, obviously does not fit for them. Therefore, in order to promote the application of LQFA concrete columns in actual building structures, capacity curve of them needs to be developed.

The capacity curve of a LQFA concrete column defines the relationship between lateral resistance and drift ratio of the column, and is indispensable to the performance-based seismic design and nonlinear dynamic analysis of the structures made of LQFA concrete columns. Besides, a sound capacity curve is also useful for predicting the ultimate failure mode of a LQFA concrete member as shown in Fig.5-1, and helping structural engineers to avoid premature and undesirable failure mode of the member and structure.

Objectives of this chapter are listed as below:

1) Development of a simple method to evaluate the capacity curve of circular LQFA concrete columns reinforced by SBPDN rebars. This method is supposed to be able to

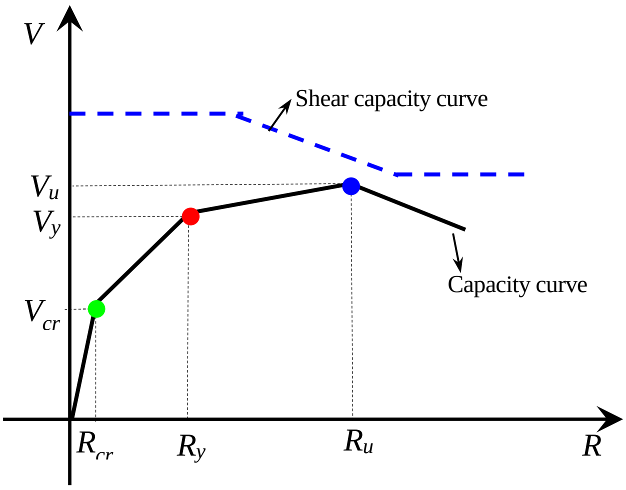

(a) Flexural failure

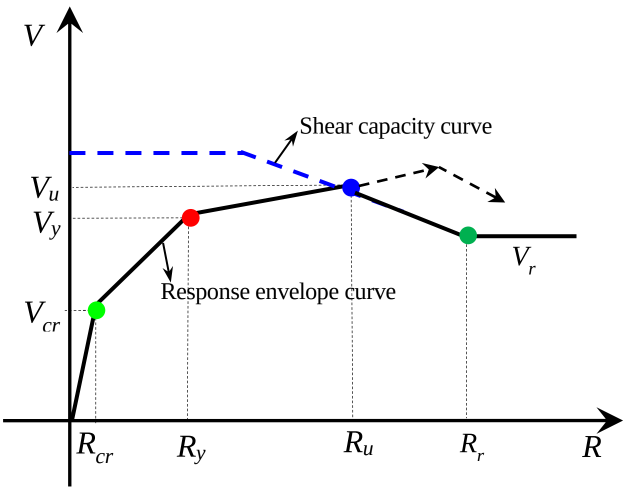

(b) Shear failure

Fig.5- 1 Prediction of failure mode of LQFA concrete members with SBPDN rebars

account for the effect of the bond slip of SBPDN rebars on the seismic capacity curve.

2) Proposal of a complete lateral resistance versus drift ratio model to depict the envelope curve of the hysteretic behavior of LQFA concrete columns. This model is intended to more simply and reasonably evaluate the performance point and predict the potential failure mode of frame structures made of LQFA concrete columns reinforced by SBPDN rebars.

5.2 SIMPLIFIED METHOD TO EVALUATE LATERAL RESISTANCE VERSUS DRIFT RATIO RELATIONSHIP OF LQFA CONCRETE COLUMNS REINFORCED BY SBPDN REBARS

Funato et al. [5.1] have proposed an integrated analytical method for the evaluation of cyclic behavior of concrete columns reinforced by normal-strength and high-strength rebars. The proposed method can account for the effects of primary structural factors, including confinement degree by transverse steels (conventional stirrups or spirals and steel tubes) and bond slippage of longitudinal rebars, on the cyclic response. This method, however, involves tedious doubly-looped iteration procedures to find the balanced depth of neutral axis in the targeted column section and to obtain the slippage of longitudinal rebars from their anchorage zones [5.1].

For structural engineers to conduct prompt and accurate seismic design of the LQFA concrete columns reinforced by SBPDN rebars, a simplified method is desirable.

5.2.1 Basic assumptions

The simplified analytical method consists of conventional finite fiber method (FFM) for the moment-curvature analysis of column section and the concept of lumped hinge region, within which the flexural displacement is concentrated. The proposed method is based on the following assumptions:

1） The tensile strength of concrete can be ignored.
2） Concrete section of column remains plane after bending.
3） The length of plastic hinge region of column can be taken as 1.0 D (D is the diameter of column section).
4） The total tip displacement includes those caused by flexural deformation, shear distortion and slippage of longitudinal rebar as shown in Fig.5-2.
5） The stress-strain relationships of materials are known. Details of them will be given later.
6） Bond slippage of longitudinal SBPDN rebar can be approximated by the total elongation of the rebar embedded in the anchorage zone.

The first three assumptions have been well adopted to the performance analysis of concrete columns. The fourth assumption is intended to include the displacement by shear distortion and bond slippage of longitudinal rebars. In current design codes [5.2, 5.3], when predicting deformation capacity of concrete columns, only deformation due to flexure within plastic hinge region is considered. Ignorance of the bond slippage is acceptable for the columns reinforced by general deformed rebars because high bond-strength of deformed rebars keeps the deformation due to slippage to an ignorable level [5.4]. As observed in chapter two and chapter three, however, ignorance of bond slippage may result in large discrepancy between the experimental capacity curve and the calculated one for the concrete columns reinforced by SBPDN rebar, whose bond-strength is only about one-fifth of that of deformed rebar [5.1].

From the fourth assumption, the total displacement of concrete column can be written as

$$\Delta = \Delta_f + \Delta_s + \Delta_{slip} \tag{5-1}$$

where Δ_f, Δ_s and Δ_{slip} represent the displacement by flexural deformation, shear distortion and steel slippage, respectively. Based on the concept of lumped hinge and the third assumption, the displacement due to flexural deformation can be obtained by Eq. (5-2) (see Fig.5-3).

$$\Delta_f = \begin{cases} \phi L^2/3, & \phi \le \phi_y \\ \Delta_y + (\phi - \phi_y) L_p (L - 0.5 L_p), & \phi > \phi_y \end{cases}; \quad \Delta_y = \frac{\phi_y L^2}{3} \tag{5-2}$$

Where ϕ is the curvature of column section in hinge region, ϕ_y is the yield curvature, L is shear span, L_p is the length of plastic hinge of column.

Since there has been little information available on the extent or degree that inelastic shear deformation occupies in the total displacement, only the displacement by elastic shear distortion will be taken into consideration. Besides, it has been well known that for the concrete columns with common proportion, the percentage of shear displacement in the total displacement is very small as compared with the flexural displacement. Then the displacement due to shear deformation can be obtained by Eq. (5-3).

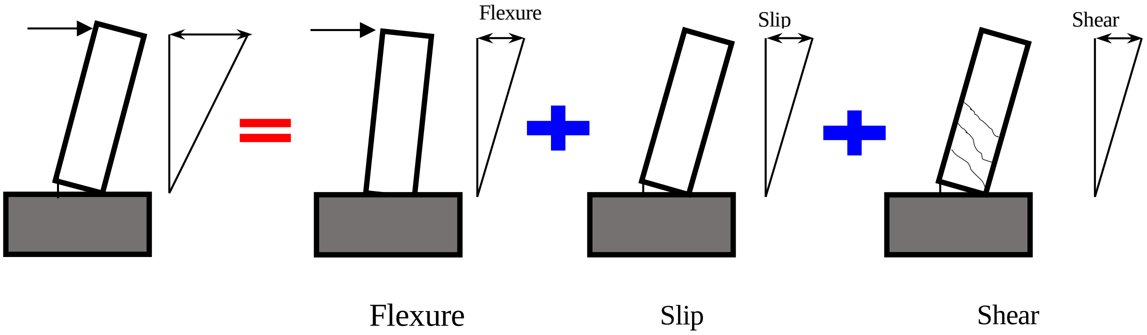

Fig.5- 2 Components of displacement in a typical concrete column

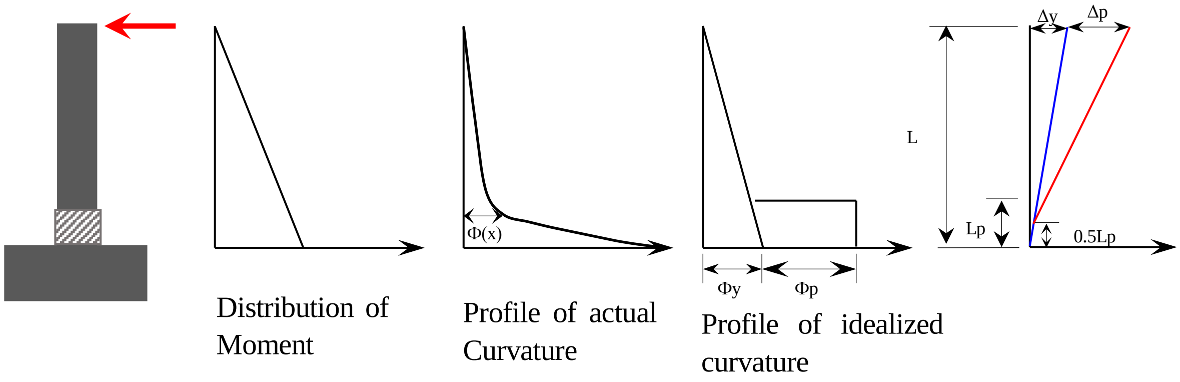

Fig.5- 3 Concept of lumped hinge for flexural deformation

$$\Delta_s = \frac{VL}{AG} = \frac{2(1+\mu)VL}{AE_c} \tag{5-3}$$

Where V is the shear force, G and E_c are the elastic shear modulus and elastic modulus of concrete, respectively, and μ is Poisson′s ratio of concrete and will be taken as 0.167.

The fifth and sixth assumptions will be described below in details.

5.2.2 Stress-strain relationships of materials

5.2.2.1 Stress-strain relationship of concrete

Reliability and accuracy of the analytical capacity curves for LQFA concrete columns are dependent upon the accuracy of the constitutive laws adopted for the materials, concrete and steels. This paper will adopt the compressive stress-strain model proposed by Sun and Sakino [5.5] for LQFA concrete, because reliability and accuracy of this model have been verified by many researchers for general concrete members without fly ash. Fig.5-4 displays outlines of the stress-strain models.

According to the model by Sun and Sakino, for a given strain ε_c, the corresponding stress of concrete f_c can be obtained as follow:

$$f_c = Kf_p \frac{aX + (b-1)X^2}{1 + (a-2)X + bX^2} \tag{5-4}$$

Where, $K=f_{cc}/f_p$ is the strength enhancement ratio of concrete confined by conventional spirals or stirrups and steel tubes, f_p is the unconfined concrete strength, which is taken as 0.85 of the strength of concrete cylinder, f_{cc} is the confined concrete strength, a is the factor governing the ascending portion, b is the factor governing the shape of descending portion, and X is the nominal strain of concrete $=\varepsilon_c/\varepsilon_{co}$, where, ε_{co} is the peak strain of confined concrete.

The parameters for determining the stress-strain relationship can be obtained as follows:

$$K=\frac{f_{cc}}{f_p}=\begin{cases}1+2.05\left(1-\dfrac{s}{2D_c}\right)^2\cdot\dfrac{\rho_h f_{yh}}{f_p}, & \text{hoop}-\text{confinement}\\ 1+4.1\left(\dfrac{2}{D'/t-2}\right)\cdot\dfrac{f_{yt}}{f_p}, & \text{tube}-\text{confinement}\end{cases} \tag{5-5}$$

$$\begin{gathered}a=\frac{E_c}{E_{\sec}}=\frac{E_c\varepsilon_{c0}}{Kf_p},\quad b=1.5-0.017f_p+\gamma\sqrt{\frac{(K-1)f_p}{23}}\\ E_c=\left(0.69+0.332\sqrt{f_p}\right)\times10^4,\ \gamma=\begin{cases}1.6, \text{hoop - confinement}\\ 2.4, \text{tube - confinement}\end{cases}\end{gathered} \tag{5-6}$$

$$\begin{gathered}\frac{\varepsilon_{c0}}{\varepsilon_0}=\begin{cases}1+4.7(K-1), & K\le1.5\\ 3.35+20(K-1.5), & K>1.5\end{cases}\\ \varepsilon_0=0.94\left(f_p\right)^{1/4}\cdot10^{-3}\end{gathered} \tag{5-7}$$

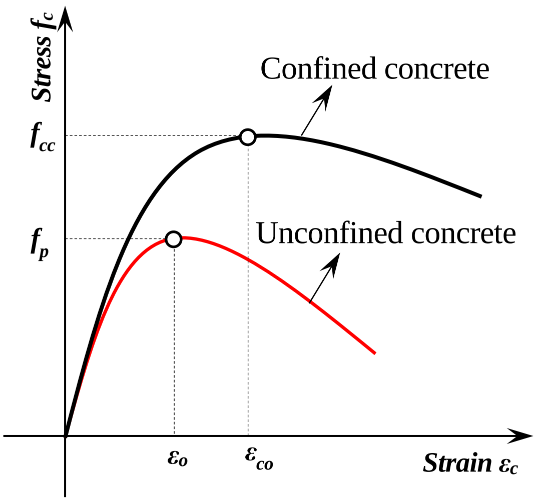

Fig.5- 4 Stress-strain relationship of concrete

In Eq. (5-6) and Eq. (5-7), s is the spacing of transverse steels including stirrups and tubes, D_c is the diameter of confined core section, ρ_h is the volumetric ratio of transverse steels, f_{yh} and f_{yt} are the yield strength of stirrups and that of steel tubes, respectively, E_c is the young modulus of unconfined concrete, E_{sec} is the secant modulus of confined concrete at the peak.

5.2.2.2 Stress-strain relationship of longitudinal rebar

The SBPDN rebar exhibits nonlinear stress-strain behavior when axial strain is beyond the yield strain ε_y as shown in chapter two or chapter three. For simplicity, a bilinear model will be used to approximate the stress-strain curve of steel rebar in form of

$$f_s = \begin{cases} E_s \varepsilon_s, & \varepsilon_s \le \varepsilon_y \\ f_y + 0.01E_s(\varepsilon_s - \varepsilon_y), & \varepsilon_s > \varepsilon_y \end{cases} \tag{5-8}$$

Where, f_s and ε_s are the stress and strain of steel, respectively, E_s is the Young's modulus, f_y and ε_y are the yielding strength and strain of steel, respectively. Fig.5-5 shows the stress-strain model for steel rebar.

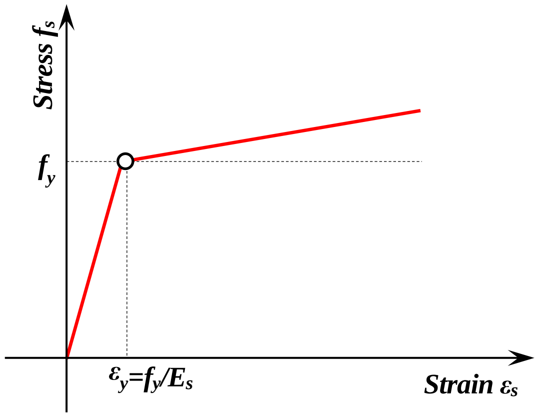

Fig.5- 5 Idealized stress-strain relationship of steel

5.2.3 Displacement due to the slippage of longitudinal rebars

In conventional analysis of structural properties of concrete members, effect of the slippage of longitudinal rebars is generally ignored if the rebars have sufficiently long anchorage or are soundly anchored by certain methods. However, due to the penetration of axial strain along anchorage length of the tensile rebars embedded inside the beam-column joint or base beam or base column, and the deterioration of bond resistance between the rebar and surrounding concrete due to cycling of external forces, the slippage of longitudinal rebars at the interface section on the total displacement may become significant, in particular for the concrete members reinforced by the rebars having low bond strength.

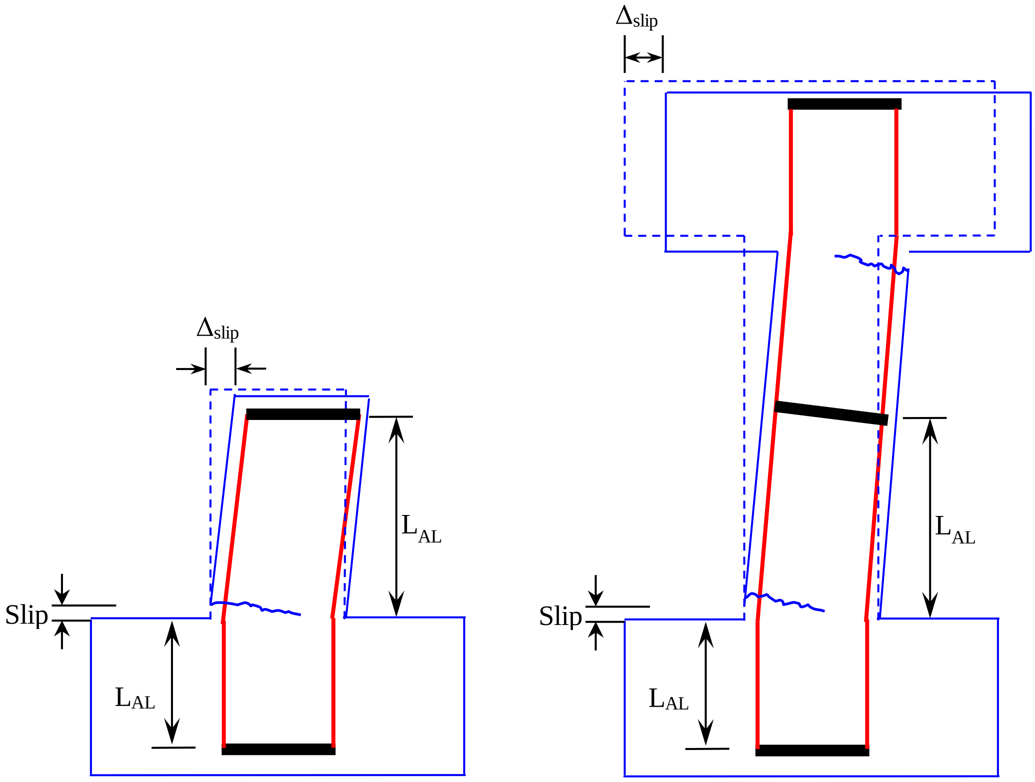

Fig.5- 6 Displacement due to slippage of tensile rebars

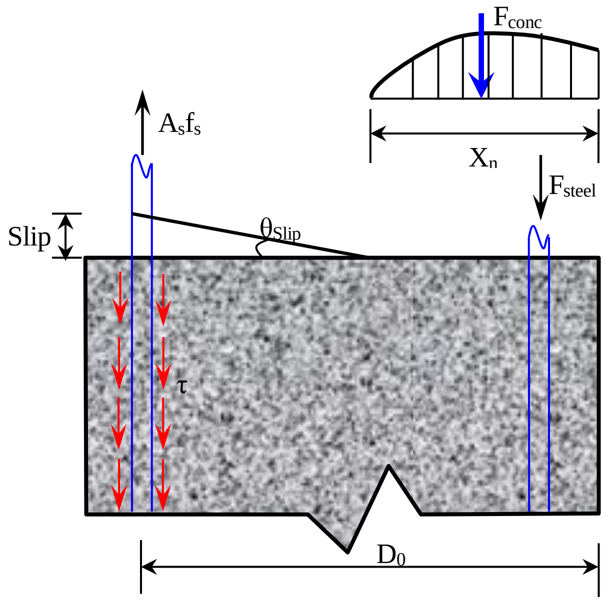

Fig.5- 7 Diagram of cross section at interface

The slippage of tensile rebars may result in additional fixed-end rotation and increase the total lateral displacement considerably. The displacement due to slippage of tensile rebars is illustrated in Fig.5-6 for cantilever column as well as beam-column. Fig.5-7 shows the way to evaluate the fix-end rotation (θ_{slip},) induced by the slip of tensile SBPDN rebar at the interface section or the end section of column.

It is obvious from Fig.5-6 and Fig.5-7 that rotation of the end section θ_{slip} and the displacement Δ_{slip} due to slippage of tensile rebars can be calculated by Eq. (5-9) and Eq. (5-10), respectively.

$$\theta_{Slip} = \frac{S_{lip}}{D_0 - X_n} \tag{5-9}$$

$$\Delta_{Slip} = \begin{cases} \theta_{Slip} \cdot L, & cantilevercolumn \\ \left(\theta_{Slip,top} + \theta_{Slip,bottom}\right) \cdot L, & beam\text{-}colum \end{cases} \tag{5-10}$$

where, θ_{slip} is fixed-end rotation, S_{lip} is the slippage of longitudinal rebar, D_0 is the distance from the centroid of tensile rebars to the extreme compressive fiber of column section, and X_n is the depth of neutral axis.

As obvious from Eq. (5-10) and Fig.5-6, the displacement due to slippage of beam-columns can be represented by that of cantilever columns. Therefore, the discussion will be limited to cantilever columns hereafter.

Fig.5-9 illustrates outlines of the calculation of the S_{lip}. There are five cases for the S_{lip} to be calculated, according to the axial strain of longitudinal rebar at beam-column interface and the anchorage length of SBPDN rebars (l_{AL}). In the case that the axial strain of longitudinal bar at beam-column interface does not reach yielding strain, as shown in Fig.5-8 (a), the bond stress of tensile rebars (τ_u) is assumed to be constant and equal to the bond strength of longitudinal rebar within the necessary development length (l_d) for simplicity. However, for the case that the tensile longitudinal rebar at beam-column interface reaches yielding, as shown in Fig.5-8 (b), the bi-linear bond stress-slip model is adopted [5.6], in which the uniform bond stress is taken as half of the bond strength (τ_u), as shown in Fig.5-9 (Case two and Case five). From the equilibrium of the axial forces, l_d can be obtained as follow

$$l_d = \frac{f_{se} d_b}{4\tau_u} \tag{5-11}$$

where d_b is the nominal diameter of tensile SBPDN rebar; f_{se} is the stress of longitudinal bar at beam-column interface. The S_{lip} corresponding to each case shown in Fig.5-9 can be obtained as follows:

Case one $\varepsilon_{se} < \varepsilon_y$:

$$S_{lip} = \frac{\varepsilon_{se} l_d}{2},\ f_{se} = E_s \varepsilon_{se},\ l_d = \frac{f_{se} d_b}{4\tau_u} \tag{5-12}$$

Case two $\varepsilon_{se}>\varepsilon_y$:

$$S_{lip}=\frac{\varepsilon_y l_{dy}}{2}+\frac{l_{dn}}{2}\left(\varepsilon_{se}+\varepsilon_y\right), l_{dy}=\frac{f_y d_b}{4\tau_u}, l_{dn}=\frac{\left(f_{se}-f_y\right)d_b}{2\tau_u} \tag{5.13}$$

Case three $l_{AL}>l_d$ and $\varepsilon_{se}<\varepsilon_y$:

$$S_{lip}=\frac{\varepsilon_{se} l_d}{2},\ l_d=\frac{f_{se} d_b}{4\tau_u},\ \varepsilon_{se}=\frac{f_{se}}{E_s} \tag{5-14}$$

Case four $l_{AL}<l_d$ and $\varepsilon_{se}<\varepsilon_y$:

$$S_{lip}=\frac{l_{AL}}{2}\left(\varepsilon_{se}+\varepsilon_{so}\right), \varepsilon_{se}=\frac{f_{se}}{E_s}, \varepsilon_{so}=\frac{f_{so}}{E_s} \tag{5-15}$$

Case five $l_{AL}<l_d$, and $\varepsilon_{se}>\varepsilon_y$:

$$S_{lip}=0.5\left(\varepsilon_{se}+\varepsilon_y\right)\cdot l_{dn}+0.5\left(\varepsilon_y+\varepsilon_{s0}\right)\cdot l_{dy}, l_{dn}=\frac{\left(f_{se}-f_y\right)d_b}{2\tau_u} \tag{5.16}$$

where *Slip* is slip displacement of tension longitudinal bar at interface of beam-column interface; ε_{so} is axial strain at bottom of reinforcing bar; ε_{se} is axial strain at beam-column interface; f_{se} is stress of tension longitudinal bar at interface of beam-column; f_{s0} is stress at bottom of reinforcing bar; E_s is the young modulus of tension longitudinal bar; l_{dy} is development length of elastic region; d_b is diameter of reinforcing bar; ε_y is axial yield strain of reinforcing bar; f_y is yield stress of reinforcing bar; l_{dn} is length of the strain-hardening region; l_{AL} is basic anchorage length; τ_u is the bond strength of SBPDN rebar in MPa.

The bond strength of SBPDN rebar proposed by Funato et al. [5.1] will be adopted. According to the results of pull-out tests by Funato et al., the bond strength of SBPDN rebar, which was surrounded by concrete with compressive strength of 40 MPa, was about 3.0 MPa. On the other hand, it has been well known that the bond strength of rebars is generally influenced by the concrete strength [5.7], and therefore, it is necessary to modify the proposed bond strength for SBPDN rebar and to consider the high compressive strength of LQFA concrete. According to the CEB code [5.8], influence of compressive strength of concrete on the bond strength of rebar can be taken into account in form of

$$\tau=3.0\sqrt{\frac{f_c'}{40}} \tag{5-17}$$

where, f_c' is the compressive strength of concrete cylinder in MPa.

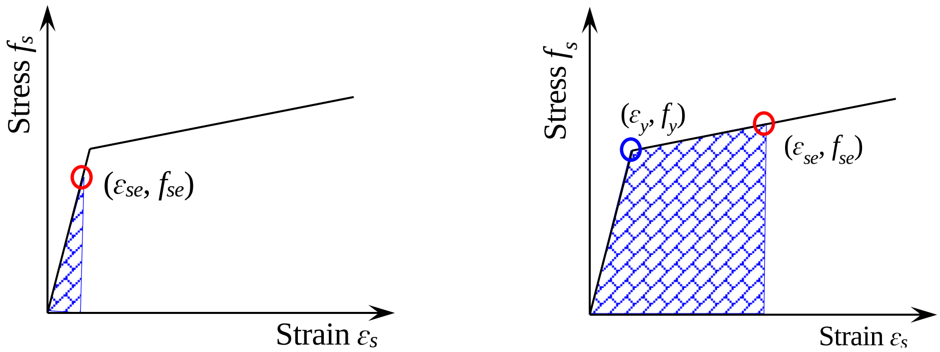

(a) Strain within elastic region (b) Strain beyond elastic region

Fig.5- 8 Calculation of stress of reinforcing bar at the top of anchorage region

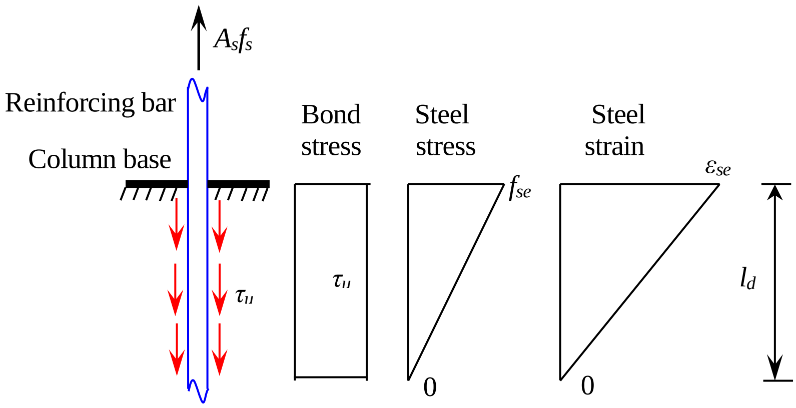

Case one

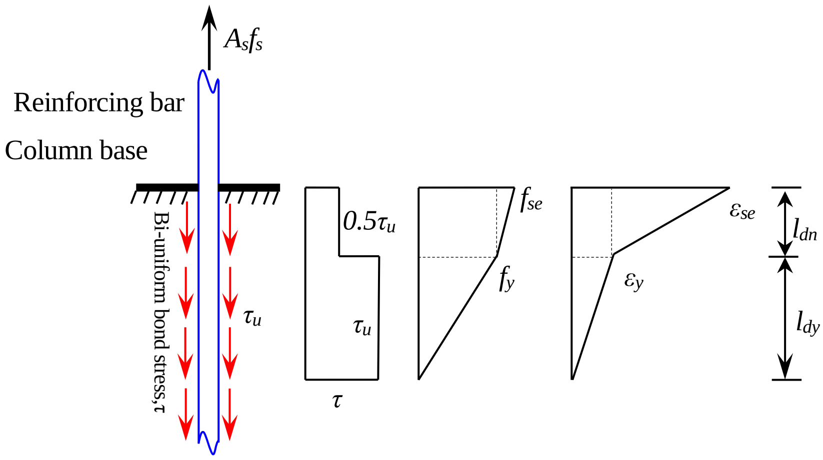

Case two

Fig.5-9 Strain and stress distribution of rebar in anchorage zone (Continued)

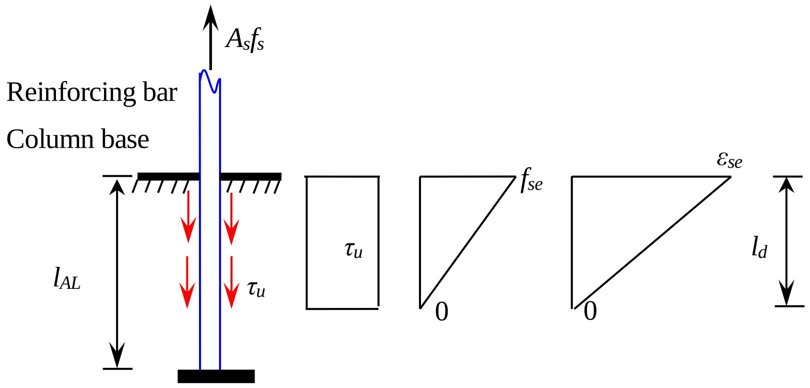

(c) Case three

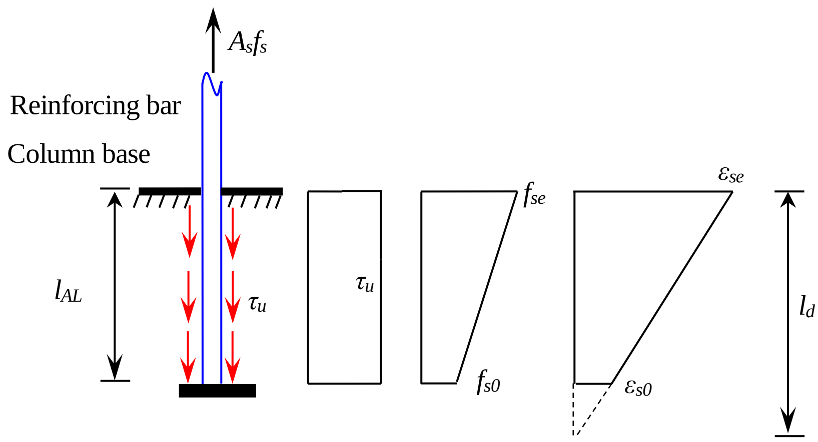

(d) Case four

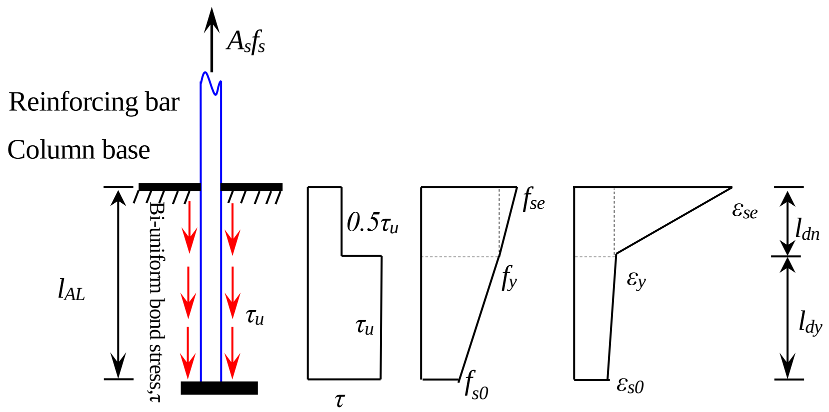

(e) Case five

Fig.5- 9 Strain and stress distribution of rebar in anchorage zone

5.2.4 Procedures of moment-curvature analysis

The widely used finite fiber method is adopted to conduct the moment-curvature analysis of the circular LQFA concrete columns. As shown in Fig.5-10, concrete in the circular section will be divided into N_{con} fibers, each of which has a same thickness but a varying width along the depth of section.

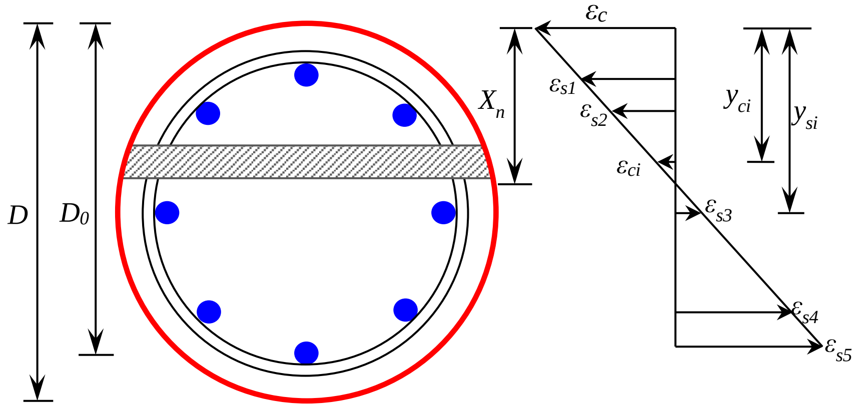

Fig.5- 10 Discretion of column section and strain profile

The procedures for computing the moment M_i corresponding to a given curvature ϕ_i can be summarized below.

1) Assume an initial value of the depth of neutral axis X_n.
2) On the basis of the second assumption above described, calculate the strains for the concrete fibers and the longitudinal steel layers as follow:

$$\varepsilon_{cj} = \left(X_n - y_{cj}\right)\phi_i, \quad \varepsilon_{sj} = \left(X_n - y_{sj}\right)\phi_i \tag{5-18}$$

where ε_{cj} is the strain of the j-th concrete fiber, ε_{sj} is the strain of the j-th layer of longitudinal rebars, y_{cj} is the distance measured from the extreme compressive fiber to the centroid of the j-th concrete fiber, y_{sj} is the distance from the extreme compressive fiber to the centroid of the j-th layer of rebars. Compressive strain is taken as positive.
3) Calculate the stresses of all concrete fibers and steel layers based on the stress-strain relationships assumed in this section.
4) Calculate the axial forces sustained by concrete and longitudinal rebars in form of

$$N_{ci} = \sum_{j=1}^{Ncon} A_{cj} \cdot f_{cj}, \quad N_{si} = \sum_{j=1}^{Ns} A_{sj} \cdot f_{sj} \tag{5-19}$$

where, N_{ci} is the axial force sustained by concrete, A_{ci} is the area of the j-th concrete fiber, f_{cj} is the stress of the j-th concrete fiber, N_s is the number of the steel layer, N_{si} is the axial load sustained by the j-th layer of longitudinal steels, A_{sj} and f_{sj} are the area and stress of the j-th layer of steels, respectively.
5) Determine the "true" depth of neutral axis by the following criterion.

$$\left|N_{ci}+N_{si}-N\right|\leq N_{res} \tag{5-20}$$

where N is the axial load applied and N_{res} is the unbalanced axial force. The N_{res} should be zero to ensure equilibrium of the axial forces acting on the column section. However, the zero N_{res} may lead to divergence of the calculation. To avoid the divergence of the calculation, the N_{res} is usually taken as about 0.5% of the applied external axial force N, which can give sufficiently accurate results.

6) If Eq. (5-20) is satisfied, the assumed X_n is the "real" depth of neutral axis, and then one can proceed to the next step. If not satisfied, then assume a new X_n and return to step 2.

7) Calculate the moment M_{ii} sustained by the column section using Eq. (5-21)

$$M_{ii}=\sum_{j=1}^{Ncon}A_{cj}\cdot f_{cj}\cdot\left(\frac{D}{2}-y_{cj}\right)+\sum_{j=1}^{Ns}A_{sj}\cdot f_{sj}\cdot\left(\frac{D}{2}-y_{sj}\right) \tag{5-21}$$

where, D is the diameter of column section.

8) Modify the calculated M_{ii} by Eq. (5-22) to obtain the moment M_i.

$$\frac{M_i}{M_{ii}}=\begin{cases}1.1, & \dfrac{N}{A_g f_p}\leq 0.3\\ 1.1+0.8\left(\dfrac{N}{A_g f_p}-0.3\right)^2, & \dfrac{N}{A_g f_p}>0.3\end{cases} \tag{5-22}$$

Eq. (5-22) is proposed by Sun et al. to account for the enhancement effect of the extra confinement by the stiff loading stub or beam-column joint on the moment resistance of the concrete columns that failed in ductile flexure [5.9]. Eq. (5-23) was proposed by Priestley et al. [5.10] to account for the effect of extra confinement by loading stub, and is written as reference in form of.

$$\frac{M_i}{M_{ii}}=\begin{cases}1.13, & \dfrac{N}{A_g f_p}\leq 0.1\\ 1.13+2.35\left(\dfrac{N}{A_g f_p}-0.1\right)^2, & \dfrac{N}{A_g f_p}>0.1\end{cases} \tag{5-23}$$

9) Calculate the strain and stress distribution of tensile longitudinal rebar over the anchored length, l_{AL}, by using Eq. (5-24) and Eq. (5-25), according to the calculated result of Eq. (5-19).

- $\boldsymbol{f_{se}\leq f_y}$:

$$f_{si} = f_{se} - \tau_u \cdot p_d \cdot l_i / A_s \tag{5-24}$$

- $f_{se} > f_y$:

$$f_{si} = \begin{cases} f_{se} - \dfrac{f_{se} - f_y}{l_{dn}} \cdot l_i, & l_i \le l_{dn} \\ f_y - \tau_u \cdot p_d \cdot (l_i - l_{dn}) / A_s, & l_i > l_{dn} \end{cases} \tag{5-25}$$

where, l_i is the distance from the beam-column interface; f_{si} is the axial stress of tensile rebar at l_i; p_d is perimeter of reinforcing bar; A_s is the area of tensile longitudinal rebar.

The above-described calculation procedure will be repeated by incrementing curvature ϕ_i until ϕ_i reaches a targeted level.

5.2.5 Procedures of lateral resistance –drift ratio analysis

The procedure to compute the lateral resistance versus drift ratio of LQFA concrete columns can be summarized below.

1) Calculate the displacement due to flexural deformation and slippage of steel as follows:

$$\Delta_{f,i} = \phi_i l_p \left(L - \frac{l_p}{2} \right) \tag{5-26}$$

$$\Delta_{slip,i} = \theta_{slip,i} L = \frac{S_{lip}}{D_o - X_n} L \tag{5-27}$$

The first equation of Eq. (5-26) is a simplification of Eq. (5-2) by ignoring effect of the elastic deformation outside the lumped hinge region on the displacement due to flexural deformation (see Fig. 5-3). S_{lip} in Eq. (5-12) ~Eq. (5-16) can be obtained by substituting the tensile stress of extreme tensile rebar obtained at step 3 and Eq. (5-17) into Eq. (5-11) through (5-16).

2) Calculate the lateral force V_i corresponding to the given ϕ_i in form of

$$V_i = \frac{M_i}{L} - \frac{N(\Delta_{f,i} + \Delta_{slip,i})}{L} \tag{5-28}$$

where, N is the axial load applied, L is the shear span.

3) Calculate the drift ratio R_i by Eq. (5-29) after computing the shear displacement by Eq. (5-3).

$$R_i = \frac{\Delta_{f,i} + \Delta_{slip,i} + \Delta_{s,i}}{L}, \quad \Delta_{s,i} = \frac{2(1+\mu)}{E_c A_g} V_i L \tag{5-29}$$

where, E_c are the elastic modulus of concrete, μ is Poisson ratio of concrete and will be taken as 0.167, and A_g is the gross area of column section.

5.2.6 Verification of the proposed analytical procedures

While the analytical method described-above is proposed to predict the envelope curve, in other words, the capacity curve, of circular LQFA concrete columns reinforced by SBPDN rebars, the proposed method can also be applied to the concrete columns reinforced by normal- and high-strength deformed rebars only if the bond stress versus slip relationship of them is given.

To verify accuracy of the proposed method, the measured envelope curves in push direction of the test columns described in chapters two and three are compared with the calculated capacity curves in Fig.5-11 for cantilever columns and beam-columns, respectively. Comparisons are conducted in two aspects; 1) the lateral resistance versus drift ratio relationship and 2) end moment versus drift ratio relationship.

It is noted that only three beam-columns are compared in Fig.5-11 because the specimen CFNBN26 did not have fixing steel plate at the mid-height of column to anchored SBPDN rebar, which enables the application of the cantilever-based method to the beam-column. Besides, when calculating the capacity curves of specimens FANUS and FATUS reinforced by deformed USD685, the bond strength of the USD 685 rebar was taken as 15 MPa following the experimental research conducted by Funato et al. [5.1]. In Fig.5-11, the curves expressed with legend "Sun" represent the calculated results by Sun and his colleagues [5.11]. For specimen FATSB, two calculated curves are displayed in Fig. 5-11. One with legend "Mi:Sun" expresses the calculated base moment amplified by Eq. (5.22), while the other with legend "Mi: Priestley" represents the base moment enhanced by Eq. (5.23).

It can be seen from Fig.5-11 that the predicted results by the simplified analytical method exhibit very good agreement with the measured capacity curves of both cantilever columns and beam-columns, having the same accuracy as the integrated analytical method, even for specimen FATSB in which the accuracy of the result enhanced by Eq. (5-23) was better than that of the result enhanced by Eq. (5-22). This fact means that the proposed simple method can be used to the quick and accurate evaluation of lateral capacity curve for circular LFQA members.

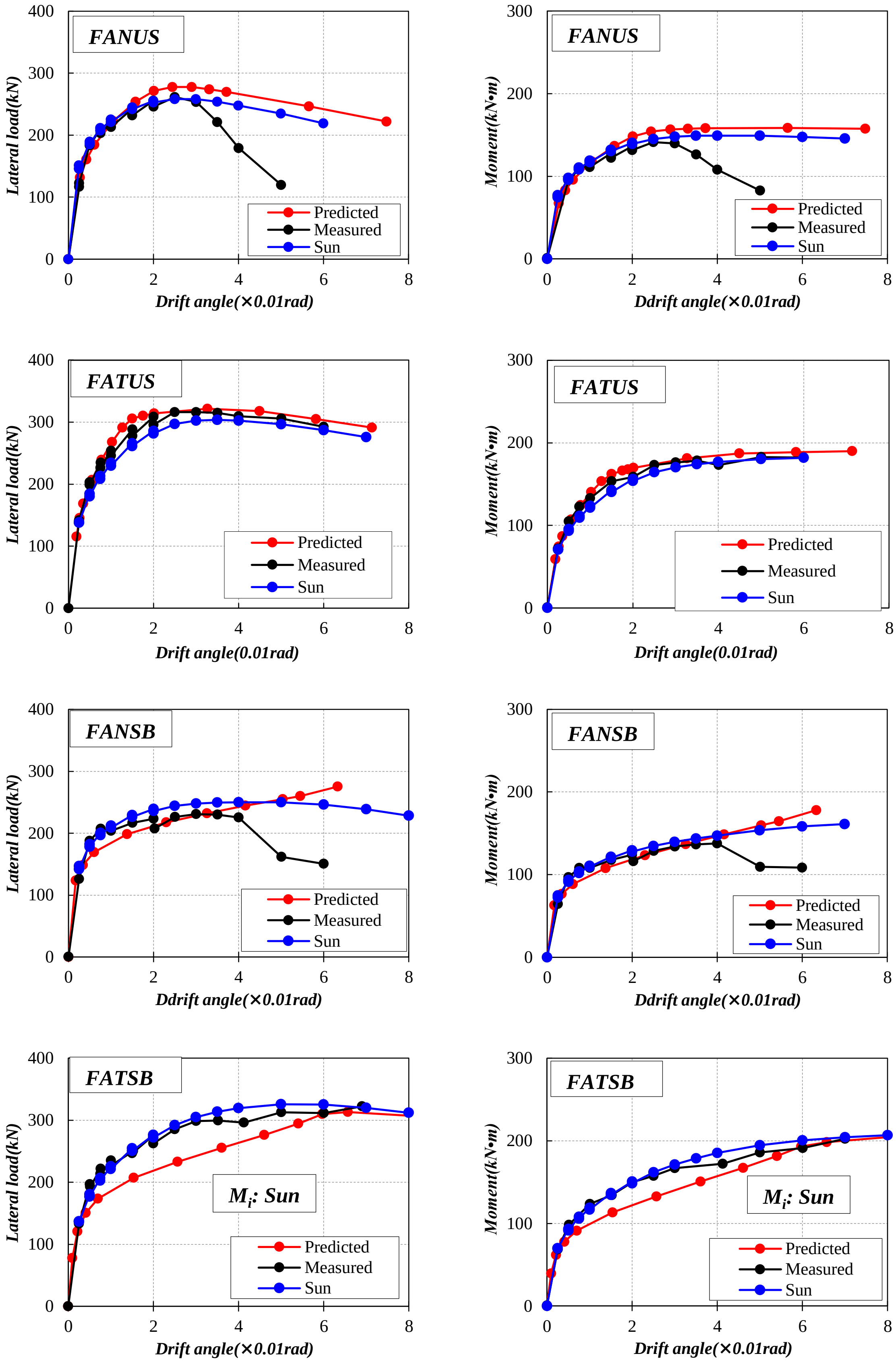

Fig.5- 11 Comparisons of capacity curves(Continued)

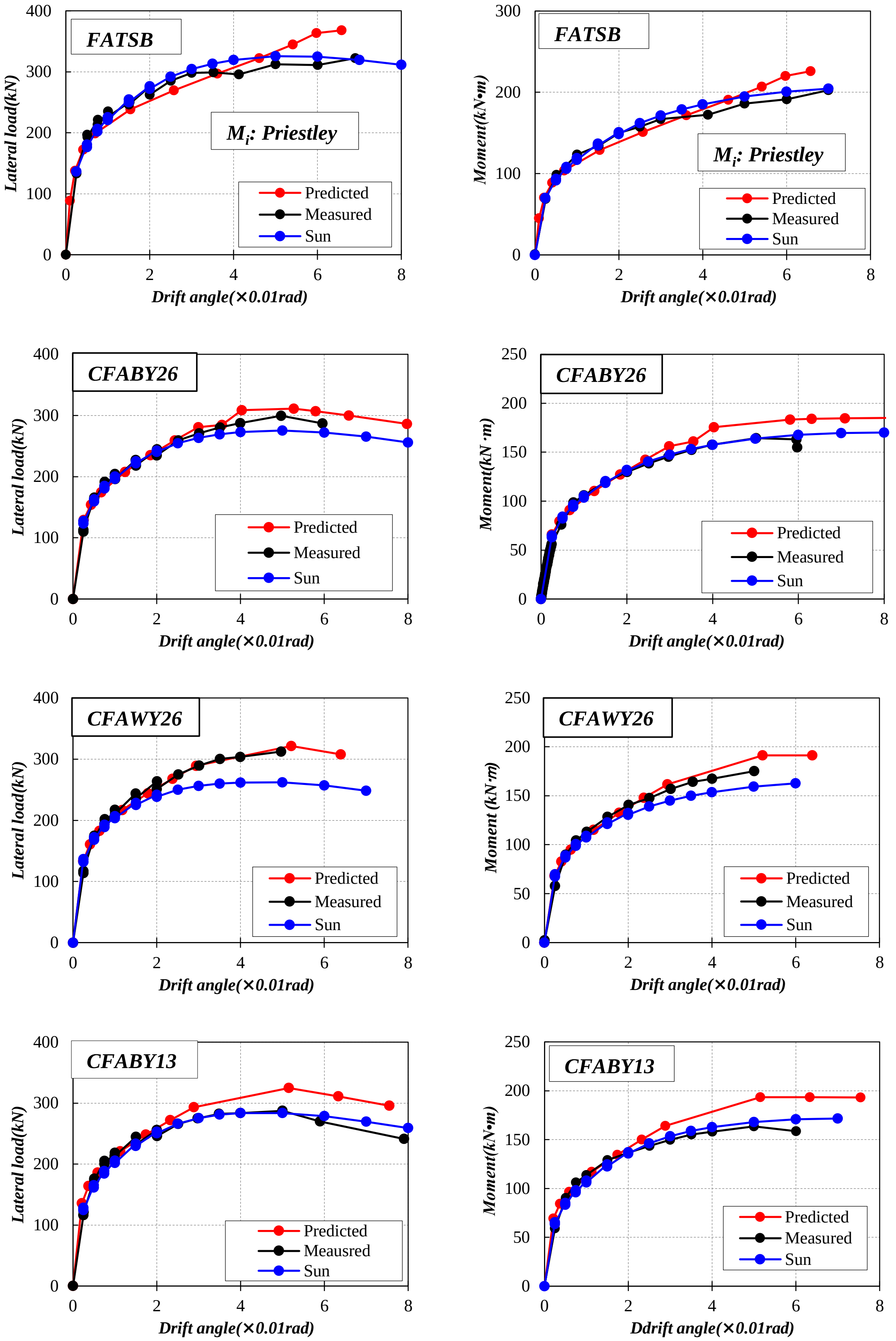

Fig.5- 11 Comparisons of capacity curves

To better see to what extent the slippage of tensile rebars influences the overall displacement response for the LQFA concrete columns with SBPDN rebars, Fig.5-12 and Fig.5-13 show the percentage of each calculated component of displacement to the total displacement of cantilever columns and beam-columns, respectively. The specimen CFNBN26 is again not included in Fig.5-13 due to the same reason as mentioned before.

For cantilever columns, when reinforced by USD 685 deformed rebars whose bond strength is about five times of that of SBPDN rebars, the displacement due to flexural deformation is dominant and occupies 60% to 80 % of the total displacement. Displacement due to shear deformation is very little. Displacement due to slippage of tensile rebars reaches about 40 % of the total one, but confinement by steel tube can reduce the percentage to about 15%.

However, for cantilever columns and beam-columns reinforced by SBPDN rebars, the displacement due to slippage of tensile steels increases along with drift ratio, occupying at most 60 ~70 % of the total displacement from the drift level of 0.03 rad on. Difference of confinement method has little, if any, influence on the displacement due to slippage of tensile rebars as observed in the columns with USD 685 deformed rebar.

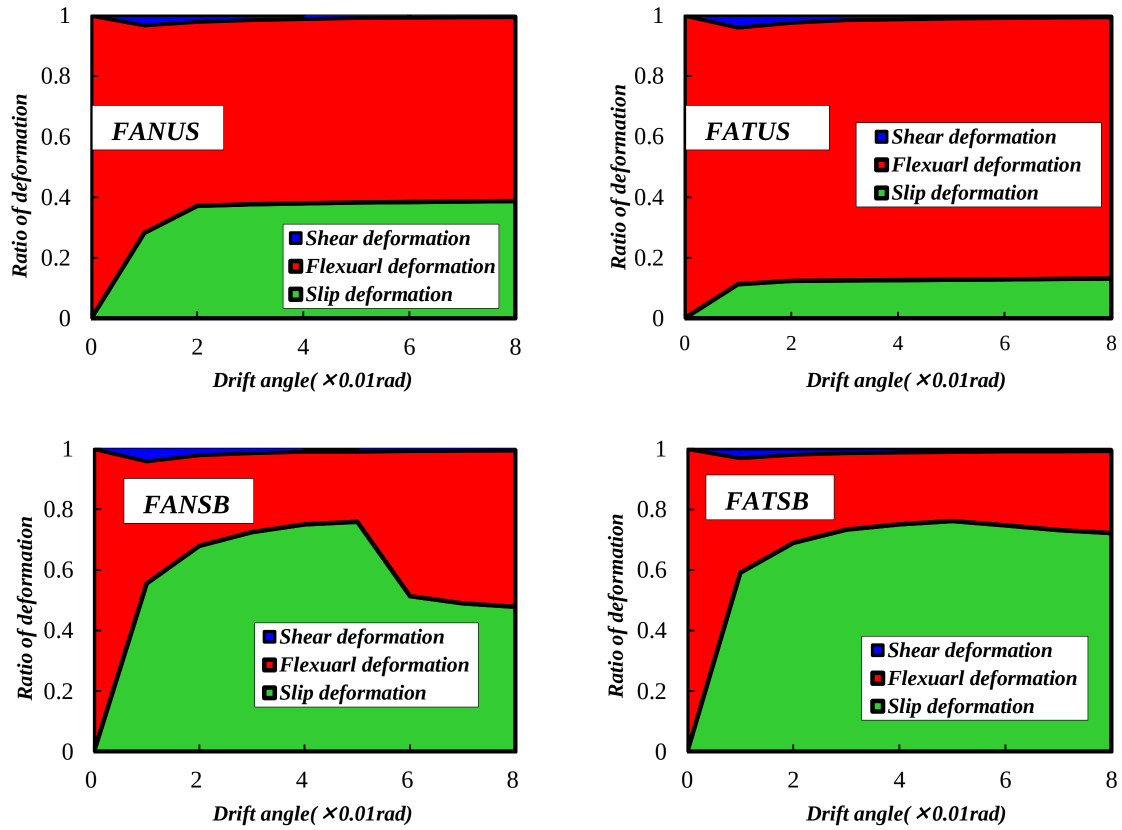

Fig.5- 12 Percentage of each component of displacement to the overall displacement of cantilever columns

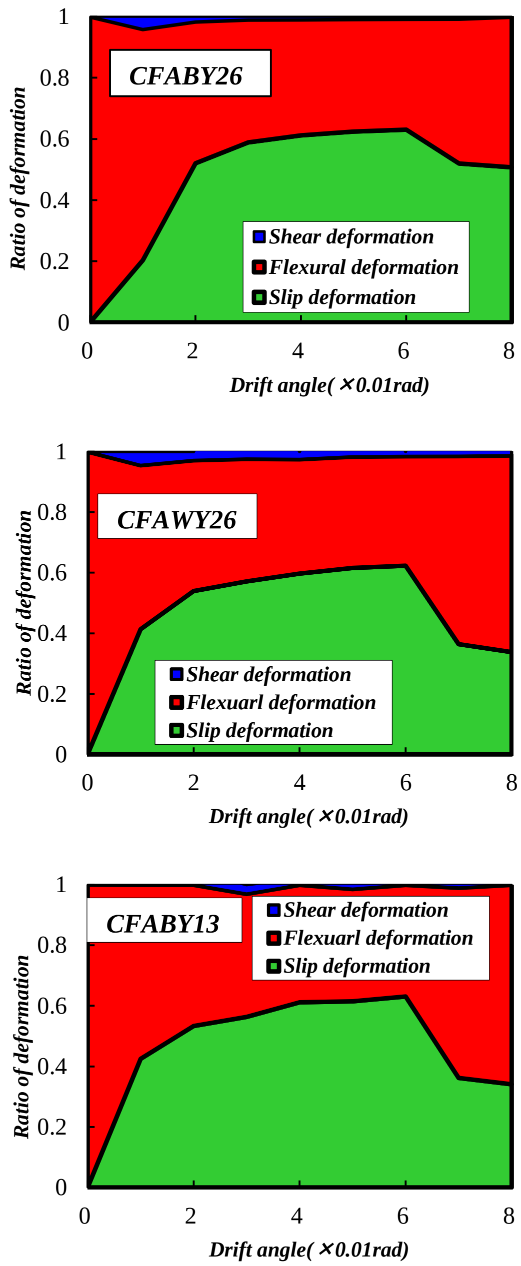

Fig.5- 13 Percentage of each component of displacement to the overall displacement of beam-columns

It is interesting to note that the displacement due to slippage of tensile rebars commences decreasing from drift ratio of 0.05rad, at which the tensile rebars reach the yield strain, as shown in Fig.5-13, resulting in increase of the displacement due to flexural deformation.

Fig.5-14 shows the calculated strain profiles of longitudinal rebars of cantilever columns described in chapter two at every drift angle level. As one can see from Fig.5-14, the steel strain of USD685 rebar, which has much higher bond strength than SBPDN rebar, tends to decrease rapidly outside the hinge region. On the other hand, the steel strain of SBPDN rebar exhibits nearly uniform distribution along column height before the rebar reaches yielding. This observation approximately coincides with the test results shown in Fig.2-14, which implies that the proposed analytical method could reasonably embody the influence of bond strength of rebar on seismic behavior of LQFA concrete columns.

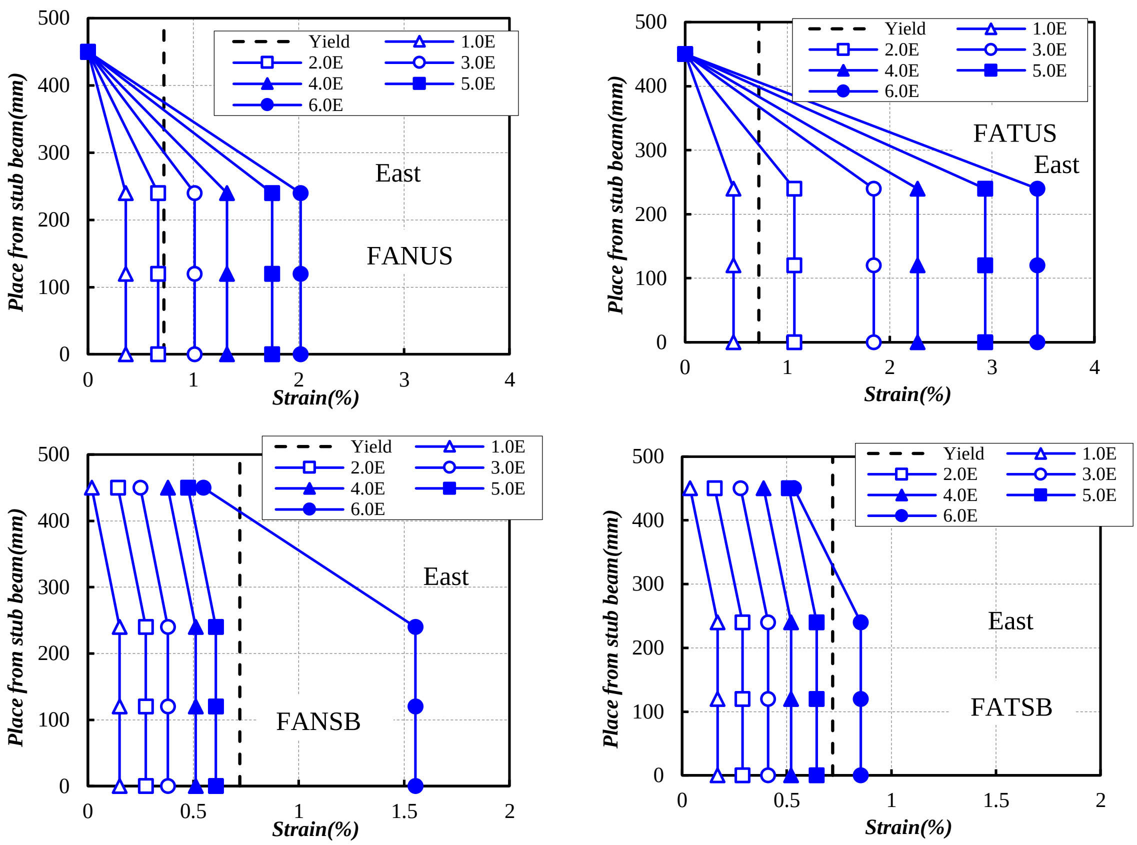

Fig.5- 14 The calculated strain profiles of longitudinal rebars along column height

Based on the results shown in Fig.5-11 through Fig.5-14, it can be said that the proposed simple method is an effective and reliable method to predict the seismic capacity of circular LQFA concrete columns.

5.3 MODELING OF THE CAPACITY CURVE

As described in the previous section, the simplified analytical method can give fairly good and accurate prediction to the capacity curve of LQFA concrete columns, but it still involves tedious iteration inherent in the moment-curvature analysis of concrete section. To help engineers to conduct prompt and reliable analysis of seismic performance of LQFA concrete columns, this section will be devoted to development of a multi-linear model for the capacity curve. Fig.5-15 illustrates outlines of the model.

As shown in Fig.5-15, the multi-linear model is governed by seven parameters listed below.

1) The initial elastic stiffness (K_e)
2) The force at which flexural crack firstly occurs (V_{cr})
3) The tangent stiffness at the stage soon after the elastic stage (K_y).
4) The tangent stiffness for the drift-hardening stage (K_s)
5) The peak lateral resistance (V_u) and the corresponding drift ratio (R_u)
6) The degrading slope (K_u) after the peak.

Formulae to define these parameters will be presented in the following sub-sections.

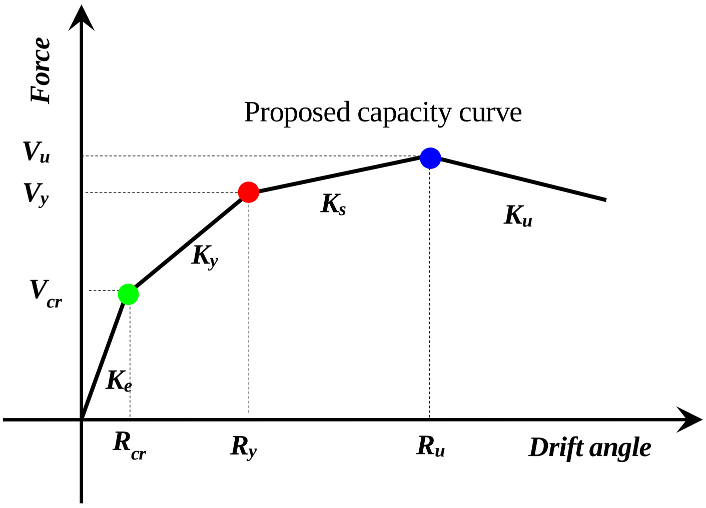

Fig.5- 15 Outline of the proposed capacity curve

5.3.1 The initial elastic stiffness K_e and cracking force V_{cr}

The initial elastic stiffness can be approximately calculated by Eq. (5-30), where effect of longitudinal rebars is ignored for simplicity.

$$K_e = \frac{3E_c I_g}{L^2} \text{ (in kN/rad)} \tag{5-30}$$

where, I_g is the moment of inertia of gross concrete section with longitudinal rebars being excluded. The lateral force that causes flexural crack V_{cr} and the corresponding drift ratio R_{cr} can be calculated with Eq. (5-31), which is recommended in the ACI-318 code [5.12].

$$V_{cr} = \frac{M_c}{L} = \frac{M_{cr} + ND/6}{L}, \quad M_{cr} = \frac{f_r I_g}{y_t}, \quad R_{cr} = \frac{V_{cr}}{K_e} \tag{5-31}$$

where, M_{cr} is the moment that causes flexural crack, N is the axial load applied and compression is taken as positive, D is the diameter of column section, f_r is the modulus of rupture of concrete, y_t is the distance from the centroid axis of gross section to the extreme tensile fiber.

5.3.2 Tangent stiffness K_y and K_s

To derive formulae to predict the tangent stiffness K_y and K_s, based on the method shown in Fig.5-16, the measured K_y and K_s of the specimens described in chapters two and three are obtained and displayed in Fig.5-17 and Fig.5-18 along with several structural factors, respectively. The factors include the transverse steel index, the tensile steel index and concrete strength.

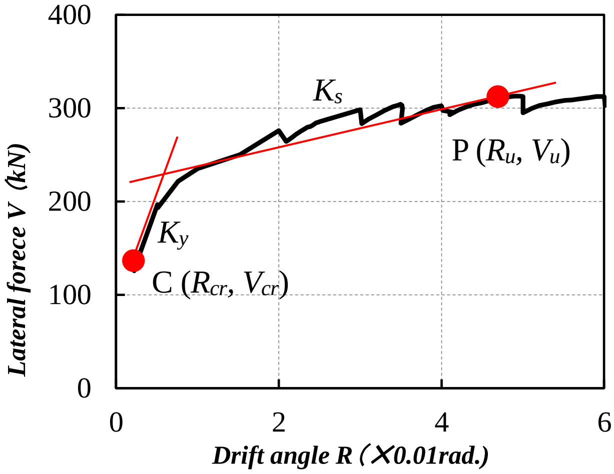

Fig.5- 16 Method to calculate measured K_y and K_s

The concrete procedure to obtain the experimental values for K_y and K_s is, 1) from point C and P (see Fig.5-16) arbitrarily draw two straight lines with gradients of K_y and K_s, respectively, 2) calculate the area covered by the drawn straight lines, 3) calculate the area covered by experimental envelop curve between point C and point P, 4) adjust the values of K_y and K_s for the area covered by them to best fit the area covered by the experimental envelop curve for each specimen.

One can see from Fig.5-17 that K_y drawn from test results does not show clear correlation with the experimental variables, which implies that. K_y is independent of these factors. The measured K_s also exhibits little correlation with the structural factors as seen from Fig.5-18. Transverse steel index (= ratio of the lateral pressure by stirrups and steel tubes to concrete strength) and tensile steel index show some correlation with measured K_s, but the correlation coefficients are so small that it is reasonable to assume that both K_s and K_y are constant for the sake of simplicity.

Based on the above observation, Eq. (5-32) and Eq. (5-33) are proposed to calculate the K_y and

K_s, respectively.

$$K_y = 0.5K_e \tag{5-32}$$

$$K_s = 0.036K_e \tag{5-33}$$

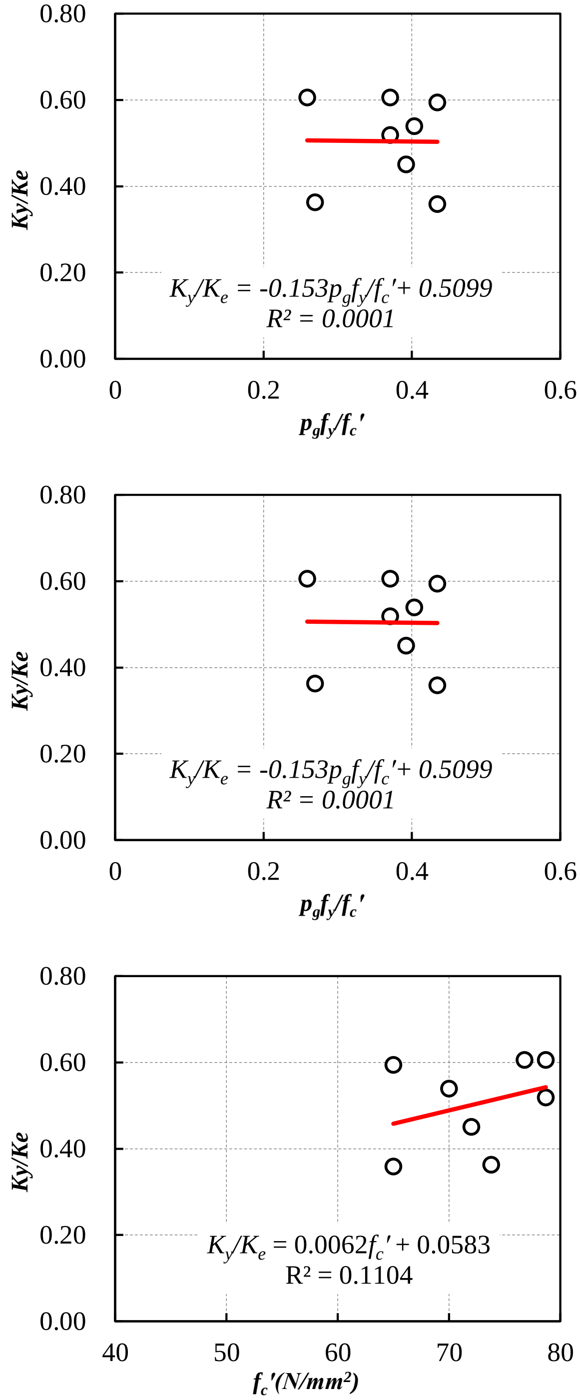

Fig.5- 17 The measured K_y and variation

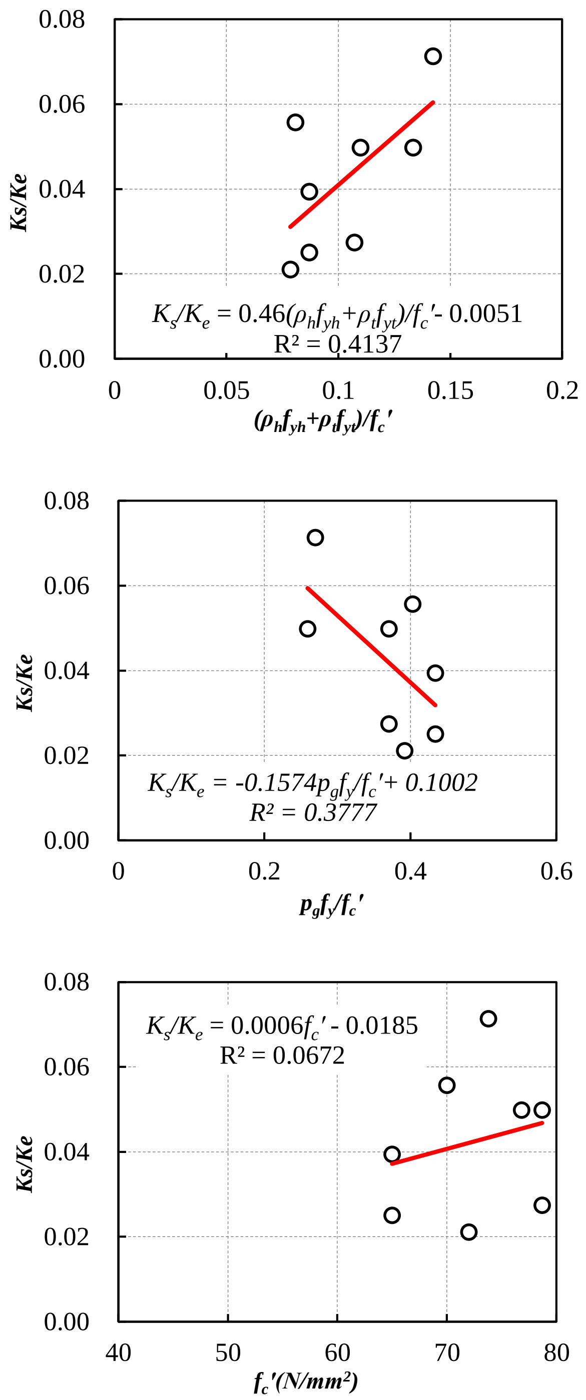

Fig.5- 18 The measured K_s and variation

If ordinates of the peak point (R_u, V_u) are known, the ordinates of the intersection point of the two straight lines with gradients of K_y and K_s can be obtained in form of

$$
\begin{aligned}
R_y &= \frac{(V_u - K_s \cdot R_u) - (V_{cr} - K_y R_{cr})}{K_y - K_s} \\
V_y &= V_{cr} + K_y \cdot (R_y - R_{cr})
\end{aligned}
\tag{5-34}
$$

5.3.3 Ordinates of the peak point (R_u, V_u)

Experimental results of specimens made of LQFA concrete and SBPDN rebars have indicated that both circular LQFA concrete cantilever columns and beam-columns reached their peak lateral resistance when the SBPDN rebar at extreme tensile fiber commenced yielding. Therefore, it is rational to assume that a LQFA concrete column reinforced with SBPDN rebars reaches its' peak resistance as the tensile SNPDN rebars commence yielding.

Based on this presumption, the strain profile along the depth of column section at the peak resistance can be illustrated in Fig.5-19. The term ε_{sy} in Fig.5-19 represents the yield strain of SBPDN rebar, while the term ε_{cm} expresses the ultimate compressive strain of confined concrete.

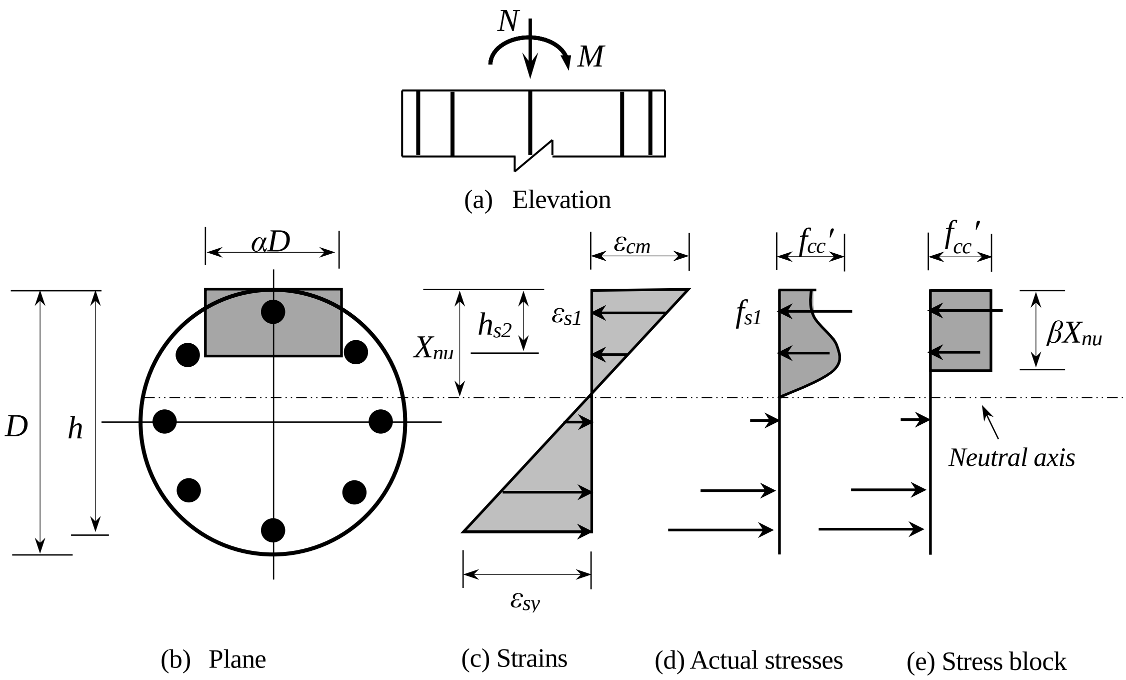

Fig.5- 19 Strain profile at peak resistance and equivalent stress block

According to the study by Sun et al. [5.13], the ultimate compressive strain of confined concrete can be calculated as follow:

$$\frac{\varepsilon_{cm}}{\varepsilon_{co}} = 1.375 + 0.108K - \frac{0.102}{K^4}\frac{f_p}{42} \tag{5-35}$$

where, K is the strength enhancement ratio of confined concrete and defined by Eq. (5-5), and ε_{co} is peak strain of confined and given by Eq. (5-7). The ultimate strains calculated by Eq. (5-35) range from 0.83% to 1.03% for the columns tested in previous two chapters.

The peak lateral resistance V_u and corresponding drift ratio R_u can be obtained if the ultimate moment of the end section or critical section of column and the corresponding curvature ϕ_u, which is referred to as peak curvature, can be predicted.

Since curvature is the gradient of the strain profile along the depth of column section, from the strain distribution illustrated in Fig.5-19, the peak curvature ϕ_u can be simply obtained by Eq. (5-36).

$$\phi_u = \frac{\left|\varepsilon_{sy}\right| + \left|\varepsilon_{cm}\right|}{D_o} \tag{5-36}$$

where, D_0 is the distance from the centroid of tensile rebar to the extreme compressive fiber. Following the assumption that the length of plastic hinge L_p is equal to the diameter of column section D and ignoring the displacement due to shear distortion, the peak drift ratio R_u can be obtained in form of

$$\begin{aligned} R_u &= R_{flexure} + R_{Slip} \\ &= \phi_u L_p \left(1 - \frac{L_p}{2L}\right) + \frac{\phi_u S_{lip}}{\phi_u D_o - \varepsilon_{cm}} L \end{aligned} \tag{5-37}$$

where, S_{lip} is the slippage of tensile rebar and is given by Eq. (5-12) ~ Eq. (5-16) according to anchorage length of the rebar within anchorage length l_{AL}. The slippage can be easily obtained by replacing the steel stress f_{se} and steel strain ε_{se} in Eq. (5-12) or Eq. (5-15) with the yield stress f_{sy} and yield strain ε_{sy}, respectively.

The ultimate moment M_u can also be calculated utilizing an equivalent stress block for the compressed concrete as shown in Fig.5-19. The stress block was developed by Sun et al. in 1998 [5.14] to directly calculate the ultimate moment capacity of circular concrete columns. This thesis will extend the stress block to the calculation of ultimate moment of LQFA concrete columns.

From Fig.5-19, the ultimate moment M_u can be expressed as follow:

$$M_u = \alpha\beta K f_p D X_{nu}\left(\frac{D}{2} - \frac{\beta}{2} X_{nu}\right) + \sum_{i=1}^{n_s} f_{si} A_{si}\left(\frac{D}{2} - h_{si}\right) \tag{5-38}$$

where, α and β are the stress block coefficients, and can be calculated in form of

$$\begin{aligned} \alpha\beta &= A(K, X_{nu}) - B(K, X_{nu})\frac{f_p}{42} \\ \frac{\beta}{2} &= C(K, X_{nu}) - D(K, X_{nu})\frac{f_p}{42} \end{aligned} \tag{5-39}$$

in which

$$\begin{aligned} A(K, X_{nu}) &= \frac{0.723 + 0.061K}{0.112 + X_{nu}} X_{nu} \\ B(K, X_{nu}) &= \frac{0.048K^{-2}}{0.072K^{-1.5} + X_{nu}} X_{nu} \end{aligned} \tag{5-40}$$

$$\begin{aligned} C(K, X_{nu}) &= (0.476 + 0.051K)(1 - 0.132 X_{nu}{}^2) \\ D(K, X_{nu}) &= 0.017\left[1 - (0.024 + 0.187K) X_{nu}{}^2\right] \end{aligned} \tag{5-41}$$

In Eq. (5-38) through Eq. (5-41), f_{si} is the stress of the i-th row of longitudinal rebars, which can be simply calculated from the stress-strain model after obtaining the steel strain form the strain profile shown in Fig.5-19, and X_{nu} is the depth of neutral axis and is written as

$$X_{nu} = \frac{|\varepsilon_{cm}|}{\phi_u} \tag{5-42}$$

After the calculation of M_u, the peak lateral resistance V_u corresponding to R_u then can be obtained as follow:

$$V_u = \frac{M_u}{L} - NR_u \tag{5-43}$$

where, L is the shear span.

5.3.4 The gradation slope K_u

As demonstrated in previous chapters, after the peak load was reached, LQFA concrete columns exhibited deterioration in lateral resistance due to two main reasons; the inherent softening property of high-strength concrete and the P-delta effect. In some specimens, the strength degradation was caused by the transition of failure mode from the initial flexure mode to shear mode due to the shear strength degradation at large deformation. However, due to lack of the experimental data, the average of degradation slope of six specimens that did not fail in shear will be adopted to predict the gradation slope in form of

$$K_u = -0.04K_e \tag{5-44}$$

5.3.5 Verification of the simplified model

In order to verify validity and accuracy of the multi-linear model, the experimental envelope curves are compared with the calculated results in Fig.5-20. In Fig.5-20, besides the multi-linear model, the shear capacity curve model developed in chapter four is also displayed for each specimen.

One can see from Fig.5-20 that the proposed multi-linear model traces the experimental result very well for specimens that exhibited stable response up to large deformation. For specimen FANSB, whose failure mode was inversed at large drift, combination of the simplified capacity curve model with the shear capacity model gives good prediction of the inverse point of the failure mode.

For specimen CFABN26, relatively big discrepancy can be observed between the measured and the calculated capacity curves at larger drift ratio than 0.03 rad. This discrepancy can be attributed to the nonexistence of fixing plate at the column mid-height. In fact, as shown in chapter three, the strain of tensile SBPDN rebar stopped increasing at that drift level and commenced degrading due to extra slippage of the rebar. This observation implies necessity of the fixing plate at the contra-flexure point of concrete columns so that one can expect stable seismic response up to the drift level that may be simply and reliably predicted by using Eq. (5-37) and related equations.

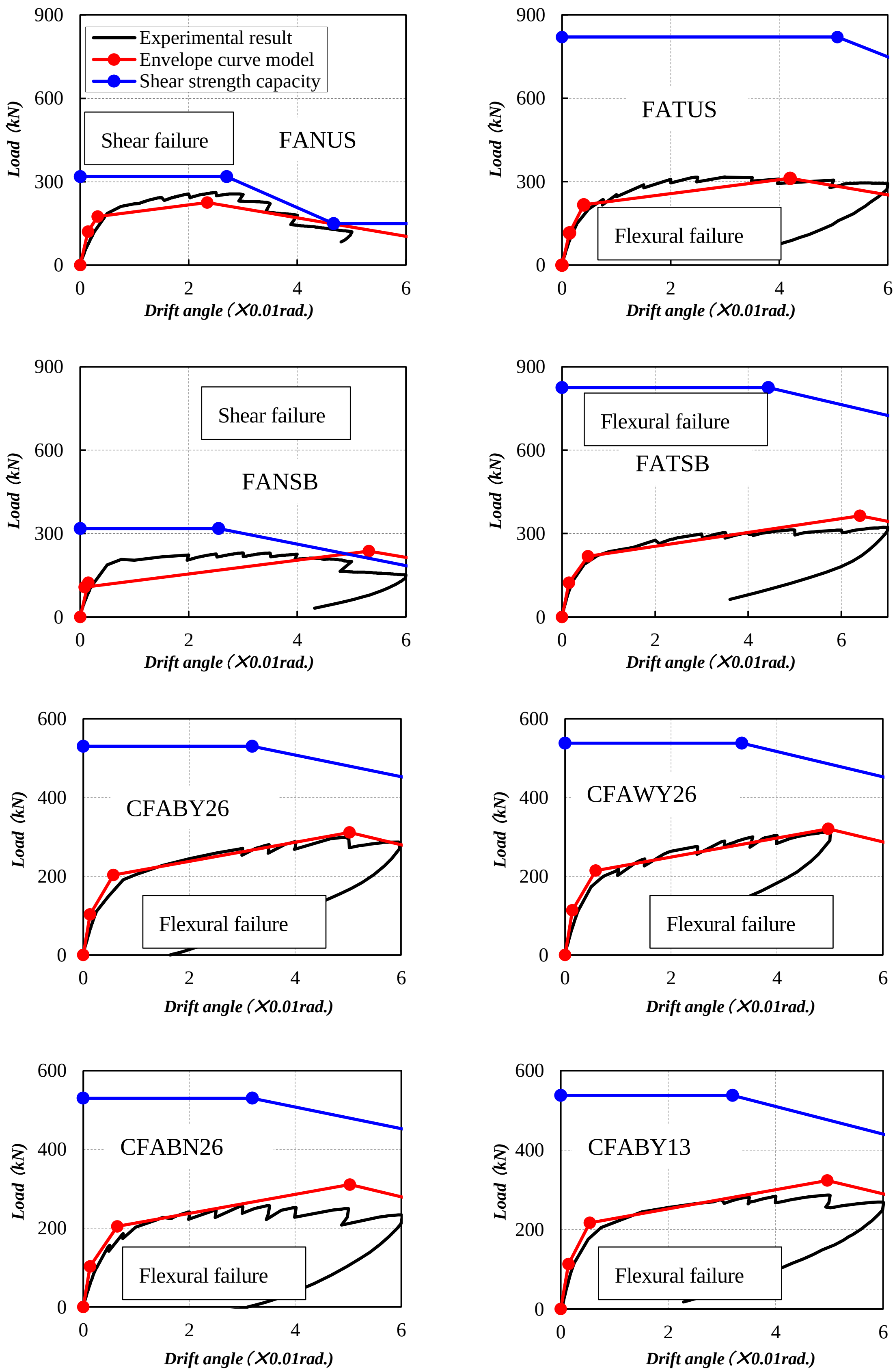

Fig.5- 20 Comparison between the predicted capacity curves and the experimental results

5.4 CONCLUSIONS

In order to develop a simple model to depict the capacity curve of circular LQFA concrete columns reinforced by SBPDN rebars that are expected to behave in a stable manner till large drift under seismic loading, an analytical method is proposed. This method can distinguish contribution of potential displacements to the total deformation of concrete columns, either made of deformed rebar or SBPDN rebar. Based on the proposed method, the monotonic lateral resistance versus drift ratio relationships are investigated. In addition, to help structural engineers to obtain prompt and reliable capacity curve for the LQFA concrete columns, a simplified semi-empirical model is proposed. From analytical works described in this chapter, the following conclusions can be drawn.

1. Based on the assumption that the displacement due to slippage of tensile SBPDN rebar is primarily induced by the elongation of the tensile rebars within the loading stub or beam-column joint, the proposed analytical method to depict the capacity curve of LQFA concrete columns can give very good prediction of the experimental curves up to large deformation.

2. The displacement due to slippage of tensile steels varies along with the bond strength and confinement degree. For the columns with deformed rebars, the displacement due to slippage of tensile steels occupies 10% to 40% of the total displacement. The stronger the confinement by transverse steels, the smaller the displacement due to slippage. On the other hand, for the specimens reinforced by SBPDN rebars, the displacement induced by the slippage of tensile steels may reach 60% - 70% of the total one before SBPDN rebar yields. Confinement degree has only little influence on the displacement due to slippage because of the inherent low bond strength of SBPDN rebar.

3. The simple semi-empirical multi-linear model involves an important presumption that the peak lateral resistance of LQFA concrete columns will be reached when the tensile rebars commences yielding, which coincides with the experimental observations of the test specimens described in chapter two and chapter three of this thesis. The model can account for effects both of confinement by transverse steels and of slippage of tensile steels. The calculated capacity curves by the model agree satisfactorily well with the measured curves till large drift level.

4. Due to its simplicity and accuracy, the proposed model can help structural engineers to give a prompt and reliable prediction to the failure mode and ultimate drift level of LQFA concrete columns, promoting the application of LQFA concrete into building structures and contributing to the reduction of environmental burden by concrete industry.

REFERENCES

[5.1] Funato, Y., Sun, Y.P., Takeuchi, T., Cai, G.C., "Modeling and Application of Bond Characteristic of High-strength Reinforcing Bar with Spiral Grooves," Proceedings of JCI. V.34, No.2, 2012, pp. 157-162.

[5.2] Hendy, C.R. and Smith, D.A., "Designer's Guide to EN 1992-2, Eurocode 2: Design of Concrete Structures. Part 2: Concrete Bridges," Thomas Telford Publishing, 2007.

[5.3] "Design Guidelines for Earthquake Resistant Reinforced Concrete Building Based on Inelastic Displacement Concept," AIJ, Architectural Institute of Japan, Tokyo, 1999.

[5.4] Sezen, H and Moehle, J.P, "Strength and Deformation Capacity of Reinforced Concrete Columns with Limited Ductility," 13th World Conference on Earthquake Engineering, No. 279, 2004, Canada.

[5.5] Sakino, K., Sun, Y.P., "Stress-strain Curve of Concrete Confined by Rectangular Hoop," J. Struct. Constr. Eng., AIJ, No.461, 1994, pp. 95-104.

[5.6] Lehman, D. E, Moehle, J. P., "Seismic Performance of Well-Confined Concrete Bridge Columns," Doctoral dissertation, University of Washington, 2000.

[5.7] Soroushian P., Choi, K.B., Park, G.H., Aslani, F., "Bond of Deformed Bars to Concrete: Effects of Confinement and Strength of Concrete," ACI Materials Journal, V.88, No.3, 1991, pp.227-32.

[5.8] CEB, "CEB-FIP Model Code 1990," CEB B INFORM, 213/214, pp.460.

[5.9] Sun Y.P., Sakino K., "Flexural Behaviour of High Strength RC Columns Confined by Rectilinear Reinforcement," Journal of Structural and Construction Engineering, No.486, 1996, pp.95-106.

[5.10] Ang B.G., Priestley, M. J. N., and Paulay, T., "Seismic Shear Strength of Circular Reinforced Concrete Columns," ACI Structural Journal, 1989, pp. 45-59.

[5.11] Cai, G.C., "Seismic Performance and Evaluation of Resilient Circular Concrete Columns," University of Kobe, 2014.

[5.12] ACI Committee 318, "Building Code Requirements for Structural Concrete (ACI 318-08) and Commentary. ACI," American Concrete Institute, Farmington Hills.

[5.13] Sun, Y.P., and Sakino K., "Simplified design method for ultimate capacities of circularly confined high-strength concrete columns," ACI special publication 193, 2000, pp. 571-586.

[5.14] Sun, Y.P., Takeuchi, T., Funato, Y., and Fujinaga, T., "Earthquake-Resisting properties and Evaluation of High Performance Concrete Columns with Low Residual Deformation," 15th WCEE, LISBOA, 2012.

Chapter 6

Conclusions and Future Works

6.1 CONCLUSIONS

In order to develop sustainable and resilient concrete structures, combination of the utilization of fly ash in large quantities and ultra-high yield strength but low bond strength longitudinal rebars was applied to making concrete members. Considering the omni-directionality and stronger confinement effect of circular columns, this doctor thesis focuses on verification of reliable resilience for circular LQFA concrete columns, whose concrete strength may exceed 70MPa due to the use of fly ash in large quantities. Furthermore, to establish performance-based design methodology, emphasis is also placed on development of capacity curves, including capacity curve for resilient response and shear capacity curve to trace shear strength degradation along with drift level.

To achieve these research goals, experimental and analytical studies were conducted to obtain basic experimental information on seismic behavior and shear behavior of LQFA concrete columns and beams. Primary findings obtained in chapter two through chapter five is summarized below as conclusions of this thesis.

In chapter two, four circular concrete cantilever columns were tested to investigate effects of combination of a large quantity of fine fly-ash, ultra-high-strength rebar with low bond strength, and confinement by thin steel plates, on seismic behavior of concrete columns under single-curvature deformation. The experimental results obtained in this chapter led to the following conclusion.

(1) Combination of a large quantity of fine fly-ash, ultra-high-strength rebar with low bond strength, and confinement by thin steel plates is a simple but effective method to create robust and resilient concrete components. The circular LQFA concrete cantilever columns with SBPDN rebars and under axial compression with axial load ratio of 0.33 showed higher resilience than the columns with USD 685 rebars.

(2) While high compressive strength of concrete due to high fly ash replacement level of 455 kg/m^3 reduced deformability or stability of LQFA concrete columns, utilization of SBPDN rebars as longitudinal rebars and proper confinement by spirals could ensure stable increment of lateral resistance up to the drift level of 0.04 rad. Confinement by steel plates in lieu of spirals could further enhance that drift level up to 0.05rad.

(3) Utilization of USD 685 rebars could ensure LQFA concrete columns stable response and higher early lateral resistance until R=0.025 rad. The high bond-strength of USD rebar, however, tended to cause yielding of it earlier than SBPDN rebar, resulting in degradation of lateral resistance of the columns after R=0.025 rad. Even the confinement by steel plates could not enhance this critical drift level.

(4) Residual drift angle, a well-known and adopted indicator for the reparability of concrete components, was primarily dependent upon if the longitudinal rebars yielded. Confinement method exhibited little, in any, influence on the residual drift angle. Once longitudinal rebars commenced yielding, tensile or compressive, the residual drift would increase at a much higher rate than that before the yielding, which implies that delay of the yielding of longitudinal rebar is crucial to the resilience of concrete members.

Chapter three described four circular columns which were fabricated and tested to investigate robustness and resilience of circular LQFA concrete beam-columns reinforced with SBPDN rebars and confined by thin steel plates. The main findings about the seismic performance and structural detailing of LQFA beam-columns are listed below.

(1) Combination of a large quantity of fly-ash, ultra-high strength rebar with low bond strength and confinement by thin steel plates is a simple and effective method to make sustainable and resilient concrete beam-columns.

(2) While compressive strength of LQFA concrete was beyond 70MPa, combination of SBPDN longitudinal rebar and partial confinement by thin steel plates could ensure circular LQFA concrete beam-columns sufficient resilience until drift angle reached 0.05rad even when the columns were under relatively high axial compression with axial

load ratio of 0.33.

(3) Uniting steel plates by bolts and nuts to form a steel tube could provide high strength concrete the same confinement effect as the welded steel tube. When using thin steel plates to confine high-strength concrete, the bolted tube can work more reliably that the welded tube, which has a risk of rupture near the welding portion at large deformation.

(4) To ensure LQFA concrete beam-columns a resilience up to 0.05 rad, the tie plate should be embedded at the contra-flexure section of column to anchor SBPDN rebars and reduce their slippage.

(5) Shorting the anchorage length of longitudinal bar within beam-column joint had little, in any, influence on the overall seismic performance of LQFA columns.

Chapter four presented twenty concrete beams that were tested under combined shear and bending in order to obtain basic information on the shear behavior of LQFA concrete beams. The emphasis was placed on the evaluation of ultimate shear strength and deformability as well as the proposal of a shear capacity curve suitable for not only rectangular beams but also circular columns. Based on the test results, a complete shear capacity model were developed to trace the shear resistance of LQFA concrete members along with deformation. The experimental and analytical works described in this chapter led to following conclusions about the shear behavior and capacity of LQFA concrete members.

(1) While the compressive strength of LQFA concrete was beyond 70 MPa, shear failure of LQFA concrete beam occurred along a primary diagonal plane by about 45-degree with respect to the beam axis as observed in general normal-strength concrete beams despite the difference in the shear span and the steel ratio of hoop.

(2) The shear resistance by the concrete in LQFA concrete beams was strongly affected by the shear span (a/d) ratio, a factor indirectly accounting for the so-called size effect of structural member on the concrete strength. For the short LQFA concrete beams with the a/d ratio of 1.0, the ultimate shear strength and chord rotation depended more upon the shear span ratio than the steel ratio of stirrup. Increasing the steel ratio of stirrup from 0.19% to 0.76% only brought about 10% increment in ultimate shear strength and chord rotation. On the other hand, for the LQFA concrete beams with the a/d ratio larger than 1.5, the ultimate shear strength and chord rotation increased significantly along with the steel amount of stirrup.

(3) Based on the equilibrium of the forces acting on the diagonal shear plane and Mohr-Coulomb criteria for LQFA concrete, equations (Eq. (4-7) and Eq. (4-8)) were developed to predict the ultimate shear strength of rectangular and circular LQFA concrete members, including beams and columns. These equations can reasonably and accurately account for effect of the shear span ratio on the shear resistance by LQFA concrete, and give more accurate prediction of the measured shear strength than the equations prescribed in current design codes. The ratio of the experimental/calculated shear strength has a mean value of 1.02, and a standard deviation of 0.14.

(4) The ultimate chord rotation or drift ratio of LQFA concrete members exhibited very strong correlation with the factor β, which is the ratio of the calculated shear strength to the calculated flexural strength. A linear equation (Eq. (4-9)) was proposed to predict the ultimate deformation. The proposed equation gives a relatively accurate prediction of the measured results. The ratio of the experimental/calculated deformation has a mean value of 0.99, and a standard deviation of 0.21.

(5) On the basis of test results of LQFA concrete beams which failed in shear, a complete shear capacity curve for LQFA concrete members was developed. The proposed model defines the shear resistance of LQFA concrete members as a multi-linear function of drift ratio or chord rotation, and hence can trace the change or degradation of shear strength along with deformation. The predicted shear capacity curves exhibited fairly good agreement with the measured results of both rectangular LQFA concrete beams and circular LQFA concrete columns, which implies reliability and accuracy of the proposed model.

(6) Due to their simplicity and accuracy, the proposed equations enable structural engineers to conduct reasonable and reliable shear design of LQFA concrete members, promoting the application of LQFA concrete to building structures and contributing to reducing environmental burden by concrete industry.

Emphasis of chapter five was placed on the development of a simple model to depict the capacity curve of circular LQFA concrete columns reinforced by SBPDN rebars that are expected to behave in a stable manner till large drift under seismic loading. At first, an analytical method was proposed to simply trace and distinguish contribution of potential displacements to the total deformation of concrete columns, made of either deformed rebar or SBPDN rebar. In addition, to help structural engineers to obtain prompt and reliable capacity curve for the LQFA concrete columns, a simplified semi-empirical model for the capacity curve was proposed. From analytical works described in this chapter, the following conclusions can be drawn.

(1) Based on the assumption that the displacement due to slippage of tensile SBPDN rebar is primarily induced by the elongation of the tensile rebars within the loading stub or beam-column joint, the proposed analytical method to depict the capacity curve of LQFA concrete columns can give very good prediction of the experimental curves up to large deformation.

(2) The displacement due to slippage of tensile steels varies along with the bond strength and confinement degree. For the columns with deformed rebars, the displacement due to slippage of tensile steels occupies 10% to 40% of the total displacement. The stronger the confinement by transverse steels, the smaller the displacement due to slippage. On the other hand, for the specimens reinforced by SBPDN rebars, the displacement induced by the slippage of tensile steels may reach 60% - 70% of the total one before SBPDN rebar yields. Confinement degree has only little influence on the displacement due to slippage because of the inherent low bond strength of SBPDN rebar.

(3) The simple semi-empirical multi-linear model involves an important presumption that the peak lateral resistance of LQFA concrete columns will be reached when the tensile rebars commences yielding, which coincides with the experimental observations of the test specimens described in chapter two and chapter three of this thesis. The model can account for effects both of confinement by transverse steels and of slippage of tensile steels. The calculated capacity curves by the model agree satisfactorily well with the measured curves till large drift level.

(4) Due to its simplicity and accuracy, the proposed model can help structural engineers to give a prompt and reliable prediction to the failure mode and ultimate drift level of LQFA concrete columns, promoting the application of LQFA concrete into building structures and contributing to the reduction of environmental burden by concrete industry.

6.2 SUGGESTIONS FOR FUTURE WROKS

The study described in this thesis has covered fundamental aspects of circular LQFA concrete members, including resilient capacity curve and shear capacity curve. However, due to the constraint of time, there are still several important issues remained to be dealt from the viewpoint of promotion of the proposed sustainable and resilient concrete columns in the actual facilities as listed below:

(1) Quantitative influence of the replacement level of fly ash on the mechanical behavior of LQFA concrete members needs to be made clear. This study concentrated on the replacement level of 455 kg/m^3 of fly ash, but the quantitative relationship between the replacement level and the mechanical properties of LQFA concrete members is obviously indispensable to amplify the application of fly ash to building and civil structures.

(2) Effect of shear span ratio on the overall seismic behavior of circular LQFA concrete columns should also be clarified. The specimens tested in this study only represented typical columns used in building structures. For the columns at the lower stories of high rise buildings or highway bridge piers, the shear span ratio may be much larger than 2.0 due to higher mode of vibration or construction requirements. In particular, the larger the shear span ratio, the more significant the so-called P-delta effect on the overall performance of columns or piers.

(3) Effect of axial load level on seismic performance of LQFA concrete columns needs to be investigated. Observations described in this paper are based on the experimental results of test columns with axial load ratio of 0.33.

(4) Applicability of the detailing method for the anchorage of SBPDN rebars at the contra-flexure section of circular beam-columns to the rectangular LQFA concrete columns needs to be verified. The findings about seismic properties of LQFA concrete members stated in this study are all for circular columns. It is necessary to clarify if these findings can be observed for the rectangular columns, which are adopted in actual structures much wider than circular columns.

(4) Effect of several important structural factors on the proposed multi-linear capacity curve model is not yet clear. These factors include the axial load level, concrete strength and confinement degree by transverse steels. They are presumed to influence the tangent stiffness *Ks* of the capacity curve soon after the commencement of slippage of tensile rebars. The empirical expression for *Ks* presented in chapter five plays a vital role in evaluating the resilience of the proposed sustainable concrete columns, but was derived from the test results of only eight specimens. Further verification of the formula for the *Ks* is necessary.

List of Publications

[1]. Junhua, Wang, Takashi Takeuchi, Tomoyuki Koyama, Yuping Sun, Mechanical Properties and Evaluation of Concrete Beams made of a Large Amount of Fine Fly Ash，Proceedings of IABSE Conference NARA, 8pages, 2015.5

[2]. Junhua Wang, Takashi Takeuchi, Tomoyuki Koyama, Yuping Sun, Seismic Behavior of Circular Fly Ash Concrete Beam-Column Reinforced by SBPDN Rebars and Steel-plate Jacketing, Proceedings of the Japan Concrete Institute, Vol.37, No.2, pp.193-198, 2015.

[3]. Junhua Wang, Takashi Takeuchi, Tomoyuki Koyama, Yuping Sun, Seismic behavior of circular fly ash concrete columns reinforced by ultra high strength rebar and steel plates, Proceedings of the Japan Concrete Institute, Vol.36, No.2, pp: 115-120,2014.

[4]. Junhua Wang, Yuping Sun, Tomoyuki Koyama, Hua Zhao, Takashi Takeuchi, Ultimate Shear Strength and Chord Rotation of High-Volume Fly Ash Concrete Beams, Structural Concrete, 2016. (under review)

[5]. Junhua Wang, Sargsyan Grigor, Yuping Sun, Takashi Takeuchi, Influence of Bond Strength of Longitudinal bar on Seismic Behavior of Concrete Member, Materials and Structures, (will be submitted)

Doctor Thesis, Kobe University
Seismic Behavior and Evaluation of Concrete Members Made of A Large Quantity of Fly Ash, 133 pages
Submitted on July, 6, 2016
The date of publication is printed in cover of repository version published in Kobe University
Repository Kernel